

Chapter 4

Advanced Modulation Formats

4.1 Introduction

This chapter presents some of our previous work including **1:** Experimental demonstration of the DQPSK signal generation using a dual-drive Mach-Zehnder modulator (DD-MZM). We show that using RZ impulse shaping can exceed more than 5 dB gain over NRZ with this generation scheme. The theoretical investigations of optical spectrum and bit error rate are also given. **2:** Encoding the ASK labeled RZ-DPSK signal by using one DD-MZM. Compared to the previous approach this cost-effective scheme has a 2 dB gain for the label and a comparable performance for the payload after 120 km fiber transmission. **3:** We also evaluate the quantum limit for 4ASK with optimum level spacing. Compared to OOK format, there is around 5 dB penalty due to multi-level detection. **4:** A phase modulated 4ASK (PM-4ASK) format is proposed with the advantages of better tolerances to the CD, PMD and optical filtering effects. Please find details of the backgrounds and overviews regarding to the advanced modulation formats in chapter 2.

4.2 DQPSK Format Generation by Using One Dual-Drive Mach-Zehnder Modulator

4.2.1 Introduction

With the rapid growth of internet traffic congestion, efficiently using signal bandwidth is essential to increase the transmission capacity over already installed optical fibers and amplifiers. Differential quadrature phase-shift keying (DQPSK) is a quaternary phase

modulation format [1], which has received increasing attention owing to its greater spectra efficiency (SE) than binary formats, such as that associated with intensity modulation or differential binary phase-shift keying [2]. To simplify the DQPSK transmitter, one phase modulator with four-level electrical drive signals has been proposed [3]. Recently, a more flexible QAM generator employing single DD-MZM is provided in [4]. In this paper [4], three generation methods for DQPSK signals with four-, three- and two-level electrical drive signals have been introduced. Among those methods, the two-level signal is the simplest, and compatible with the conventional on-off keying (OOK) coding scheme. However, the generated signal suffers from ripples caused by the rise-fall time of the input drive signals, and the RZ format is suggested to mitigate these impacts [4].

In this letter, the performance of a DQPSK signal generated by one DD-MZM with and without a pulse carver is experimentally evaluated. Different RZ duty cycles, - 33%, 50% and 67% -, are used to estimate the impact of ripples on transmission performance. All three duty cycles can effectively suppress the ripples below those associated with NRZ format. Though the 33% RZ format offers the best sensitivity, i.e. about 2 dB better than the 67% RZ format, the sensitivity of all three RZ formats is 3.5 dB better than that of the NRZ format before transmission. Following 60 km standard single mode fiber (SSMF) transmission, all RZ formats have negligible transmission penalties (less than 0.2 dB), while the NRZ format exhibits a larger transmission penalty (~0.5 dB).

4.2.2 Concept

Figure 4.1(a) shows the principle of the generation of a DQPSK signal by a single DD-MZM. A continuous wave is externally modulated by a DD-MZM. With one arm of the biased voltage set at $3V_{\pi}/2$, two independent electrical data streams, V_1 and V_2 , with peak-to-peak amplitudes (V_{pp}) that equal the switching voltage, V_{π} , are sent to the DD-MZM. This is a great relief from the requirement of high driving voltages ($2V_{\pi}$) in conventional DQPSK

signal generation combining two DPSK signals with $\pi/2$ phase shift. The output electrical field can be expressed as [6]:

$$E_{out} = E_{in} e^{j\left(\frac{V_1+V_2+V_{b1}+V_{b2}}{2V_\pi}\pi\right)} \cos\left(\frac{V_1-V_2+V_{b1}-V_{b2}}{2V_\pi}\pi\right) \quad (4-1)$$

where $V_{b1}-V_{b2} = 3V_\pi/2$ is the bias voltage. Figure 4.1(b) depicts the corresponding data positions determined using the above equation. The inset presents a symbol constellation diagram, with four phase positions, determined by the input signals V_1 and V_2 . Since the symbol transition possibly passes through the minimum and the maximum of the transfer curve, the power will fluctuate around the symbol edge owing to the rise-fall time of the electrical drive signal [5].

As displayed in Fig. 4.2, a transmission test link is established to demonstrate the feasibility of this scheme and evaluate the system performance. A DFB laser, operated at a wavelength of 1545 nm, is firstly modulated using a DD-MZM driven by two electrical 10 Gbps data signals with a length of $2^{15}-1$. To de-correlate the two input data streams [7], an electrical delay line is added to one data stream with a delay equal to the time of 28-bit interval. For RZ formats, a pulse carver is inserted to generate different RZ formats. An erbium-doped fiber amplifier (EDFA) and an optical fiber delay line (FDL) between the two MZMs are inserted to compensate for the loss of MZMs and synchronize the data to the pulses, respectively. The fiber medium contains a span of 60 km standard single mode fiber (SSMF), an EDFA, and dispersion-compensating fibers (DCF) to compensate the dispersion caused by SSMF. At the receiving end, an optical attenuator is placed before the optical pre-amplifier to adjust the input power to the DQPSK receiver. A 40 GHz optical band-pass filter is employed to remove the residual amplified spontaneous emission (ASE) noise. To demodulate the DQPSK signal, two delay-interferometers in a parallel architecture with phase difference of $+\pi/4$ and $-\pi/4$ are required to extract simultaneously the in-phase and quadrature-phase information [1]. A single DI with either a $+\pi/4$ or a $-\pi/4$ phase difference

is utilized to demodulate one data stream at a time [8]. The signal is single-ended detected by the following photodiode and clock recovery circuit and sent into the 10 Gbps error detector (ED). Since differential encoding was not applied, the expected data patterns at the receiver were calculated and programmed into the error detector to measure the bit error ratio (BER). Two additional attenuators are inserted through the link after the transmitter and before the DCF, to alter the input power such that it equals 0 dBm.

4.2.3 Experimental Results

Figure 4.3 shows the optical spectra of different signal formats with a resolution bandwidth of 0.01 nm. The narrowest bandwidth is that of NRZ-DQPSK format, for which the mainlobe has the same width as that associated with NRZ-OOK but carries double the amount information. Appropriately adjusting the bias point and the input clock signals of the pulse carver yields pulses with duty-cycles of 33%, 50% and 67%. As expected, the optical spectra in Fig. 4.3 indicate that the 67% RZ signal has the narrowest mainlobe while the 33% RZ signal has the widest mainlobe. Notably, spectra obtained using the new generation scheme differs interestingly from that of the conventional schemes. Instead of the nulls among the sidelobes in the conventional scheme, new generation method yields peaks at the valley points in all data formats, especially the case of NRZ format. They are believed to be induced by the time domain ripples around the symbol transitions. Figure 4.4 presents their corresponding eye diagrams, a high speed oscilloscope with a bandwidth of 53 GHz (Agilent 86116A) is used to observe the details of the ripples. The NRZ signal suffers most from the ripple effect and is seriously degraded in the demodulated eye pattern. The suppression of ripples in RZ formats in the three different duty-cycles can be readily observed. Although most of the ripples can be removed by a pulse carver, the amounts of residual ripples are different with the three different duty cycles at the rise-fall traces. The residual ripples with a smaller duty cycle, 33%, are smaller than those with a 67% duty cycle. The back to back (b2b) demodulated eye

patterns are also shown below in Fig. 4.4. In the demodulated eyes, the ripple effect is almost completely removed from the 33% RZ format, while 50 and 67% RZ formats still slightly suffer from ripple effects. However, all three duty-cycle RZ formats considerably suppress the ripples and yield much clearer demodulated eyes than the NRZ format.

Figure 4.5 plots the measured bit error ratio (BER). Except for the NRZ format, in which the ripples seriously distort the signal, the RZ formats have receiving sensitivities of around -30 dBm. The performance of the 33% RZ format is best for two reasons. Firstly, in this format, more power near the edges is carved out, where the signal most suffers from ripples most. Secondly, a narrower pulse format inherently has a better sensitivity because more power falls into the decision window [9]. Following 60 km SSMF and DCF, the transmission penalties for RZ formats are under 0.2 dB whereas that for the NRZ format is 0.5 dB. The insets display the demodulated eyes after transmission. Although the NRZ-DQPSK signal can be generated by only one MZM, the RZ formats are preferred scheme with good sensitivities of -30 dBm. The measured results for RZ formats are similar to that in [10], and confirm that this generation scheme is a good alternative choice with simpler structure and lower cost. The receiver sensitivity can be further improved by using double balanced detection.

4.2.4 Summary

An optical DQPSK signal using only one DD-MZM is experimentally generated and transmitted. With an additional pulse carver, the RZ formats are generated to eliminate the power of ripples inherently occurred in NRZ formats. The BER results indicate that all the RZ formats in such a generation scheme outperform the NRZ format, and the 33% RZ format, with the narrowest pulse width, is the most robust against ripples. The sensitivity of all three RZ formats exceeds that of the NRZ format by more than 3.5 dB, which manifests the necessity of using a pulse carver.

4.3 Theoretical Investigations for DQPSK Signal Generated by One Dual-Drive Mach-Zehnder Modulator

4.3.1 Introduction

With the rapid growth of Internet traffic congestion, efficiently using signal bandwidth is essential to increase the transmission capacity over already installed optical fibers and amplifiers. Differential quadrature phase-shift keying (DQPSK) is a quaternary phase modulation format [11], which has received increasing attention owing to its greater spectra efficiency (SE) than binary formats, such as that associated with intensity modulation or differential binary phase-shift keying [12]. To simplify the DQPSK transmitter, one phase modulator with four-level electrical drive signals has been proposed [13]. Recently, a more flexible QAM generator employing single DD-MZM is provided in [14]. In this paper [14], three generation methods for DQPSK signals with four-, three- and two-level electrical drive signals have been introduced. Among those methods, the two-level signal is the simplest, and compatible with the conventional on-off keying (OOK) coding scheme. As indicated by the authors, the generated signal suffers from ripples caused by the rise-fall time of the input drive signals, the return to zero (RZ) format is suggested. However, they did not evaluate the impact of the ripples which would possibly appear even in RZ format when there is an asynchronization between the data modulator and the pulse carver. Besides, due to the different generation method, the DQPSK signal is with a different power spectra compared to the conventional scheme.

In this letter, we analytically computed the optical spectra of the one-MZM generated DQPSK signal and compared it with that of the conventional one. With the noise modeled by the Karhunen-Loeve (KL) expansion and the bit error rate (BER) computed by the saddle point approximation [15], we evaluated the sensitivity improvement when a RZ format was used, and the sensitivity impairment when there was a timing mismatch between the data and

the pulse modulator. The simulation results are validated by the Monte Carlo error counting method. In addition, we firstly, to the authors' knowledge, demonstrated the one-MZM generated DQPSK signal by measuring the optical spectra and corresponding eye patterns in NRZ and RZ formats.

4.3.2 Optical Spectra and Bit Error Rate Analysis

An optical DQPSK signal can be generated by using two parallel x-cut MZMs [11] or by using one z-cut DD-MZM [14], as shown in Fig. 4.6(a) and (b). We will compare these two schemes in terms of their optical spectra and bit error rate performance.

Optical Power Spectra

The optical spectra were computed based on the method in [16]. We firstly considered the spectra of the one-MZM generated signal. We ignored the chirp effect and considered the following electrical field: $e(t) = \frac{1}{2}\{exp[j\eta\phi_1(t)] + jexp[-j\eta\phi_2(t)]\}$ where $\eta = \pi/2$ is the modulation index and $\phi_i(t) = \sum_{k=-\infty}^{\infty} b_i(k)p(t - kT)$ is the two independent data signals with $i = 1, 2$. $b_i(k)$ is the data bit and $p(t)$ is the pulse waveform. This formula is similar to eq. (2) in [16] except the value of modulation index and the independency of the two data streams $\phi_1(t)$ and $\phi_2(t)$. The power spectra density (PSD) is the same form as eq. (12) in [16], which consists of a continuous spectrum and discrete frequency tones.

For the case of 2-MZMs generated signal, the output electrical field of the two parallel DPSK modulators can be written as

$$e(t) = e_1(t) + je_2(t) = \frac{1}{2}\{exp[j\eta\phi_1(t)] - exp[-j\eta\phi_1(t)]\} + j\frac{1}{2}\{exp[j\eta\phi_2(t)] - exp[-j\eta\phi_2(t)]\}$$

After some manipulations, we can get the average autocorrelation function, $\bar{R}(\tau)$.

$$\bar{R}(\tau) = \frac{1}{T} \int_0^T \left[\prod_{k=-\infty}^{\infty} \cos\{[p(t + \tau - kT) - p(t - kT)]\} \right. \\ \left. - \prod_{k=-\infty}^{\infty} \cos\{[p(t + \tau - kT) + p(t - kT)]\} \right] dt$$

and the PSD follows

$$\Phi_e(f) = 2Re\left\{ \int_0^{(K+M)T} \bar{R}(\tau) e^{-j2\pi f\tau} d\tau \right\}$$

where K and M are defined in [16]. The periodic terms are cancelled and only the continuous parts remain.

Bit Error Rate

The bit error rate evaluation is based on the Karhunen-Loeve series expansion and saddle point approximation [15]. We consider an optically pre-amplified receiver in which ASE is the dominant noise. As shown in Fig. 4.6(c), the ASE noise is added to the signal with one polarization, single-sided power spectra density of $h\nu n_{sp}(G - 1)$ where G is the gain of the EDFA. A followed optical filter removes the residual noise. An optical delay interferometer, with one arm delayed by one bit duration and an additional phase shift of $\pm\pi/4$, is located after the optical bandpass filter forcing the signal to OOK format. The demodulated signal is then converted to electrical signal by the following squared law detector with balanced architecture. The signal is then filtered by an integrated-and-dump circuit, sampled and fed to the decision circuit. The bit error rate are computed by approximating the saddle point integration of the moment generating function (MGF) of the decision variable.

4.3.3 Numerical Results

Optical Spectra

The optical spectra versus various pulse waveforms of the signals generated by one and two

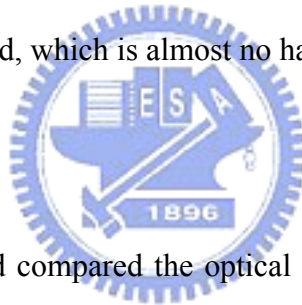
MZMs are plotted in Fig. 4.8. The input electrical waveform is the raised-cosine pulses described in [16]. Figure 4.7(a) depicted the signal spectra of the two-MZMs scheme with $\beta = 0, 0.5,$ and 1.0 . As expected, for all the three input waveforms, the spectra are continuous and no frequency tones are observed. However, the signals of one-MZM scheme have both the continuous spectra and the discrete tones if the electrical pulse waveform is with a nonzero rise-fall time as shown in Fig. 4.7(b). These tones are induced by the time domain rippling effect between two adjacent symbols. These tones carry no information and thus will make the signal having worse sensitivity.

Bit Error Rate

In this section we will lay emphasis on the suppression of the ripples induced in the one-MZM scheme. The ripple will become significant when NRZ format is used or there is a timing mismatch between the data and the pulse. As a validation of the KL technique in the presence of receiver impairments, Fig. 4.8(a) shows the BER of the one-MZM scheme which is a comparison between the results obtained using the KL method and numerical simulations where the BER is estimated through Monte Carlo error counting. Each point is derived with at least 30 errors. The data rate is 10-Gbps and the bandwidth of the Gaussian optical filter is 20 GHz. The KL method approximates well even with a 20-ps timing mismatch between the data and the pulse modulator. Since using the balanced detection can get a better sensitivity, we only show results with balanced detection hereafter. Fig. 4.8(b) shows the timing mismatch tolerances of the one-MZM scheme with different RZ duty cycles. The rise-fall time of the input electrical signal is 25 ps. The RZ-50% of the two-MZMs scheme is also provided for comparison. For penalty less than 1 dB, the tolerances of the three RZ pulses are 25, 30, 35 ps for duty cycles of 67, 50 and 33%, respectively. Since the ripples are near the symbol edges, narrower pulse will hardly carve the ripple into signal while the broader pulse will easily contain the ripple power and enhance the power penalty. The penalty of the two-MZMs

scheme can be ignored when the timing mismatch is up to ± 20 ps.

Figure 4.9 shows the bit error rate of the signals of the two schemes. In the two-MZMs scheme, the required OSNR for RZ and NRZ are about 14 and 14.4 dB when electrical inputs with rectangular waveforms are used; while they are 14 and 14.6 dB when the electrical inputs are with a rise time of 25 ps. The reason for better sensitivities of RZ formats can be explained in [17]. The 0.2 dB gain of the rectangular input signal over that with a nonzero rise-time might be the match filtering of an integrated and dump circuit to a rectangular waveform. In the case of the signal with one MZM, we found that NRZ format is very sensitive to the rise-fall time of the electrical inputs because of the inherent ripples appearing at the symbol edges. With an input rise-fall time of 25 ps, at least a 2.6 dB optical penalty for the NRZ format is observed. However, with a pulse carver, the ripples are largely suppressed and only little penalty is induced, which is almost no harm to the system.



4.3.4 Summary

We theoretically computed and compared the optical spectra and the exact bit error rates of two DQPSK signals generated by different methods. The inherent ripple impact appearing in NRZ format and timing mismatch between data and pulse modulators is evaluated by optical power penalty. Finally, we showed the demodulated eyes opened and demonstrated the possibility of the one-MZM scheme.

4.4 Encoding ASK Labeled CSRZ-DPSK Payload by Using Only One Dual-Drive Mach-Zehnder Modulator with Enhanced Label Performance

4.4.1 Introduction

Optical Label Switching (OLS) had been proposed to enable more effective and flexible utilization of the capacity of WDM optical networks [18]. Optical-label packet transmission based on amplitude shift keying/return-to-zero differential phase shift keying (ASK/RZ-DPSK) orthogonal modulation format was recently proposed [19, 20], in which the payload is modulated by RZ-DPSK format, while the label is transmitted by ASK format. It was found that when DPSK is used for high speed payload transmission (40 Gbps and beyond), the temperature stability and polarization insensitivity of the delay interferometer (DI) are significantly improved after the laser linewidth requirements are reduced [19]. A variation over the standard RZ-DPSK is carrier-suppressed return to zero DPSK (CSRZ-DPSK) format. It has been shown that CSRZ-DPSK is more resilient to fiber nonlinearity and, with optical signal filtering, is the optimized format for achieving ultrahigh spectral efficiency (0.8 bits/s/Hz) at 40 Gbps [21, 22]. However, to implement such an ASK/CSRZ-DPSK orthogonal modulation format, three cascaded optical modulators are required for phase encoding, pulse carving and label impressing [19, 20], an arrangement that is extremely costly and difficult to manage due to the size and the electronic components required in each modulator. In addition, the heritage loss is usually so high that two EDFAs will be needed in the transmitting end.

In this paper, we propose a simple and elegant method to generate ASK/CSRZ-DPSK signal which only needs one dual-drive Mach-Zehnder modulator (DD-MZM). Similar schemes producing CSRZ-DPSK signal with one DD-MZM can be found in [23, 24]. We theoretically study and compare the performance differences between these two schemes with 40 Gbps CSRZ-DPSK payload and 1.25 Gbps ASK label over 120 km standard single mode fiber (SSMF) transmission. It is found that, under our new scheme, the receiver sensitivities of the label signal is 2 dB better, while the payload is only 0.2 dB worse than the previous scheme after 120 km standard single mode fiber (SSMF) transmission.

4.4.2 Concept

Figure 4.10 shows the principle of the proposed scheme. The label signal is first modulated onto a half payload data rate clock. Then the precoded payload and label are synchronously combined and sent into the DD-MZM, with one arm of label signal being inverted. The output electric field E_{out} can be written as [25]:

$$\begin{aligned}
 E_{out} &= \frac{E_{in}}{\alpha^{1/2}} e^{j\left(\frac{V_1+V_2}{2V_\pi}\pi\right)} \cos\left(\frac{V_1-V_2}{2V_\pi}\pi\right) \\
 &= \frac{E_{in}}{\alpha^{1/2}} e^{j\pi d_p(t)} \cos\left(\frac{1}{2}\pi d_L(t) \cos(2\pi f_c t) + \frac{\pi}{2}\right)
 \end{aligned} \tag{4-2}$$

where α and V_π are the power loss and the switching voltage of the modulator. $V_1 = V_\pi d_p(t) + 0.5V_\pi d_L(t) \cos(2\pi f_c t) + V_{b1}$ and $V_2 = V_\pi d_p(t) - 0.5V_\pi d_L(t) \cos(2\pi f_c t) + V_{b2}$ are voltages employed on the two electrode arms. $d_L(t) = \{x, 1\}$ is the label signal which modulates the clock with a frequency of $f_c = B/2$, where “x” is the electrical level representing label bit “0” range between (0, 1) depending on the required optimized extinction ratio of the label. Bias voltages on the two arms V_{b1} and V_{b2} are $+V_\pi/2$ and $-V_\pi/2$, respectively, which bias the MZM at the null point of transmission curve. The first term of E_{out} contains the phase information encoded by the payload and the second term carves the payload into pulses with the label modulated clock. Thus the MZM output will contain CSRZ-DPSK payload with impressed ASK label. Notably, in practice, the ‘+’ in Fig. 4.10 can be realized using a linear RF combiner/coupler, and the ‘-1’ can be implemented using a π -phase shifter. Since the pulse carving clock is amplitude modulated, the output pulses of the payload will have label dependent duty-cycle. Thus the spectrum of the payload will be label dependent, which might introduce label interference to the payload after narrow band filtering. However, a simple adjustment of the eraser extinction ratio (ER) can easily alleviate the label interference effect with minimum impact on the system performance.

4.4.3 Numerical Results

To demonstrate the feasibility of the proposed scheme, a transmission link is established as shown in Fig. 4.11, which contains three main parts: payload/label transmitter, transmission fiber, and payload/label receiver. A 40 Gbps CSRZ-DPSK payload with 1.25 Gbps label is generated and transmitted with input power of 1.7 dBm over 120 km SSMF with fiber loss of 0.2 dB/km, dispersion parameter of $D=16$ ps/(nm)(km) and nonlinear coefficient $\gamma = 1.314$ (1/W.Km). The signal is then amplified using the inline erbium doped fiber amplifier (EDFA) with 20 dB gain and 5 dB noise figure and the SSMF dispersion is fully compensated by the following dispersion compensating fiber (DCF) in a post compensation scheme. At the receiving end, the signal is optically amplified by an EDFA with 30 dB gain and 5 dB noise figure and then passes through a 2nd order Gaussian filter with a 3 dB bandwidth of 2.4 nm. It is then split into two branches for payload and label extraction. In the upper branch, the ASK label is erased by an electro-absorption (EA) modulator. As suggested in [19], the transmitted label is inverted and directly fed into the remote label erasure to focus on new scheme performance. A delay-interferometer is used to demodulate the CSRZ-DPSK payload and detected by a balanced-photodiode. The 4th order Bessel electrical filter with a 3 dB bandwidth of 30 GHz is used to eliminate the residual noise. In the lower branch, the signal is directly fed into a photodiode and goes through a low pass 4th order Bessel filter with a 3 dB bandwidth of 1 GHz to extract the label information. For comparison, we also simulated previous proposed scheme [19, 20] with the same system parameters as our new scheme.

The performance evaluation was conducted using a commercial simulation tool, VPItransmissionMaker 5.0. Both the input payload and label data are rectangular pulse, and the sequence used is the pseudorandom binary sequence (PRBS) patterns with length $2^{11}-1$. The simulation time window is set to 1.64 us which allow sufficient bit number of label and payload (≥ 2048) for more accurate estimation of bit error rate (BER). BER is calculated using the Gaussian detection statistics for both payload and label [21].

The right-hand side inset in Fig. 4.11 shows the optical spectra of ASK/CSRZ-DPSK signals using the conventional and proposed schemes. No difference is apparent between these two schemes except that the new scheme has a slightly broader main lobe. This may result from the reduced duty-cycle of the pulses impressed by label bit “0”.

Fig. 4.12 shows the back to back receiver sensitivities of the payload and label as a function of the label extinction ratio at bit error ratio (BER) equals to 10^{-12} . As expected, tradeoff between the extinction ratio requirements for the label and payload are observed. In the previous scheme [19], the duty cycle of CSRZ-DPSK is fixed, and thus the eraser can simply use the inverted label signal to remove the label. In the proposed scheme, the payload spectrum comprises two spectra from pulses with different duty-cycles, corresponding to the impressed label bits “one” and “zero”. The two spectra produce different filtering effect following a narrow band electrical filter and thus lead to label interference with payload detection. Fig. 4.13 shows that, without optimization, electrical filtering produces a multilevel eye diagram. However, with a slightly larger ER (3.6 dB, if the original ER of the label is 3 dB) in the eraser, a single level eye diagram at the decision point can be obtained after optimization. Conventionally, because the label carries routing information and is necessitated to have better sensitivity than the payload [26], we choose the label extinction ratio equals to 3 dB in both schemes for fair comparison. Bit error ratios of the labels are shown in Fig. 4.14. The inset shows the transmitted label patterns before and after filtering with 1 GHz electrical low pass filter. Compared these two schemes, the new scheme has 2 dB better label performance owing to the smaller duty cycle of the payload, indicating a larger distance between the mark and space levels [27]. Additionally, the narrower pulses (space) are filtered out more power than the broader pulses (mark), thus enlarging the ER of the label after narrow band electrical filtering. Fig. 4.15 shows the BER results of the payload. In both back-to-back and after 120 km SSMF transmission, the sensitivities of the optimized payload at $\text{BER}=10^{-12}$ are only 0.2 dB worse than the previous scheme. These results clearly indicate

that the new scheme has better label sensitivity, which is crucial in packet switching network; almost the same payload performance and much lower cost since only single modulator is needed.

4.4.4 Summary

We propose a novel scheme which generates ASK/CSRZ-DPSK signals using only one DD-MZM. By synchronously combining the payload data with the pulse carving clock modulated by label, the new method is much simpler and more cost-effective because only a single modulator and no EDFA is required. Performance of the novel scheme is studied and investigated theoretically. We setup a transmission link with 40 Gbps CSRZ-DPSK payload impressed by 1.25 Gbps ASK label over 120 km SSMF. It is found that the label is 2 dB better than the previous scheme and the payload has only 0.2 dB worse sensitivity at $BER=10^{-12}$.

4.5 Quantum Limit of Optimum Four-Level ASK Signals with Direct Detection Optically Pre-amplified Receivers

4.5.1 Introduction

With the rapid growth of Internet traffic congestion, efficiently using signal bandwidth is essential to increase the transmission capacity over already installed optical fibers and amplifiers. Multilevel amplitude-shifted-keying (ASK) format such as 4ASK has recently attracted much attention because it offers an increased spectral efficiency at a reduced symbol rate without too complex transmitting and receiving ends [28-32]. Benefited from the reduced symbol rate, the tolerances to chromatic dispersion (CD) and polarization mode dispersion (PMD) are enhanced compared to traditional binary format [28, 30, 32]. In addition, the logic circuit at both the transmitter and receiver can be operated with half the bit-rate speed, thus lowering the electronic cost [32]. One interesting problem of 4ASK format is the level

spacing with an optically pre-amplified receiver, which is directly related to the bit error rate of the system. Extensive works based on the optimum level spacing have been studied [28, 33, 34]. In these papers, the noises are all simplified as Gaussian distribution to pursue the optimum level spacing and the corresponding bit error rate. Unfortunately, the accuracy and the appropriateness of Gaussian approximation to the optimum level spacing and the bit error rate have not been confirmed yet. Although the Gaussian approximation is good for calculating bit error rate in binary format, there has no report regarding the Gaussian method in predicting the optimum level in 4ASK format. An exact analysis to 4ASK will be necessary since establishing accurate estimates of the performance can yield useful insights in practical system design. Recently, the exact performance of 4ASK transmission systems was explored by using Karhunen–Loeve series expansion (KLSE) and saddle point approximation method, which generally speaking is semi-analytical and not explicit [32]. With this method, the optimum multilevel spacing of the 4ASK is achieved by scanning the middle two energy levels for each pair of optical and electrical bandwidth to get the minimum bit error rate. They also provide the optimum receiving sensitivity, which is generally called quantum limit [35], by KLSE method. However, searching the optimum multilevel spacing and threshold levels by scanning each parameter to achieve the minimum error rate would be very time consuming. Therefore, an explicit and rigorous expression for the bit error rate, which has never been investigated to the authors' knowledge, is required since it provides fast computing and gives a direct relation between the system inputs and the overall performance. In this paper, we give an exact formula of bit error rate for an optical 4ASK format with optimum level spacing using an optically pre-amplified receiver. This formula is derived under the assumption that an ideal optical filter and an integrate and dump circuit are used at the receiver. The quantum limit for a 4ASK signal is derived as 127.5 photons/bit, considering the Chi-squared distribution of each level. The exact bit error rates and optimum level spacing are compared to those evaluated by Gaussian approximation. We conclude that the Gaussian method not only

give a good evaluation to the bit error rate but also the optimum level spacing for a 4ASK format, although the three optimum decision thresholds are all underestimated. We further confirm that the inter-symbol interference (ISI) considered Gaussian approximation used for binary format [36] would still works for a practical 4ASK format when suffered by ISI.

4.5.2 The Optimum Level and Quantum Limit for 4ASK

We firstly consider the error probability formula of a receiver consisting of an ideal optical filter, a square law detector and an electrical integrate and dump circuit, and then the quantum limit will be the specific case of this formula. We assume that the ASE is the dominant noise and ignore the other noises. The baseband envelope of the transmitter output can be written as:

$$s(t) = \left\{ \sum_k a_k p(t - kT) \right\} \quad (4-3)$$

where T is the symbol duration, $a_k \in \{ \sqrt{E_y}, y = 0, 1, 2, 3 \}$ with $\sqrt{E_0} = 0 < \sqrt{E_1} < \sqrt{E_2} < \sqrt{E_3}$ is the modulated amplitude corresponding to the k_{th} symbol, $p(t)$ is the pulse shape satisfying $\int_{-T/2}^{T/2} p^2(t) dt = 1$, and thus $E_y = \int_{-T/2}^{T/2} s^2(t) dt$ represents the symbol energy. For each symbol, the signal $s(t)$ and the filtered noise $n(t)$ can be modeled by orthonormal functions $\phi_i(t)$ over the pulse interval T [37-39]: $s(t) = \sum_{i=1}^{2M} s_i \phi_i(t)$ with energy of $\sum_{i=1}^{2M} s_i^2 \in \{ E_0, E_1, E_2, E_3 \}$ and the filtered noise $n(t) = \sum_{i=1}^{2M} n_i \phi_i(t)$, where n_i 's are independent Gaussian random variables with mean and variance of 0 and $N_0/2$, respectively. $M = BT$ is proportional to the optical bandwidth B . After the electrical integrate and dump circuit, the probability density function (pdf) of the decision variable χ with symbol energy of $E_{y=1,2,3} > 0$ is [37-39]:

$$f_{S_y}(\chi) = \left(\frac{\chi}{S_y}\right)^{(M-1)/2} \exp(-\chi - S_y) I_{M-1}(2\sqrt{\chi S_y}) \quad (4-4)$$

and that with symbol energy of $E_0 = 0$ is :

$$f_{S_0}(\chi) = \frac{\chi^{M-1} e^{-\chi}}{(M-1)!} \quad (4-5)$$

where the decision random variable χ has been normalized to the noise level N_0 and $S_y = E_y / N_0$ is the normalized symbol energy. Assuming that Gray coding is used, the symbol error rate $P(e | S_i)$ for each symbol S_i can be written as :

$$P(e | S_0) = e^{-\gamma_1} \sum_{n=0}^{M-1} \frac{1}{n!} \gamma_1^n$$

$$P(e | S_i) = 1 - Q_M(\sqrt{2S_i}, \sqrt{2\gamma_i}) + Q_M(\sqrt{2S_i}, \sqrt{2\gamma_{i+1}}) \quad , \text{ for } i = 1, 2 \quad (4-6)$$

$$P(e | S_3) = 1 - Q_M(\sqrt{2S_3}, \sqrt{2\gamma_3})$$

where γ_i is the threshold normalized to the noise level N_0 ,

$Q_M(a, b) = \int_b^{\infty} \frac{x^M}{a^{M-1}} \exp(-(x^2 + a^2)/2) I_{M-1}(ax) dx$ is the Marcum's Q function, and I_M is the modified

Bessel function of the first kind. The bit error rate (BER) is almost equal to half the averaged symbol error rate under a good signal to noise ratio [40, p. 503]:

$$P_e = \frac{1}{2} \left\{ \frac{1}{4} P(e | S_0) + \frac{1}{4} P(e | S_1) + \frac{1}{4} P(e | S_2) + \frac{1}{4} P(e | S_3) \right\} \quad (4-7)$$

Usually the levels of $S_0 = 0$ and S_3 are known and we only need to find the values of $S_{1,2}$ and $\gamma_1 \sim \gamma_3$ to minimize the error rate. The minimum error rate implies that the partial derivatives of P_e with respect to $S_{1,2}$ and $\gamma_1 \sim \gamma_3$ are all equal to zeros, which means:

$$\frac{\partial P_e}{\partial S_1} = \frac{\partial P_e}{\partial S_2} = \frac{\partial P_e}{\partial \gamma_1} = \frac{\partial P_e}{\partial \gamma_2} = \frac{\partial P_e}{\partial \gamma_3} = 0 \quad (4-8)$$

The derivatives with respect to the thresholds are known as the maximum-likelihood principle and those with respect to $S_{i=1,2}$ determine the optimum locations of the middle two levels

within the given thresholds (γ_i and γ_{i+1}). Using the two partial-derivative properties of Marcum's Q functions:

$$\frac{\partial Q_M(a, b)}{\partial b} = -\frac{b^M}{a^{M-1}} e^{-\frac{1}{2}(a^2+b^2)} I_{M-1}(ab) \quad (4-9)$$

$$\frac{\partial Q_M(a, b)}{\partial a} = \frac{b^M}{a^{M-1}} e^{-\frac{1}{2}(a^2+b^2)} I_M(ab) \quad (4-10)$$

where Eq. (4-10) can be easily proved with the two following equalities:

$$Q_M(a, b) = Q(a, b) + e^{-\frac{1}{2}(a^2+b^2)} \sum_{n=1-M}^{-1} \left(\frac{a}{b}\right)^n I_n(ab) \quad \text{and} \quad I_{-n}(ab) = I_n(ab).$$

Using Eq. (4-6)-(4-10), we can obtain the following five equalities:

$$\begin{aligned} \frac{\partial P_e}{\partial \gamma_1} = 0 &\Rightarrow e^{-\frac{a_1^2}{2}} I_{M-1}(a_1 b_1) * (M-1)! \left(\frac{a_1 b_1}{2}\right)^{(1-M)} = 1 \\ \frac{\partial P_e}{\partial S_1} = 0 &\Rightarrow \left(\frac{b_1}{b_2}\right)^M e^{-\frac{1}{2}(b_1^2-b_2^2)} \frac{I_M(a_1 b_1)}{I_M(a_1 b_2)} = 1 \\ \frac{\partial P_e}{\partial \gamma_2} = 0 &\Rightarrow \left(\frac{a_2}{a_1}\right)^{M-1} e^{-\frac{1}{2}(a_1^2-a_2^2)} \frac{I_{M-1}(a_1 b_2)}{I_{M-1}(a_2 b_2)} = 1 \\ \frac{\partial P_e}{\partial S_2} = 0 &\Rightarrow \left(\frac{b_2}{b_3}\right)^M e^{-\frac{1}{2}(b_2^2-b_3^2)} \frac{I_M(a_2 b_2)}{I_M(a_2 b_3)} = 1 \\ \frac{\partial P_e}{\partial \gamma_3} = 0 &\Rightarrow \left(\frac{a_3}{a_2}\right)^{M-1} e^{-\frac{1}{2}(a_2^2-a_3^2)} \frac{I_{M-1}(a_2 b_3)}{I_{M-1}(a_3 b_3)} = 1 \end{aligned} \quad (4-11)$$

where $a_i = \sqrt{2S_i}$ and $b_i = \sqrt{2\gamma_i}$. With Eq. (4-11), we can uniquely obtain the middle two levels $S_{1,2}$ and the thresholds $\gamma_1 \sim \gamma_3$. Note that to avoid the overflow of the modified Bessel function, the exponential term should be shifted into the integrand of the integral formula of the modified Bessel function. An alternative method avoiding over- and underflow problems is to put these derivatives in the moment generating function (MGF) domain using the method similar to that described in [41].

Although Eq. (4-7) is for ideal optical filter and electrical integration circuit, it is with the same form as that of an optical matched filter $h(t) = p^*(T-t)$ when $M = 1$ [37, 42]. For the matched filter, the normalized multilevel spacing and the optimum decision thresholds under

a high signal to noise ratio ($SNR = E_b / N_0 = 1/8 * \sum_{i=0}^3 S_i$, where E_b is the averaged energy per bit) can be easily solved as $(L_0, r_1, L_1, r_2, L_2, r_3, L_3) = (0, 1/36, 1/9, 1/4, 4/9, 25/36, 1)$, where $L_i = S_i / S_3$ and $r_i = (\gamma_i - M) / S_3$. For here the crude approximation $I_0(x) \approx e^x$ and the assumption of $f_{S_0}(\gamma_1) = f_{S_1}(\gamma_1) = f_{S_1}(\gamma_2) = f_{S_2}(\gamma_2) = f_{S_2}(\gamma_3) = f_{S_3}(\gamma_3)$ are used. Note that the squared roots of the asymptotic optimum levels and thresholds are equally spaced as $(\sqrt{L_0}, \sqrt{r_1}, \sqrt{L_1}, \sqrt{r_2}, \sqrt{L_2}, \sqrt{r_3}, \sqrt{L_3}) = (0/6, 1/6, 2/6, 3/6, 4/6, 5/6, 6/6)$.

The minimum bit error rate and the optimum multilevel spacing can also be approximated by using the Gaussian method. The means and variances of the random variable χ for each symbol are $\mu_i = M + S_i$ and $\sigma_i^2 = M + 2S_i$, respectively [37]. The optimized multilevel spacing can be derived by equalizing the Q_i factors defined as $Q_i = (\mu_i - \mu_{i-1}) / (\sigma_i + \sigma_{i-1})$ of the three eyes. The optimum thresholds of the three eyes are located at $\gamma_i = (\mu_{i-1}\sigma_i + \mu_i\sigma_{i-1}) / (\sigma_i + \sigma_{i-1})$. The BER with Gaussian method is written as :

$$Pe = \frac{1}{8} \sum_{i=1}^3 \text{erfc} \left(\frac{Q_i}{\sqrt{2}} \right) = \frac{3}{8} \text{erfc} \left(\frac{Q}{\sqrt{2}} \right) \quad (4-12)$$

where $Q_1 = Q_2 = Q_3 = Q$. Note that each symbol carries two bits.

4.5.3 Numerical Results

For the results shown here we only consider the ASE noise with the same polarization as the signal. The ASE orthogonal to signal can be easily included by doubling the value of M [37, 38]. The BER versus the photons/bit are presented in Fig. 4.16 with $M = 1, 10, 30, 50$, where the photons/bit relates to SNR as photons/bit = $SNR = E_b / N_0$ [43]. The BER approximated by Gaussian scheme only slightly overestimate those of exact solutions. For various optical bandwidths M, the sensitivity differences between the chi-squared and Gaussian distributions are less than 0.2 dB. For the optical matched filter, ie: $M = 1$, the photons/bit and SNR

required to achieve a BER of 10^{-9} is about 127.5 and 21 dB, respectively, and this figures out the best performance that 4ASK format can reach under the optimum multilevel spacing. Figure 4.17(a)-(d) shows the relation between SNR and optimum levels L_i and the thresholds r_i for various optical bandwidths M . The optimum levels and the thresholds are descending as SNR increases. For poor SNR and broader optical bandwidth M , the noise is less dependent to the signal and the optimum levels are closer to be equally spaced. For high SNR and narrower optical bandwidth, the signal dependent noise dominants and the levels and the thresholds will approach the asymptotic values $(L_0, L_1, L_2, L_3, r_1, r_2, r_3) = (0, 1/9, 4/9, 1, 1/36, 1/4, 25/36)$. Figure 4.17(e) shows the optimum spacing and thresholds at a BER of 10^{-9} as a function of M . The optimum multilevel spacing predicted by Gaussian method is quite close to those by exact solution over a broad range of SNR and M while the decision thresholds are slightly underestimated.

Figure 4.18 shows the relation between the optical bandwidth M and the required photons/bit (SNR) at a BER of 10^{-9} . The results of binary format, which we have reviewed from [37], are also shown for comparison. The worse performance for 4ASK has been explained and described in [28]. In both the cases of binary and quaternary formats, the SNR are overestimated by the Gaussian approximation for a broad range of M from 1 to 100. The results from Gaussian method are more accurate as M becomes larger in both formats due to the central limit theorem when M approaches infinity. We also found that the quaternary format is not that sensitive to the bandwidth of optical filter, M . Since the variance of χ for each symbol is $\sigma_i^2 = M + 2S_i$, the quaternary format with higher SNR dominating the variance will behave more insensitive to M . This leads to the result that the gain of binary format over quaternary varies from 5.2 to 3.5 dB as M increases from $M = 1$ to 100. The gain ~ 5 dB of binary format described in previous reports [28, 43] comes from the result of using an optical

filter.

In Fig. 4.19 we show the BER for the return-to zero 4ASK (RZ-4ASK) format considering the ISI effect. The data rate is operated at 20Gbps. The exact BER, which is calculated by the Karhunen-Loeve based method [44], is compared to that of the Gaussian approximation [28, 36]. The receiver uses a 2nd order optical Gaussian band-pass and 5th order electrical Bessel low-pass filters. The 3-dB bandwidths (BW) of optical and electrical filters are 25 and 7 GHz, respectively. The results show that the BER calculated by the exact and Gaussian methods are with a difference of less than 0.2 dB in both the cases of back to back (b2b) and after 30 km standard single mode fiber (SSMF) transmission. This confirms the accuracy of using the Gaussian method for the 4 ASK signal when the ISI exists.

4.5.4 Summary

We have evaluated the exact optimum multilevel spacing and the corresponding bit error rate for the 4-level amplitude-shift keying format in presence of optical pre-amplified direct-detection receiver, and compared these results with Gaussian approximation. The quantum limit is 127.5 photons/bit considering the exact noise characteristic on each level. We have found that with the Gaussian method, the optimum multilevel spacing and the bit error rate can be well predicted and approximated while the thresholds are all underestimated. The accuracy for evaluating the optimum levels and bit error rate also implies that the ISI-considered Gaussian approximation would still works for a practical 4ASK format with arbitrary optical and electrical filters. In addition, we point out that the 4ASK format is more insensitive to the optical bandwidth and the previously proposed ~5.2-dB gain of binary over quaternary format comes from a narrowband optical filter. Note that the method in this paper for the optimum symbol spacing can also be used in other advanced modulation format such as 8ASK, 8ADPSK or 16ADQPSK [45], in which the time-consuming scanning method

would be inefficient.

4.6 Improvement of Dispersion and Optical Filtering Tolerances for Quaternary Intensity Detection Using Phase Modulation and Balanced Detection Technique

4.6.1 Introduction

Multilevel amplitude-shifted-keying (ASK) format such as 4ASK has recently attracted much attention because it offers an increased spectral efficiency at a reduced symbol rate without complex transmitting and receiving ends [46-50]. Benefited from the reduced symbol rate, the tolerances to chromatic dispersion (CD) and polarization mode dispersion (PMD) are enhanced compared to traditional binary format [46-50]. In addition, the logic circuit at both the transmitter and receiver can be operated with half the bit-rate speed, thus lowering the electronic cost [50]. The optimum level spacing of 4ASK in the presence of optical preamplifier has been proved unequally spaced as around 0: 1: 4: 9 [46, 50], for which a practical generation method will be described in this paper. The quantum limit of 4ASK with this optimum level spacing is about 5.7 dB better than that with equal level spacing. However, the smaller aperture of the lower eye with this optimum level is vulnerable to the signal distortions such as dispersions, optical filtering effect, and fiber nonlinearities, thus degrading the overall performance.

In this paper, we propose an alternative generation scheme for 4ASK by phase modulation and balanced-detection technique, which will be referred to as phase modulated 4ASK (PM4ASK) format. With a delay-interferometer and one set of balanced detector, the phase modulated signal can be converted to an equally spaced four-level signal and the dominant signal-ASE beat noise will be uniformly distributed onto each electrical level. The demodulated eyes with equal apertures can averagely bear the signal distortions and maintain

the receiving performance. We base our investigations on CD, PMD and optical filtering effect and use a Karhunen-Loeve based semi-analytical method for bit error rate (BER) calculation [51], accounting for optical noise in front of the receiver. The optical and electrical receiver bandwidths are optimized for the lowest BER in the back to back (b2b) case. The results are compared to the conventional 4ASK for both NRZ and RZ impulse shaping at a bit rate of 20 Gbps.

4.6.2 Generation of 4ASK and PM4ASK

In this section we describe the modulation and demodulation of the conventional 4ASK and the proposed PM4ASK formats. The conventional 4ASK transmitter is depicted in Fig. 4.20(a), which is a simple and direct method basically following the principle in [52]. A continuous wave (CW) is modulated by an IQ modulator consisted of two parallel Mach-Zehnder modulators (MZM1 and MZM2, shown in the figure). The first modulator MZM1 is biased at $v_{\pi}/2$ and driven by data1 electrical signal with peak to peak amplitude (V_{pp}) of V_{π} . For here v_{π} is the switching voltage of each MZM. The second modulator MZM2 is biased at $5v_{\pi}/6$ and driven by data2 electrical signal with V_{pp} of $v_{\pi}/3$. The two optical fields are summed in phase to get the optimum level 4ASK, for which the optical constellation diagram with a symbol distance of 'a' is shown in the inset. The following pulse carver is an option for RZ impulse shaping. A photodiode can directly convert the optical signal into electrical signal which is then detected by a four-level electrical decision circuit which has been described in [46, 48]. The optical spectra of the 4ASK in NRZ and RZ formats are shown in the insets. Just like the binary on-off keying format, a strong optical carrier for 4ASK can be observed in the center of the spectra. The four-level electrical eyes with and without ASE noises are also shown in the inset in which we can see the dominant signal-ASE beat noise is getting larger for higher signal levels.

For PM4ASK format as depicted in Fig. 4.20(b), the transmitter is basically the same as

the 4ASK. The difference is that the two MZMs are now biased at the minimum points to generate two independent DPSK signals. The driving signals of data1 and data2 are with $V_{pp} = 2V_{\pi}$ and V_{π} for MZM1 and MZM2, respectively. The two optical fields are then summed with one branch phase shifted by $\pi/2$. The output field can be modeled as $E_{PM} = b \cdot d_1(t) + j c \cdot d_2(t)$, where the amplitude ratio of the optical field $b: c = \sqrt{2}: 1$ and $d_1, d_2 = \{-1, 1\}$ are the bipolar data information. The generated signal is phase modulated and with the constellation points shown in the inset. A narrowband optical filter or a delay-interferometer (DI) with one symbol delay of $T_s = 1/R_s$, where R_s is the symbol rate, can be used to convert this phase modulated signal into a 4ASK signal immediately, which is similar to the conversion from DPSK to duobinary format [53]. However, the DI allocated before the receiver is suggested by virtue of the constant power transmission and balanced detection. The output current after the balanced detector is proportional to $\text{Re}[E_{PM}(t)E_{PM}^*(t - T_s)] = 2c^2 d_1(t)d_1(t - T_s) + c^2 d_2(t)d_2(t - T_s)$ and thus the four equally spaced levels are produced. The insets show the optical spectra of the PM4ASK in NRZ and RZ formats. The bandwidth is the same as that of 4ASK but there is no carrier frequency observed because of phase modulation. The demodulated signal with optical noise is also shown in the inset, in which the noises are equally distributed onto each level, which is different from the conventional 4ASK.

4.6.3 Performance Bound, Dispersion and Optical Filtering Tolerances

In this section we study the performance bound and the CD, PMD and optical filtering tolerances of 4ASK and PM4ASK. The considered bit rate is 20 Gbps. Because we consider a linear system, a higher bit rate will still result in similar conclusions. For 4ASK the optimum level spacing of around 0: 1: 4: 9 is used with the middle two levels slightly tuned for best b2b performance. For PM4ASK the ratio of $a/b = \sqrt{2}$ is used for equalized eyes and optimum b2b performance. For both 4ASK and PM4ASK the receiver uses a 2nd order optical Gaussian

band-pass and 5th order electrical Bessel low-pass filters. The 3 dB bandwidths (BW) of optical ($f_{3dB,opt}$) and electrical ($f_{3dB,el}$) filters have been optimized to reach the lowest BER in b2b case, as shown in Table 4.1.

To validate our simulation results, Fig. 4.21(a) shows the BER versus SNR for RZ-4ASK and RZ-PM4ASK formats in both Monte Carlo (MC) error counting and Karhunen-Loeve (KL) based methods. The SNR is the signal to noise ratio and is defined as $Pr/(4*No*Rs)$, where Pr is the received optical power and No is the noise power spectra density per polarization. In this paper, the ASE of both two polarizations is considered for a real world system. The MC method shows excellent agreement with the KL calculations, thus validating the semi-analytical model for both formats. The ASE-limited performance bound in terms of BER versus SNR for both the matched filter (quantum limit case, QL) and the optimum practical filter is shown in Fig. 4.21(b). We can observe that the b2b receiving sensitivity of PM4ASK is worse than that of 4ASK for both NRZ and RZ formats. This can be explained as follows: for an averaged received optical power Pr and photodiode responsivity Rp , the distance of the farthest two symbols in the electrical domain for 4ASK is $18PrRp/7$ which is larger than $2PrRp$ for PM4ASK. The sensitivity penalties of PM4ASK for NRZ and RZ formats are about 0.7 and 0.6 dB, respectively, with respect to 4ASK.

In Fig. 4.22(a) and (b) we show CD and PMD tolerances for 4ASK and PM4ASK. For PMD we consider the first order PMD similar to [54]. The CD and PMD are measured in terms of the residual dispersion R_d and differential group delay (DGD) τ . Over the various formats, the NRZ-PM4ASK is mostly vulnerable to CD and RZ-PM4ASK is with the best tolerance to CD. The RZ impulse shaping is traditionally considered as with a broader bandwidth and more vulnerable to CD compared to NRZ. However, it has been proven in many reports that the RZ is more robust to few amounts of residual CD for multilevel (>2) phase signaling formats [54-55]. In PMD the RZ format apparently performs better than NRZ for both 4ASK and PM4ASK formats. For the PMD alone, there is almost no difference

between 4ASK and PM4ASK. The tolerances to CD and PMD for 3-dB SNR penalties with respect to the b2b values are given in Table 4.1.

Figure 4.23 depicts the PMD tolerance with residual CD of 255 and 510 ps/nm for 4ASK and PM4ASK in RZ impulse shaping. When the CD kicks in, the tolerance to the PMD for the 4ASK and PM4ASK is very different. The 3-dB SNR penalties of the PMD tolerance with the two residual CD values are shown in Table 4.1. With 255 ps/nm of CD, the PMD tolerance for PM4ASK is almost the same as that with zero CD. While in the case for 4ASK, the PMD tolerance for 4ASK is degraded with nonzero CD. Further with 510 ps/nm of CD, the 3-dB PMD tolerance for PM4ASK still 9 ps outperforms that for 4ASK. In Fig. 4.24 we show the optical filtering effect for RZ-4ASK and RZ-PM4ASK formats. To fairly compare their tolerance to the optical filtering, we set the 3-dB electrical filter bandwidth at 8 GHz for both formats and evaluate their performances with different values of optical bandwidth. The results indicate that the performance of RZ-PM4ASK surpasses that of RZ-4ASK at the optical bandwidth of around 17.2 GHz. The new format also shows better tolerance to the optical filtering effect, which would make the PM4ASK format more suitable for the DWDM application.

The reason for the better tolerance to the dispersions and optical filtering for PM4ASK comes from the equalized eyes after demodulation. The lower eye for 4ASK is with the smaller aperture compared to the upper eyes, which makes it very sensitive to the signal distortions. The overall performance will be dominated by the lower strongly distorted eye. On the other hand, the PM4ASK is with the eyes of equal apertures, the contribution of any signal distortion can be equally distributed onto each level and the distortion would be partially cancelled by the balanced detection technique. The similar behavior is also observed in NRZ impulse shaping. In a real world the transmitted signal often suffers from the distortions such as residual CD, PMD and optical filtering, the PM4ASK would be an alternative choice for the conventional 4ASK.

4.6.4 Summary

We provide a new PM4ASK format employing phase modulation with balanced-detection scheme. We compare its CD, PMD and optical filtering tolerances to those of conventional 4ASK. It turns out that the CD, PMD and optical filtering tolerances are enhanced by PM4ASK in RZ format although the b2b receiving sensitivity is about 0.6 dB worse than 4ASK. In addition, the PM4ASK is with the potential of combating with fiber nonlinearity due to the constant power transmission.



Reference

- [1] R. A. Griffin and A. C. Carter, "Optical differential quadrature phase-shift keying (oDQPSK) for high capacity optical transmission," OFC'02, paper WX6.
- [2] M. Rohde, C. Caspar, N. Heimes, M. Konitzer, E. J. Bachus, and N. Hanik, "Robustness of DPSK direct detection transmission format in standard fiber WDM systems," *Electron. Lett.*, vol. 36, no. 17, pp. 1483-1484, Aug. 2000.
- [3] C. Wree, J. Leibrich, and W. Rosenkranz, "RZ-DQPSK format with high spectral efficiency and high robustness towards fiber nonlinearities," in *Proc. ECOC'02*, 2002, paper 9.6.6.
- [4] M. Ohm, and T. Freckmann, "Comparison of different DQPSK Transmitters with NRZ and RZ impulse shaping," *LEOS'04*, paper ThB2.
- [5] K. P. Ho, and H. W. Cui, "Generation of arbitrary quadrature signals using one dual-drive modulator," *J. Lightwave Technol.*, vol. 23, no. 2, Feb, pp. 764-770, 2005.
- [6] P. J. Winzer, C. Dorrer, R. J. Essiambre, and I Kang, "Chirped return-to-zero modulation by imbalanced pulse carver driving signals," *IEEE Photon. Technol. Lett.*, vol. 16, pp. 1379-1381, May 2004.
- [7] T. Miyazaki and F. Kubota, "Superposition of DQPSK over inverse-RZ for 3-bit/symbol modulation-demodulation," *IEEE Photon. Technol. Lett.*, vol. 16, pp. 2643-2645, Dec. 2004.
- [8] H. Kim and P. J. Winzer, "Robustness to laser frequency offset in direct-detection DPSK and DQPSK systems," *J. Lightwave Technol.*, vol. 21, pp. 1887-1891, Sept. 2003.
- [9] M. Pauer, P. J. Winzer, and W. R. Leeb, "Bit error probability reduction in direct detection optical receivers using RZ coding," *J. Lightwave Technol.*, vol. 19, pp. 1255-1262, Sept. 2001.
- [10] C. Wree et al., OFC'03, paper ThE5.

- [11] R. A. Griffin and A. C. Carter, "Optical differential quadrature phase-shift keying (oDQPSK) for high capacity optical transmission," OFC'02, Paper WX6
- [12] C. Wree, J. Leibrich, and W. Rosenkranz, "RZ-DQPSK format with high spectral efficiency and high robustness towards fiber nonlinearities," in Proc. ECOC'02, 2002, Paper 9.6.6.
- [13] M. Ohm, and T. Freckmann, "Comparison of different DQPSK Transmitters with NRZ and RZ impulse shaping," LEOS'04, paper ThB2.
- [14] K. P. Ho, and H. W. Cui, "Generation of arbitrary quadrature signals using one dual-drive modulator," J. Lightwave Technol., vol. 23, no. 2, Feb, pp. 764-770, 2005.
- [15] G. Bosco, and P. Poggiolini, "The impact of receiver imperfections on the performance of optical direct-detection DPSK," J. Lightwave Technol., vol. 23, pp.842-848, 2005.
- [16] K. P. Ho, and J. M. Kahn, "Spectrum of externally modulated optical signals," J. Lightwave Technol., vol. 22, pp.658-663, 2004.
- [17] M. Pauer, P. J. Winzer, and W. R. Leeb, "Bit error probability reduction in direct detection optical receivers using RZ coding," J. Lightwave Technol., vol. 19, pp. 1255-1262, Sept. 2001.
- [18] D. J. Blumenthal, A. Carena, L. Rau, V. Curri, and S. Humpries, "All-optical label swapping networks and technologies," *J. Lightwave Technol.*, vol. 18, pp. 2058-2075, Dec. 2000.
- [19] N. Chi, C. Mikkelsen, L. Xu, J. Zhang, P. V. Holm-Nielsen, H. Ou, J. Seoane, C. Peucheret, and P. Jeppesen, "Transmission and label encoding/erasure of orthogonally labeled signal using 40Gb/s RZ-DPSK payload and 2.5Gb/s IM label," *Electron. Lett.*, vol. 39, pp. 1335-1336, Sept. 2003.
- [20] X. Liu, X. Wei, Y. Su, J. Leuthold, Y. H. Kao, I. Kang, and R. C. Giles, "Transmission of an ASK-labeled RZ-DPSK signal and label erasure using a saturated

SOA,” *IEEE Photon. Technol. Lett.*, vol. 16, pp. 1594-1596, June 2004.

[21] G. Bosco, A. Carena, V. Curri, R. Gaudino, and P. Poggiolini, “Modulation formats suitable for ultrahigh spectral efficient WDM systems,” *IEEE J. Sel. Top. Quantum Electron.*, vol. 10, pp. 321-328, 2004.

[22] B. Zhu, L. E. Nelson, S. Stulz, A. H. Gnauck, C. Doerr, J. Leuthold, G. Nielsen, M. O. Pedersen, J. Kim and R. L. Lingle, Jr., “High spectral density long-haul 40-Gb/s transmission using CSRZ-DPSK format,” *J. Lightwave Technol.*, vol. 22, No. 1, pp. 208-214, Jan. 2004.

[23] Y. J. Wen, A. Nirmalathas, and D. S. Lee, “RZ/CSRZ-DPSK and chirped NRZ signal generation using a single-stage dual-electrode Mach-Zehnder modulator,” *IEEE Photon. Technol. Lett.*, vol. 16, pp. 2466-2468, Nov. 2004.

[24] D. S. Lee, M. S. Lee, Y. J. Wen, and A. Nirmalathas, “Electrically band-limited CSRZ-DPSK signal with a simple transmitter configuration and reduced linear crosstalk in high spectral efficiency DWDM systems,” *IEEE Photon. Technol. Lett.*, vol. 16, pp. 2135-2137, Sep. 2004.

[25] P. J. Winzer, C. Dorrer, R. J. Essiambre, and I. Kang, “Chirped return-to-zero modulation by imbalanced pulse carver driving signals,” *IEEE Photon. Technol. Lett.*, vol. 16, pp. 1379-1381, May 2004.

[26] N. Chi, J. Zhang, P. V. Holm-Nielsen, C. Peucheret, and P. Jeppesen, “Transmission and transparent wavelength conversion of an optically labeled signal using ASK/DPSK orthogonal modulation,” *IEEE Photon. Technol. Lett.*, vol. 15, pp. 760-762, May 2003.

[27] M. Pauer, P. J. Winter, W. R. Leeb, “Bit error probability reduction in direct detection optical receivers using RZ coding,” *J. Lightwave Technol.*, vol. 19, pp. 1255-1262, Sept. 2001.

- [28] S. Walklin, and J. Conradi, "Multilevel signaling for increasing the reach of 10Gbps lightwave systems," *J. Lightwave Technol.* 17, 2235 (1999).
- [29] S. K. Ibrahim, S. Bhandare, and R. Noe, "Narrowband 20-Gbps quaternary intensity modulation generated by duobinary 10-Gbps modulation in 2 quadratures," *ECOC 2005 Paper Th 2.6.5*.
- [30] S. K. Ibrahim, S. Bhandare, and R. Noe, "20-Gbps quaternary intensity modulation based on duobinary modulation with unequal amplitude in two polarizations," *IEEE Photon. Technol. Lett.* 14, 1482 (2006).
- [31] S. K. Ibrahim, S. Bhandare, and R. Noe, "Narrowband 2x10 Gbit/s Quaternary Intensity Modulation Based on Duobinary Modulation in Two Polarizations with Unequal Amplitudes," *OFC 2006 Paper OTh12*.
- [32] J. Zhao, L. Huo, C. K. Chan, L. K. Chen, and C. Lin, "Analytical investigation of optimization, performance bound, and chromatic dispersion tolerances of 4-amplitude-shifted keying format," *OFC 2006 Paper JThB15*.
- [33] J. Rebola and A. V. T. Cartaxo, "On the quaternary level spacing signaling optimization for increasing the transmission distance in optical communication systems," in *Proc. of ConfTele2001 3rd Conference on Telecommunications*, Figueira da Foz 23, 514 (2001).
- [34] N. Avlonitis, E. M. Yeatman, M. Jones, and A. Hadjifotiou, "Multilevel amplitude shift keying in dispersion uncompensated optical systems," *IEE Proc. Optoelectron.* 153, 101 (2006).
- [35] P. J. Winzer, "Optically preamplifier receiver with low quantum limit," *Electronics Lett.* 37, 582 (2001).
- [36] L. Ribeiro, J. Da Rocha, and J. Pinto, "Performance evaluation of EDFA preamplified receivers taking into account intersymbol interference," *J. Lightwave Technol.* 13, 225 (1995).

- [37] P. A. Humblet, and M. Azizoglu, "On the bit error rate of lightwave systems with optical amplifier," *J. Lightwave Technol.* 9, 1576 (1991).
- [38] D. Marcuse, "Derivation of analytical expressions for the bit-error probability in lightwave systems with optical amplifiers," *J. Lightwave Technol.* 8, 1816 (1990).
- [39] J. P. Gordon and L. F. Mollenauer, "Effects of Fiber Nonlinearities and Amplifier Spacing on Ultra-Long Distance Transmission," *J. Lightwave Technol.* 9, 170 (1991).
- [40] L. W. Couch, *Digital and Analog Communication Systems* (Upper Saddle River, N.J. :Prentice Hall, 2001).
- [41] C. W. Helstrom, "Computing the generalized Marcum Q-function," *IEEE Transactions on Information Theory* 38, 1422 (1992).
- [42] G. Bosco, A. Carena, V. Curri, R. Gaudino, and P. Poggiolini, "Quantum limit of direct-detection receivers using duobinary transmission," *IEEE Photon. Technol. Lett.* 15, 102 (2003).
- [43] J. M. Kahn, and K. P. Ho, "Spectral efficiency limits and modulation/detection techniques for DWDM systems," *IEEE J. Selected Topics in Quantum Electronics* 10, 259 (2004).
- [44] G. Bosco and P. Poggiolini, "The Impact of receiver imperfections on the performance of optical direct-detection DPSK," *J. Lightwave Technol.* 23, 842 (2005).
- [45] K., Sekine, N. Kikuchi, and S. Sasaki, "Modulation parameter tolerance for 8- and 16-APSK (amplitude- and phase-shift keying) signals," *OFC 2006 Paper JThB13*.
- [46] S. Walklin, and J. Conradi, "Multilevel signaling for increasing the reach of 10Gbps lightwave systems," *J. Lightwave Technol.*, vol. 17, pp. 2235-2248, Nov. 1999.
- [47] S. K. Ibrahim, S. Bhandare, and R. Noe, "Narrowband 20-Gbps quaternary intensity modulation generated by duobinary 10-Gbps modulation in 2 quadratures," *ECOC 2005, Paper Th 2.6.5*.

- [48] S. K. Ibrahim, S. Bhandare, and R. Noe, "20-Gbps quaternary intensity modulation based on duobinary modulation with unequal amplitude in two polarizations," *IEEE Photon. Technol. Lett.*, vol. 14, pp. 1482-1484, July 2006.
- [49] S. K. Ibrahim, S. Bhandare, and R. Noe, "Narrowband 2x10 Gbit/s Quaternary Intensity Modulation Based on Duobinary Modulation in Two Polarizations with Unequal Amplitudes," *OFC 2006*, Paper OThI2.
- [50] J. Zhao, L. Huo, C. K. Chan, L. K. Chen, C. Lin, "Analytical investigation of optimization, performance bound, and chromatic dispersion tolerances of 4-amplitude-shifted keying format," *OFC 2006*, Paper JThB15.
- [51] G. Bosco and P. Poggiolini, "The Impact of receiver imperfections on the performance of optical direct-detection DPSK," *J. Lightwave Technol.*, vol. 23, pp. 842-848, Feb. 2005.
- [52] N. Kikuchi, K. Sekine, and S. Sasaki, "Proposal of inter-symbol interference (ISI) suppression technique for optical multilevel signal generation," *ECOC2006*, Paper Tu4.2.1.
- [53] I. Lyubomirsky and C. C. Chien, "DPSK demodulator based on optical discriminator filter," *IEEE Photon. Technol. Lett.*, vol. 17, pp. 492-494, Feb., 2005.
- [54] J. Wang and J. M. Kahn, "Impact of chromatic and polarization mode dispersions on DPSK systems using interferometric demodulation and direct detection," *J. Lightwave Technol.*, vol. 22, pp. 362-371, Feb. 2004.
- [55] M. Ohm and J. Speidel, "Optimal receiver bandwidths, bit error probabilities and chromatic dispersion tolerance of 40 Gbps optical 8-DPSK with NRZ and RZ impulse shaping," *OFC2006*, Paper OFG5.

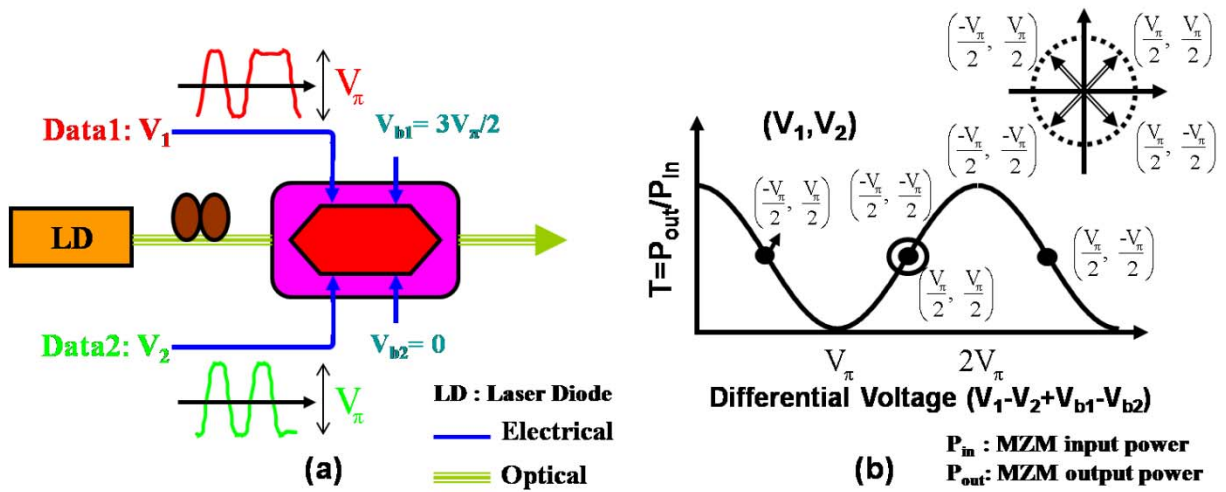


Fig. 4.1 (a) Principle of the generation of an optical DQPSK signal with a single MZM. (b) Symbol positions and the constellation diagram.

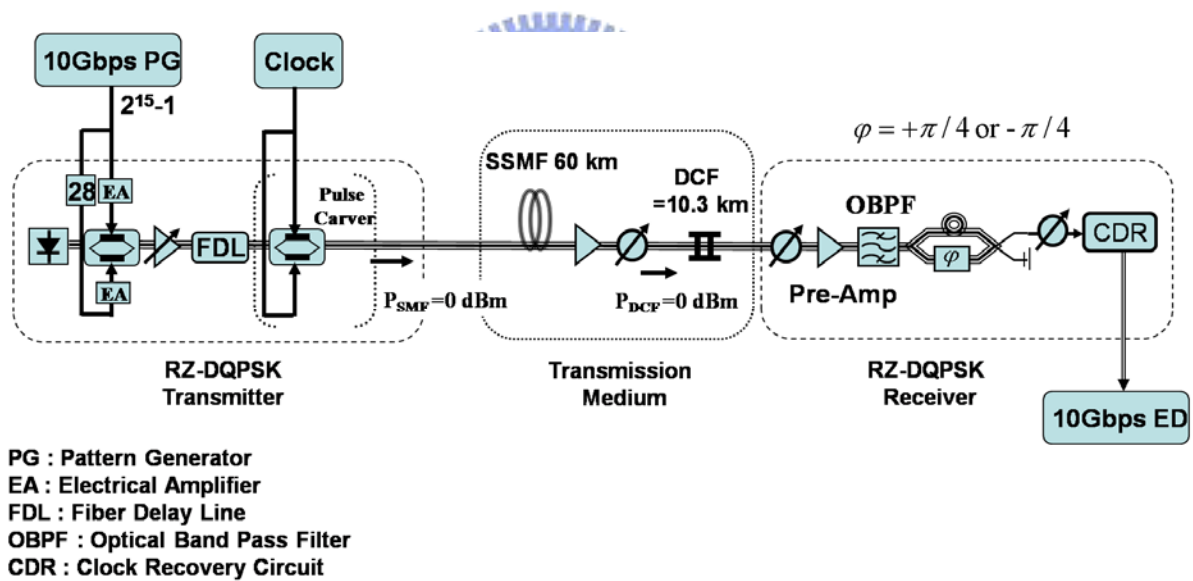


Fig. 4.2 Experimental setup.

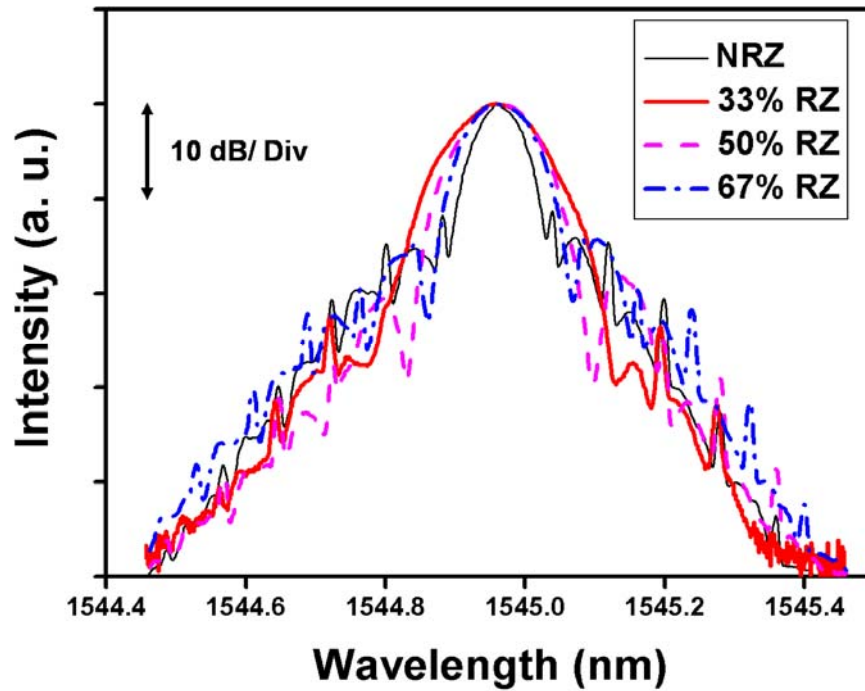


Fig. 4.3 Optical spectra of the generated NRZ, and RZ signals with different duty cycles.

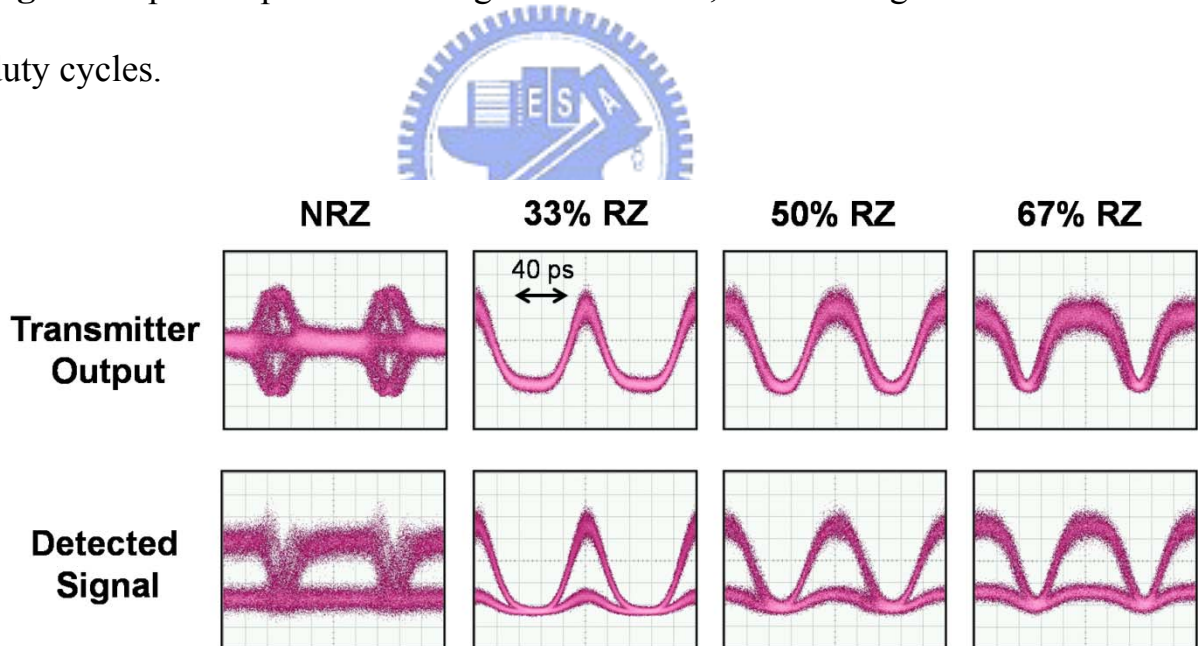


Fig. 4.4 Back to Back eye diagrams of the NRZ and RZ signals with different duty cycles before and after detection. The horizontal scales are all with 20 ps/div.

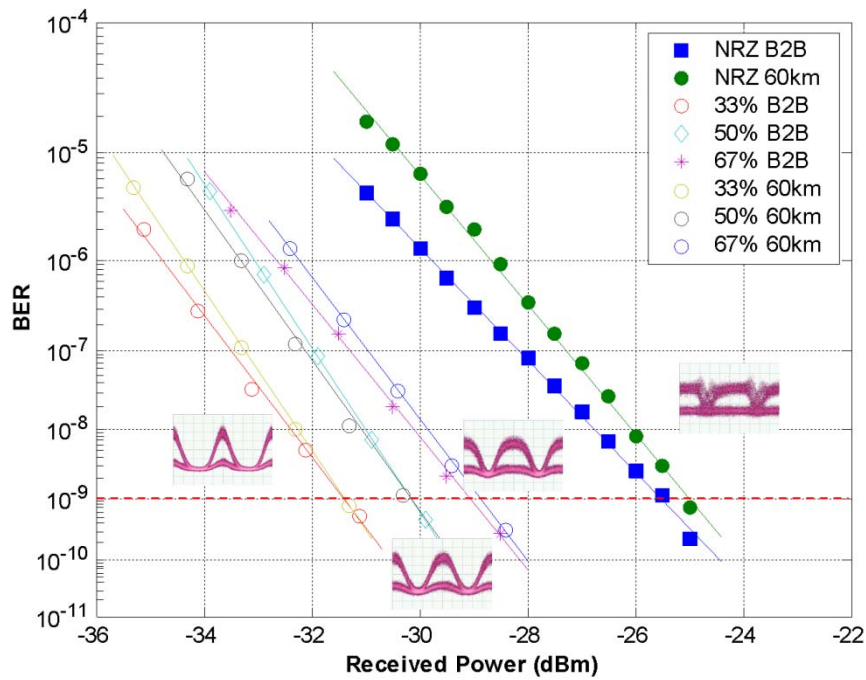


Fig. 4.5 Bit error ratio of the DQPSK signals before and after 60km fiber transmission.

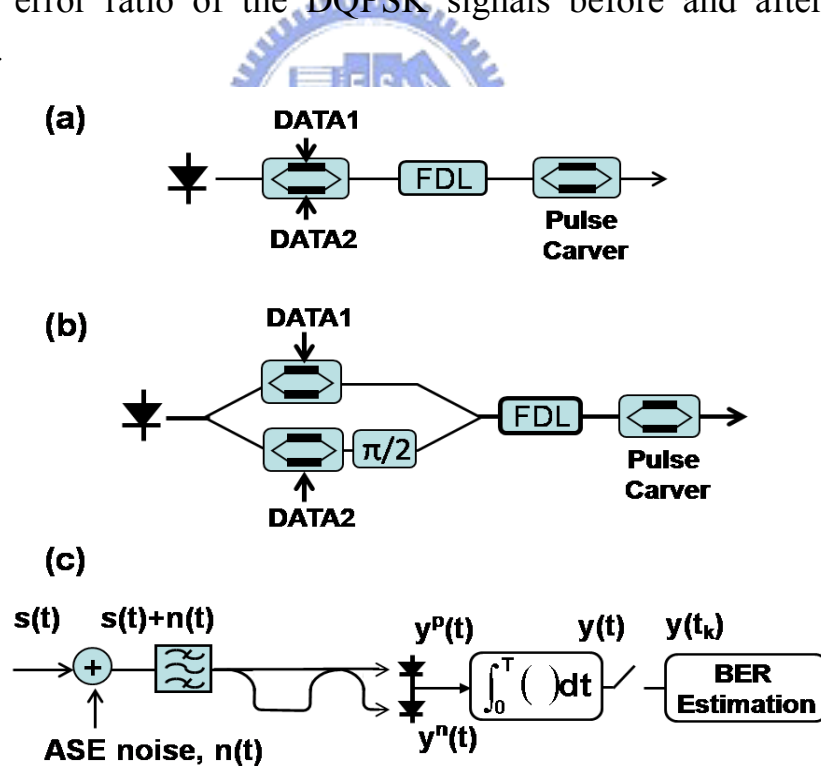


Fig. 4.6 (a) DQPSK transmitter with one DD-MZM and one pulse carver. (b) DQPSK transmitter with two parallel MZMs and one pulse carver. (c) Receiver numerical model.

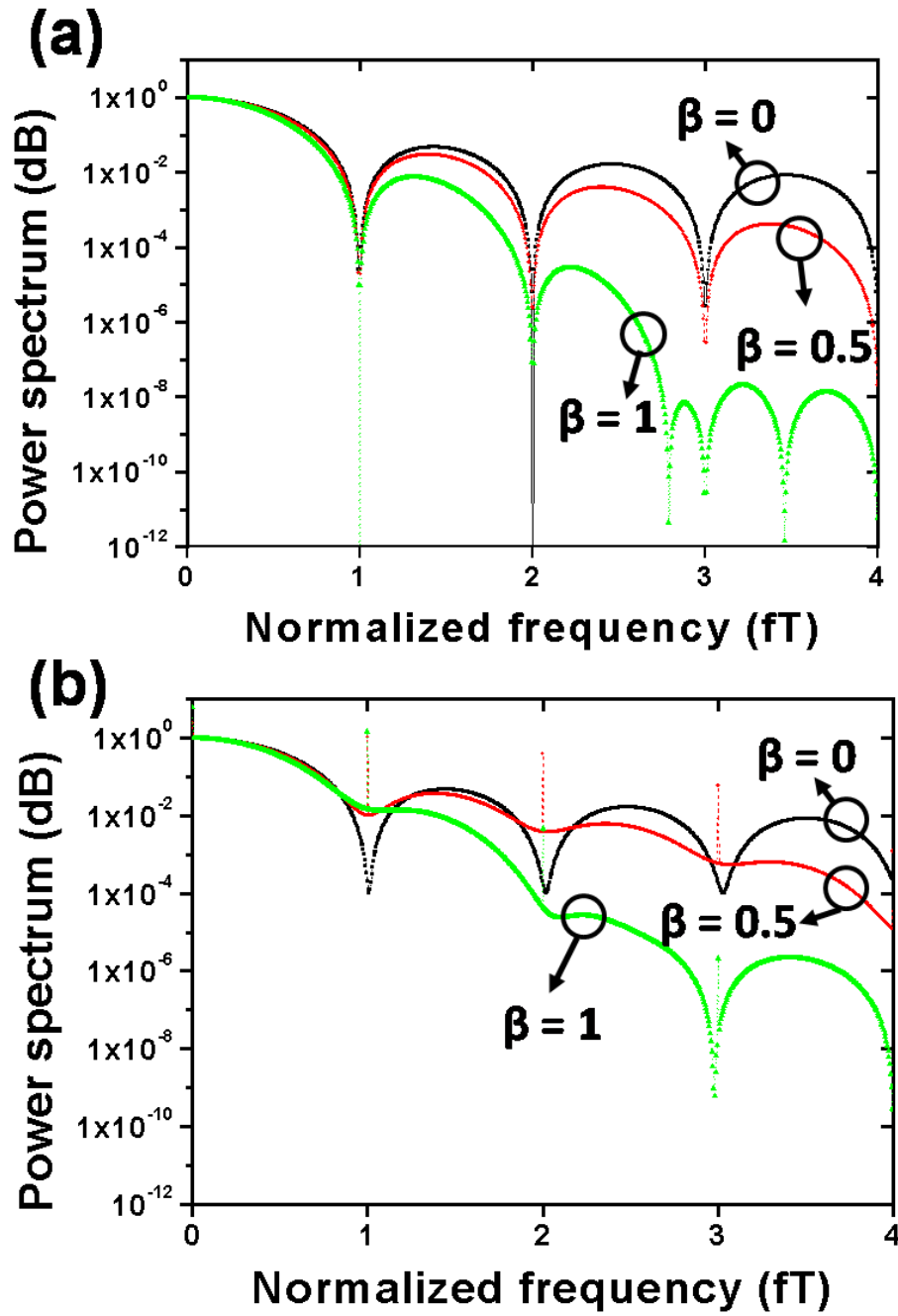


Fig. 4.7 (a) The optical spectra of the DQPSK signal generated by conventional two parallel MZMs. (b) The optical spectra of DQPSK signal generated by one DD-MZM.

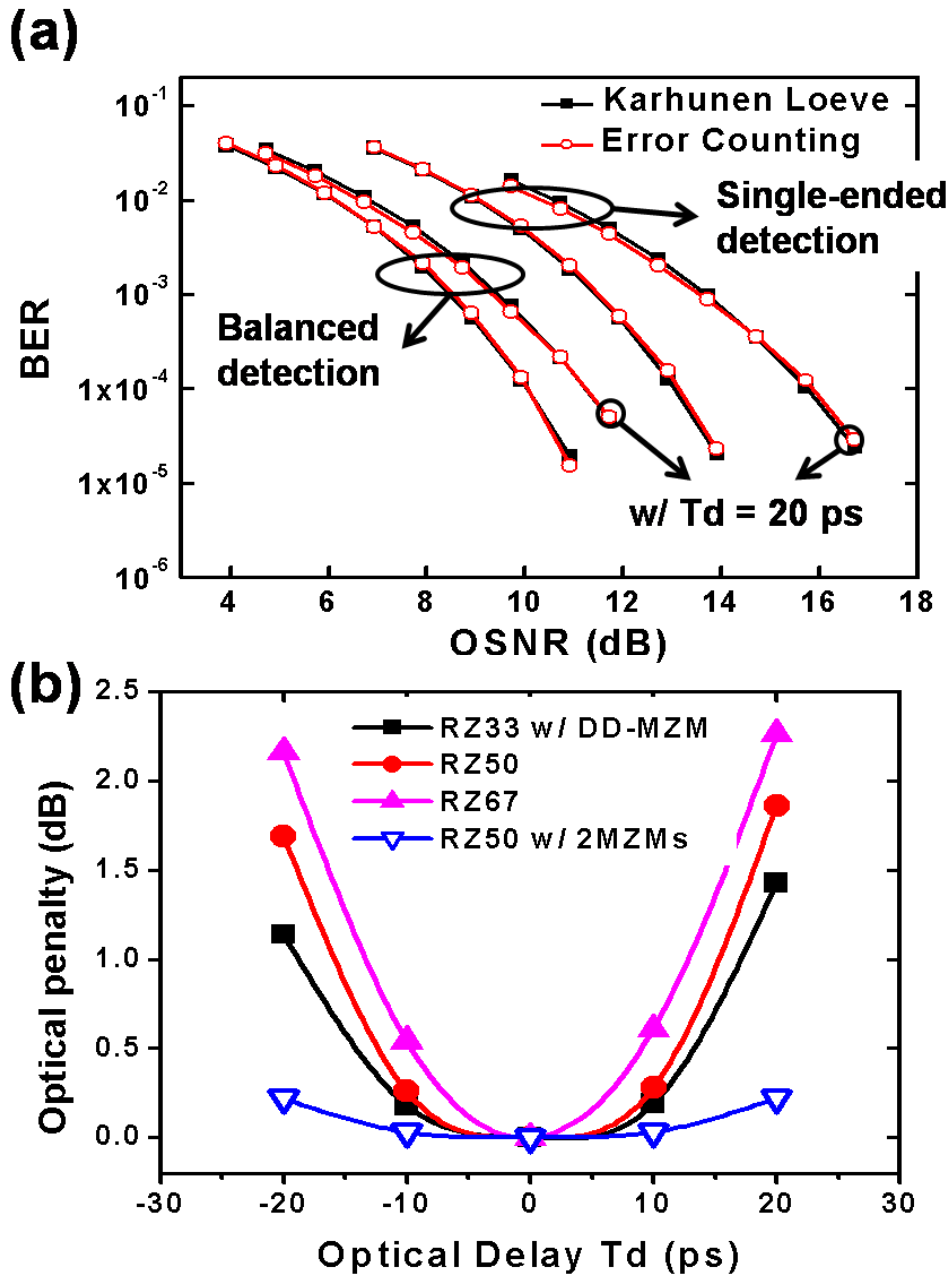


Fig. 4.8 (a) BER versus OSNR for one-MZM scheme with $T_d = 20$ ps time mismatch between the data and the pulse modulators. (b) The power penalty of the RZ formats versus the relative delay between the data and the pulse modulators.

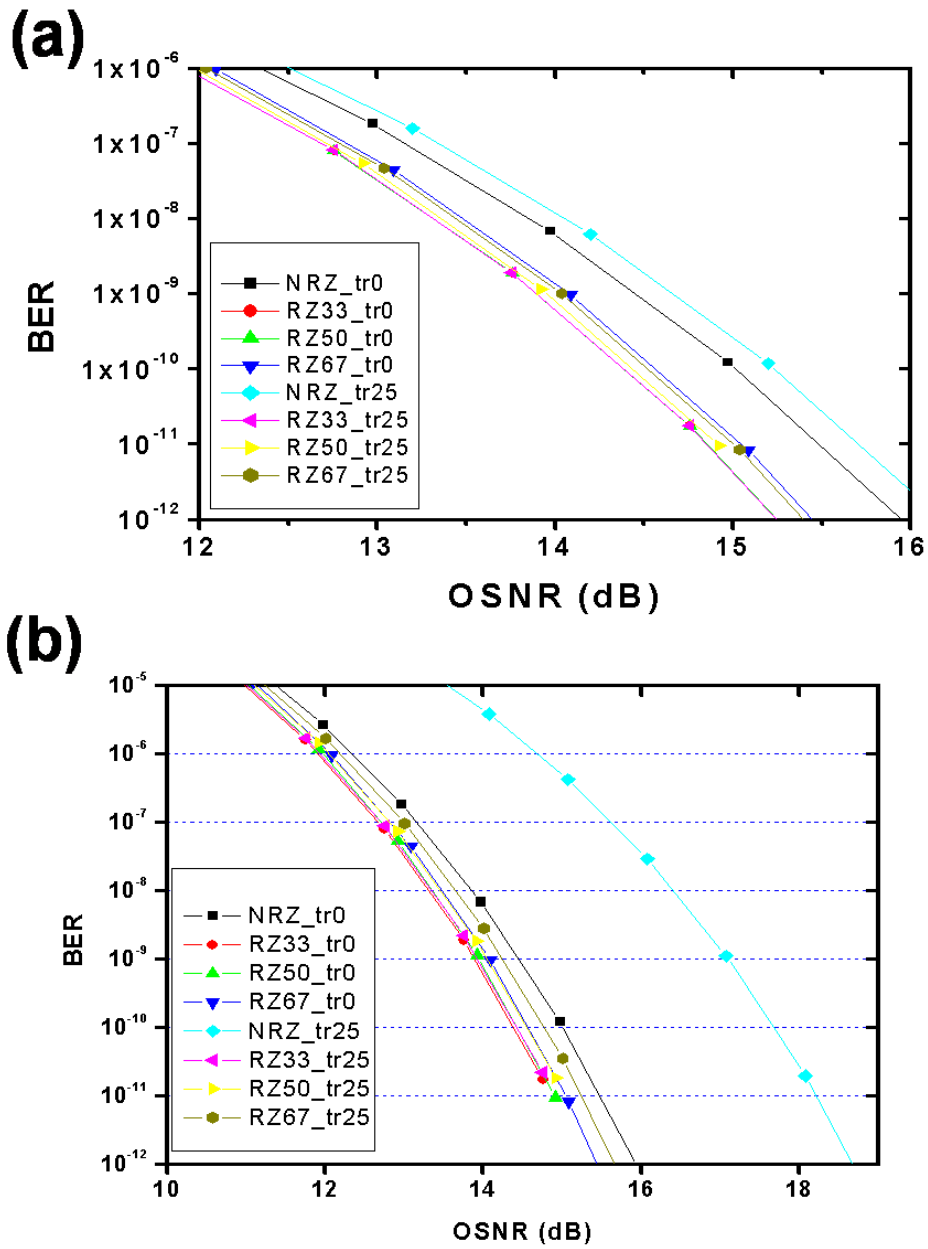


Fig. 4.9 (a) BER of the two-MZMs schemes. (b) BER of the one-MZM scheme.

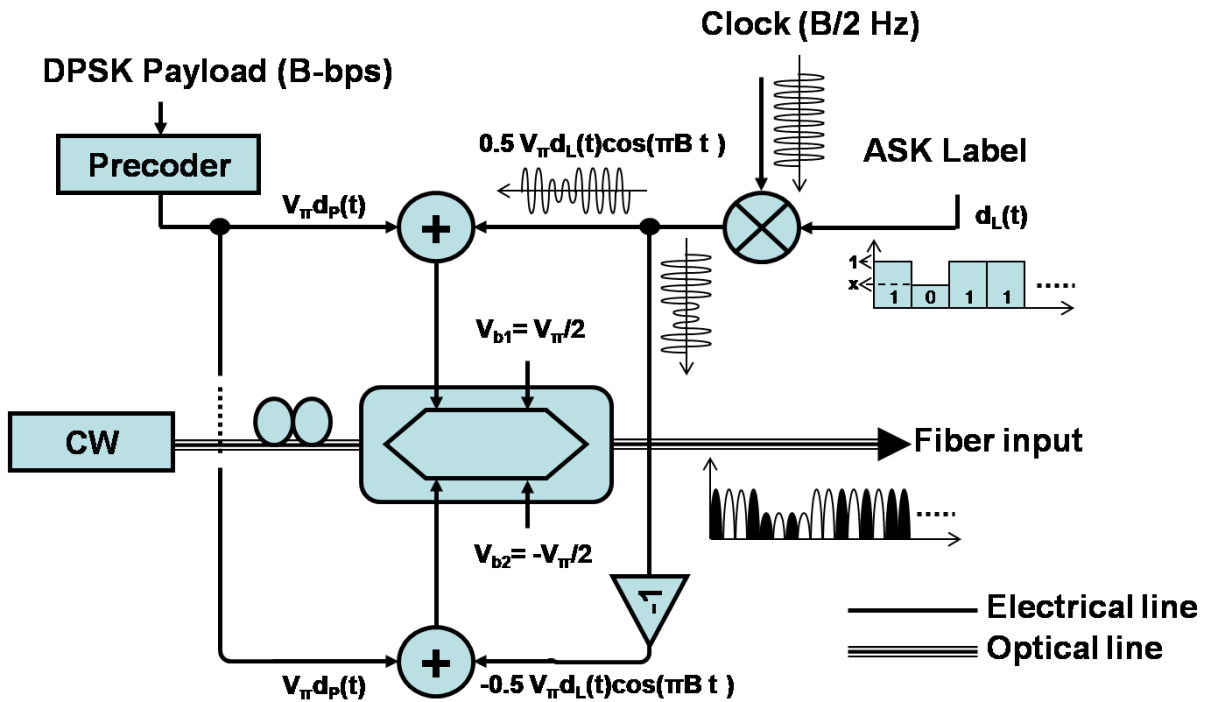


Fig. 4.10 The proposed scheme for ASK/ CSRZ-DPSK modulation.

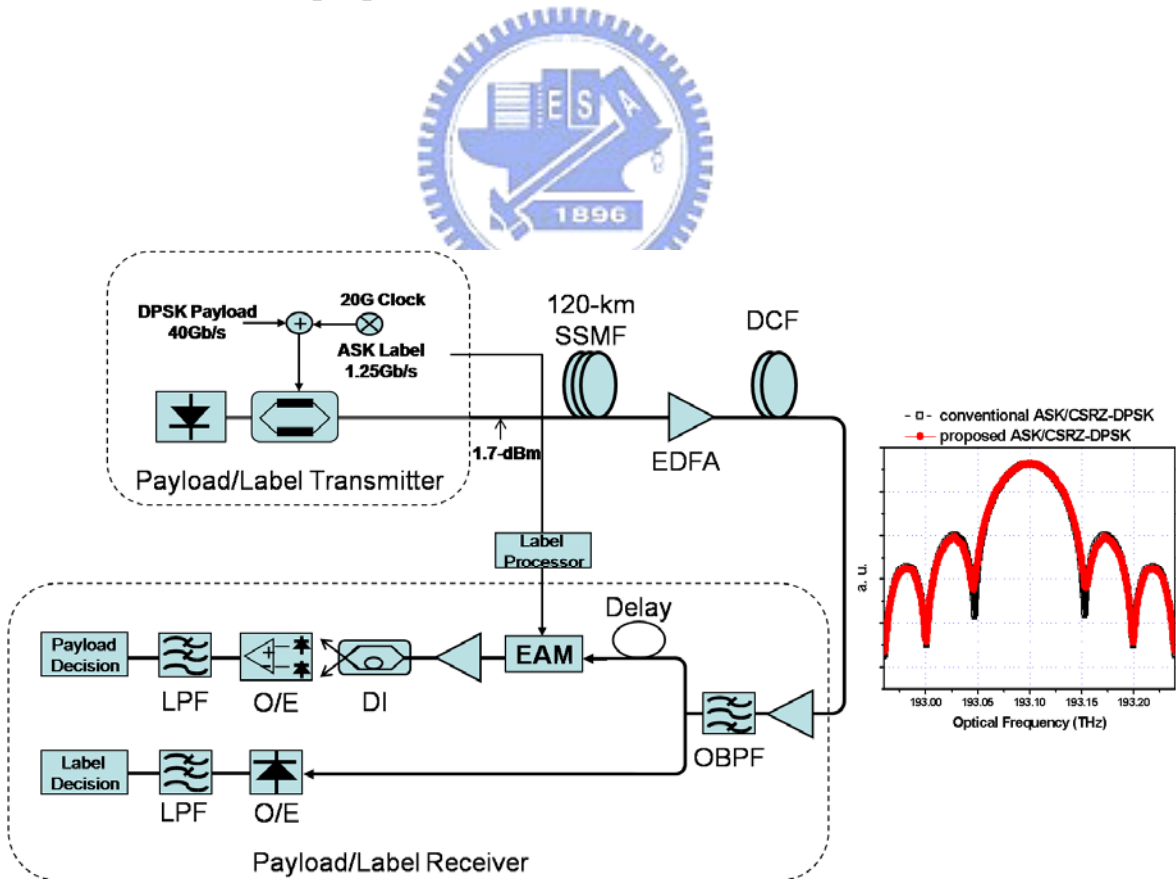


Fig. 4.11 System test link for the proposed ASK/RX-DPSK modulation scheme.

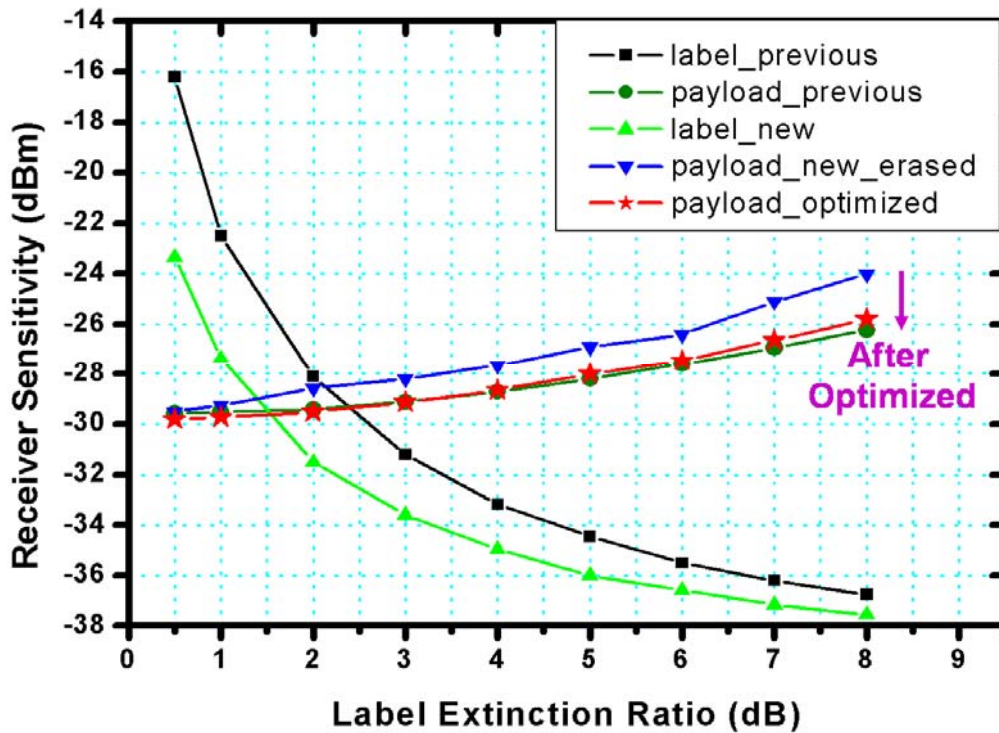


Fig. 4.12 Back to back receiver sensitivities of label and payload versus label extinction ratio.

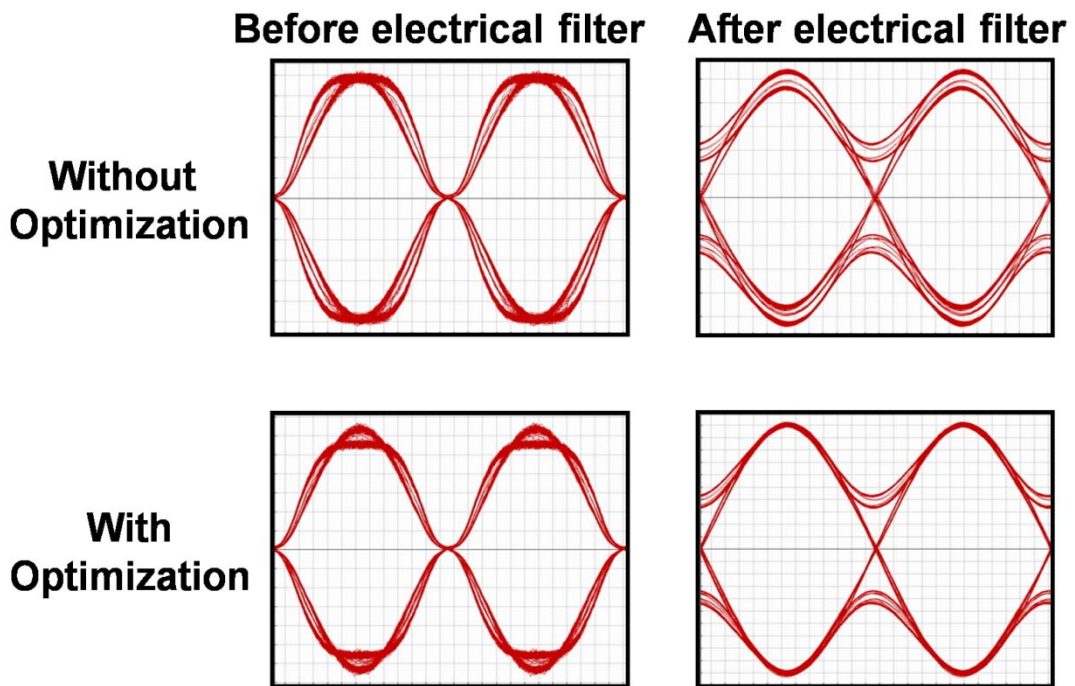


Fig. 4.13 Eye patterns of the payload before and after the low pass electrical filter, with and without the optimization scheme.

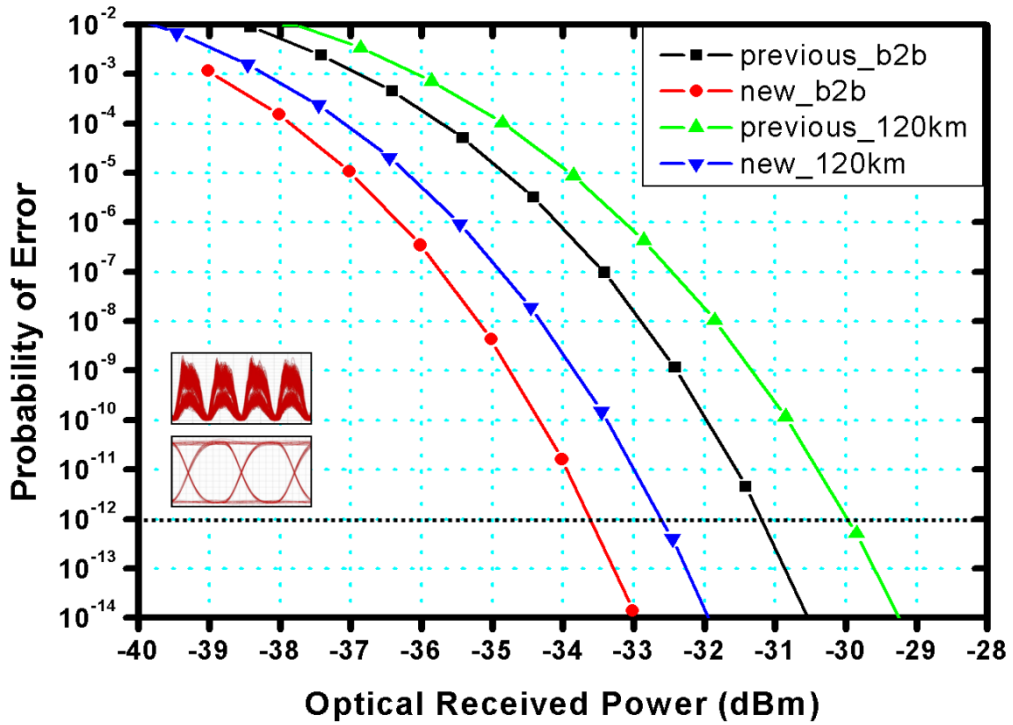


Fig. 4.14 BER performances of the label in back to back and 120 km SSMF transmission.

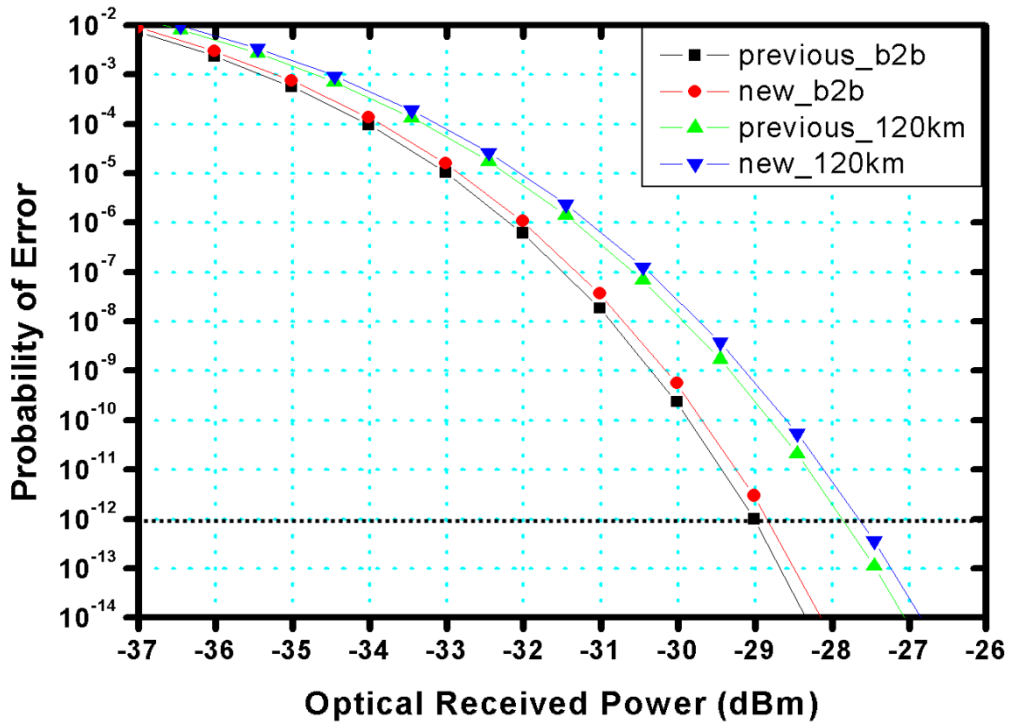


Fig. 4.15 BER performances of the payload in back to back and 120 km SSMF transmission.

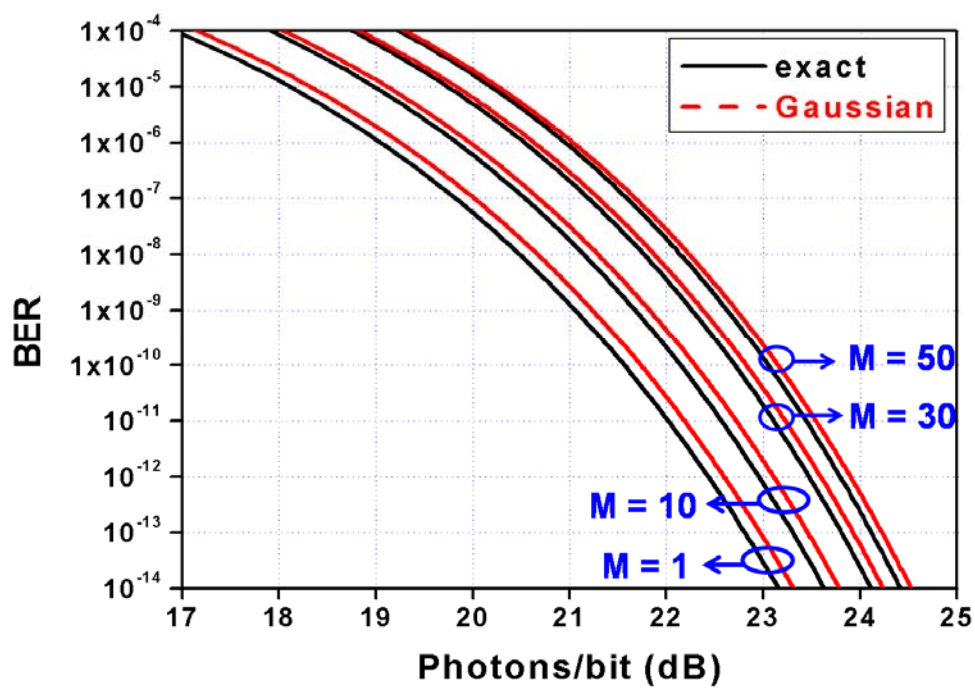


Fig. 4.16 The bit error rate for 4-ASK as a function of photons/bit with various M.



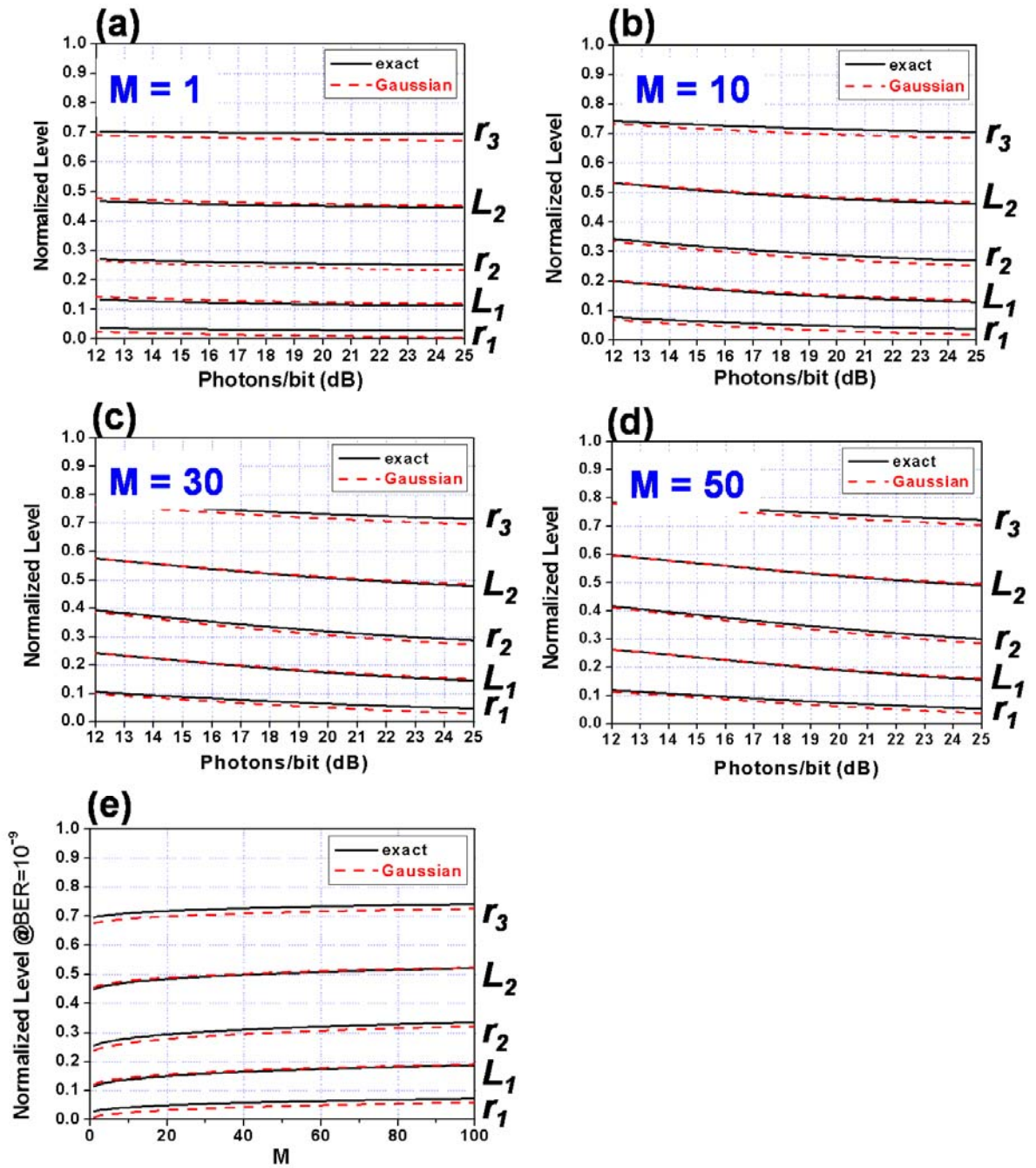


Fig. 4.17 The optimum normalized multilevel spacing and thresholds as a function of photons/ bit with (a) $M = 1$, (b) $M=10$, (c) $M=30$, (d) $M=50$. (e) The optimum normalized multilevel spacing and thresholds at a bit error rate of 10^{-9} as a function of M .

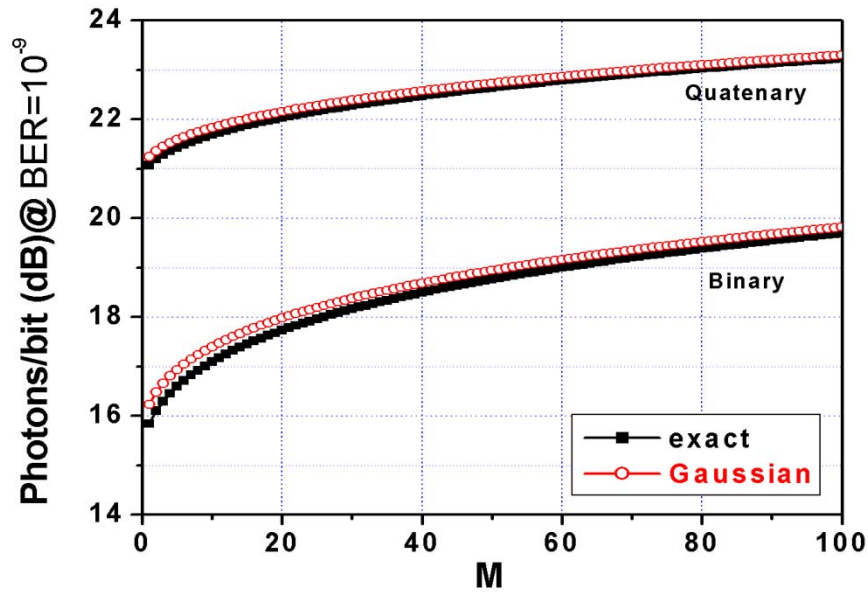


Fig. 4.18 Required photons/bit to achieve a bit error rate of 10^{-9} for both the binary and the quaternary formats.

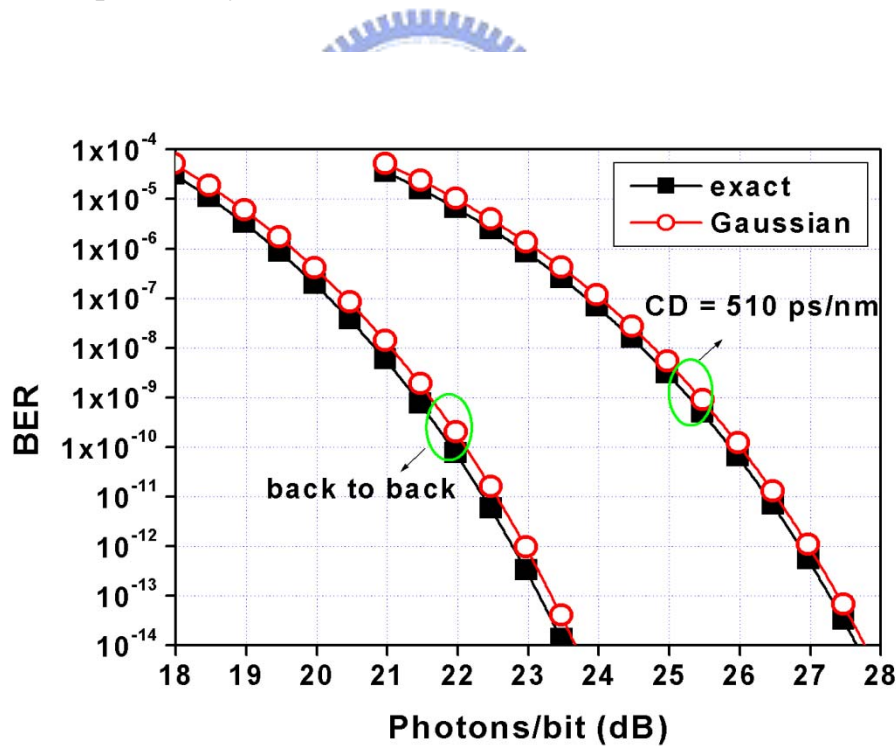


Fig. 4.19 Bit error rate versus the photons/bit for the RZ-4ASK format for the back to back and $CD = 510$ ps/nm with the exact and Gaussian approximation method.

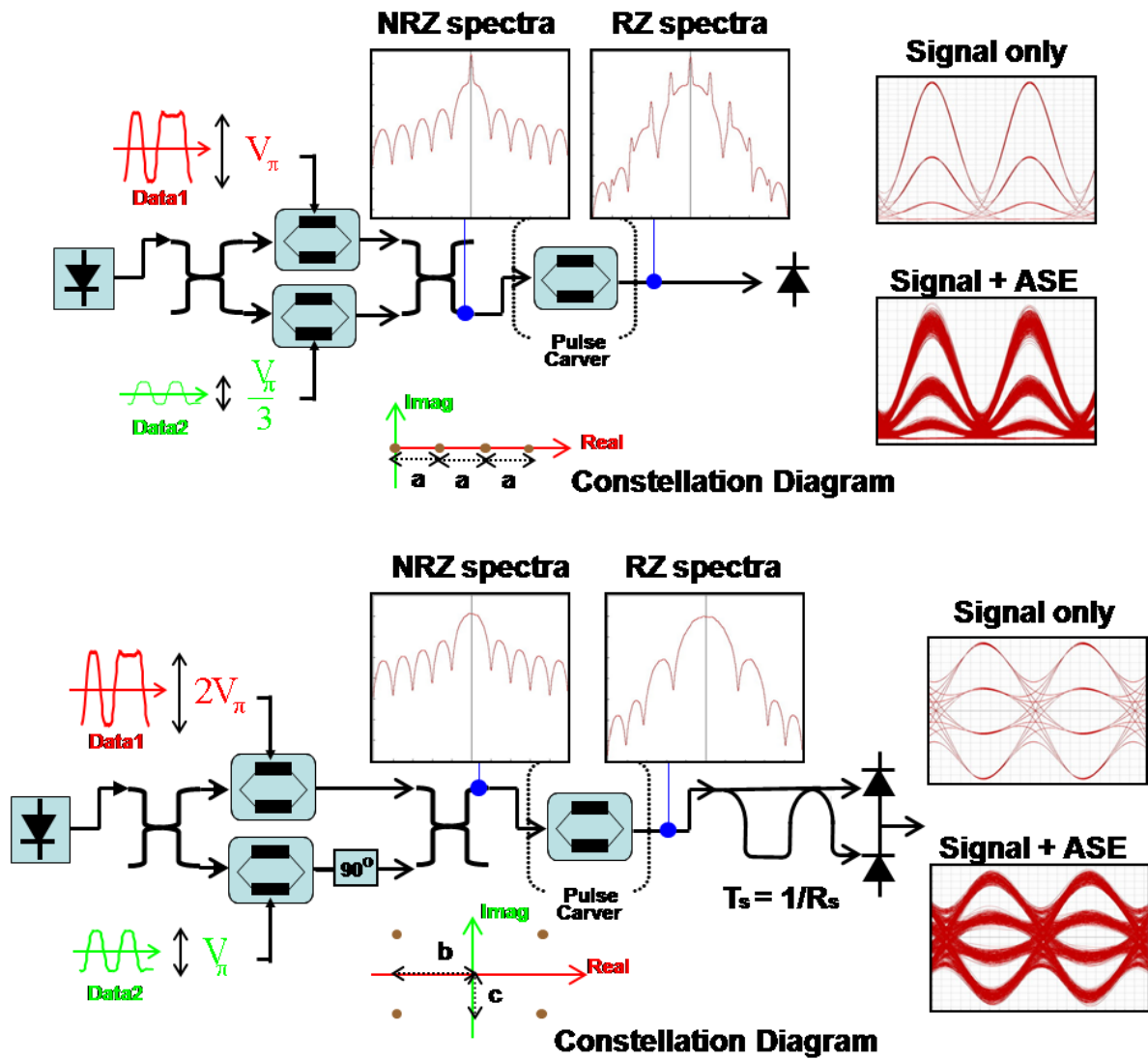


Fig. 4.20 The modulation and demodulation of (a) the conventional 4ASK and (b) the proposed PM4ASK formats.

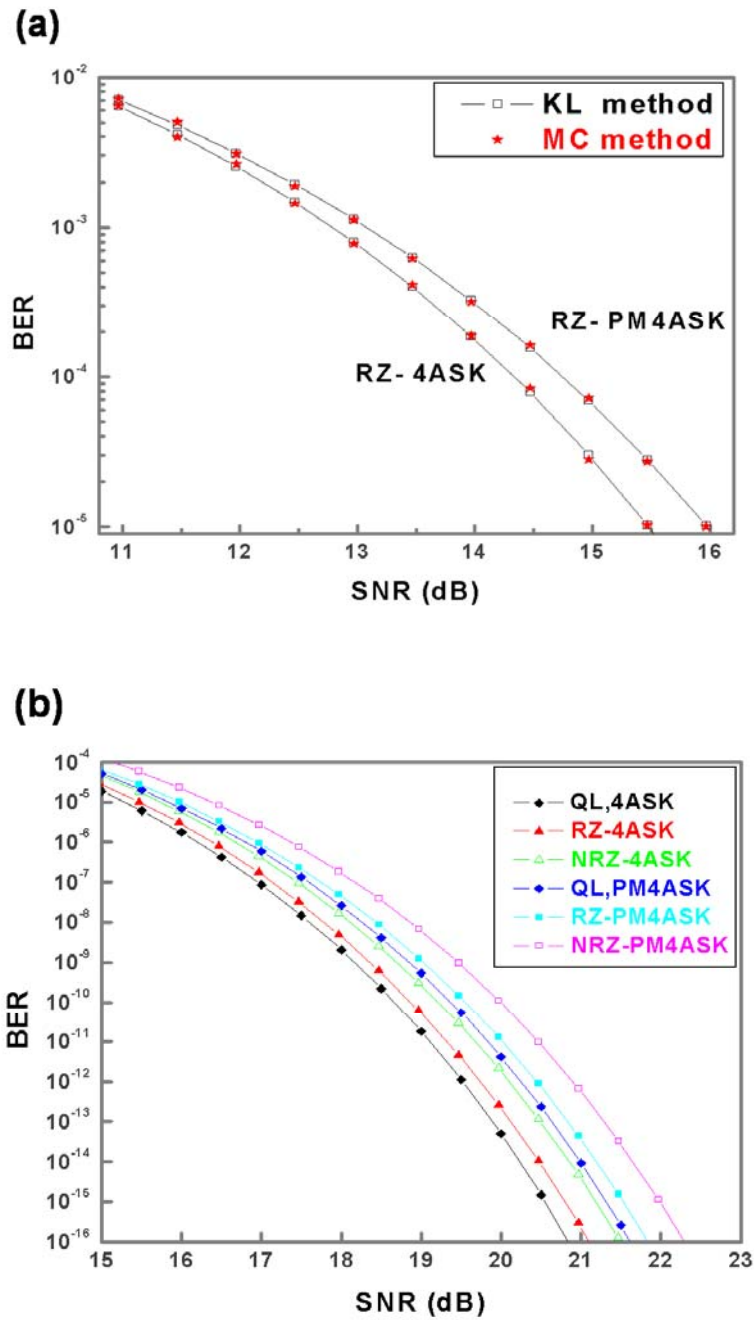


Fig. 4.21 (a) Bit error rates for RZ-4ASK and RZ-PM4ASK formats calculated by Monte-Carlo (MC) error counting and Karhunen-Loeve (KL) semi-analytical method. (b) BER versus SNR for both 4ASK and PM4ASK formats under the matched (QL) and optimum practical filters.

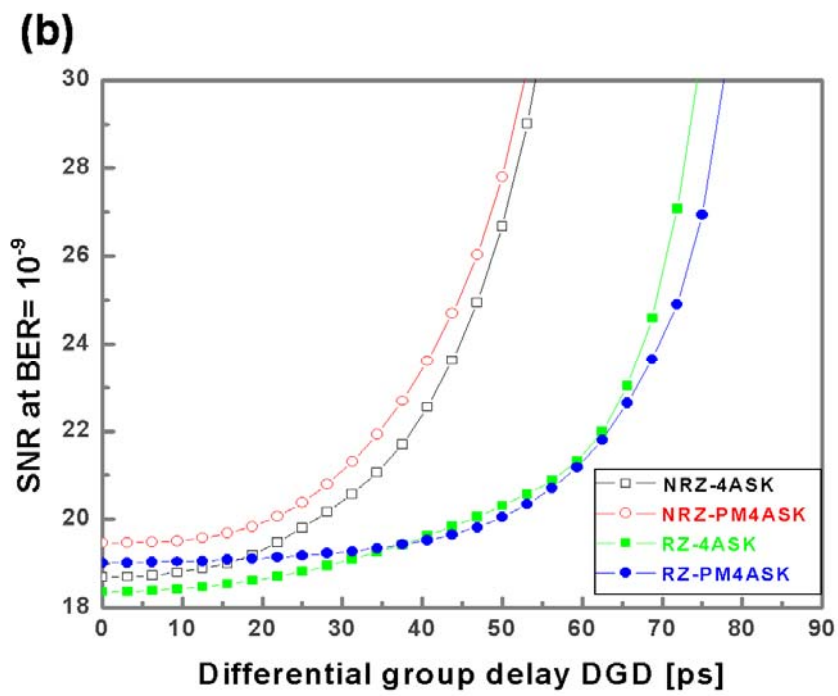
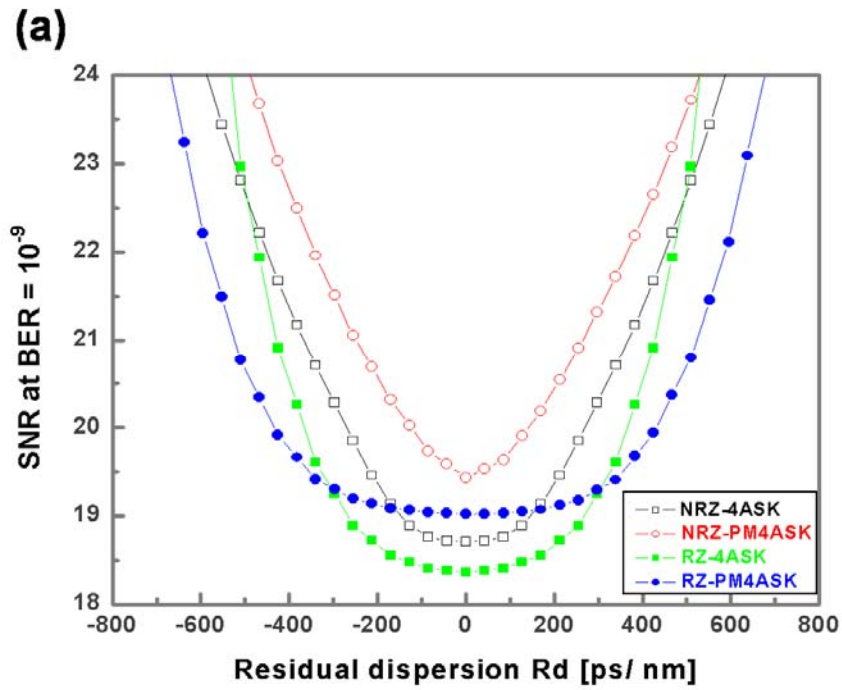


Fig. 4.22 (a) Required SNR for $BER=10^{-9}$ versus residual dispersion. (b) Required SNR for $BER=10^{-9}$ versus differential group delay.

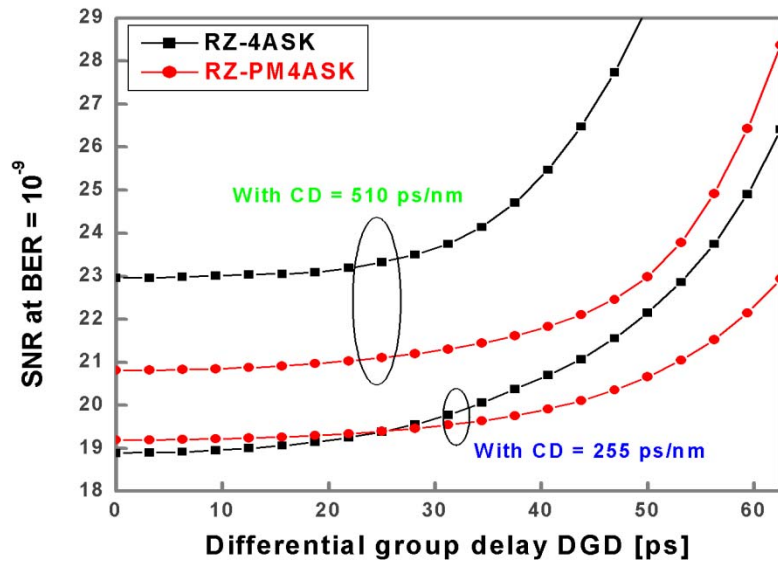


Fig. 4.23 Required SNR for BER=10⁻⁹ versus differential group delay with residual dispersion of 255 and 510 ps/ nm.

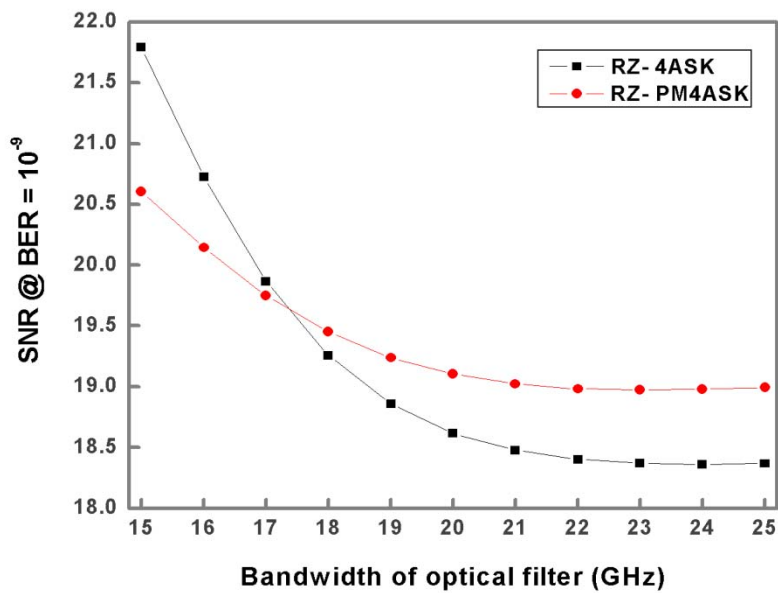


Fig. 4.24 Required SNR at BER = 10⁻⁹ versus the optical bandwidth for the conventional RZ4ASK and proposed RZ-PM4ASK formats.

| | 4ASK | | PM4ASK | |
|-----------------------------------|------|------|--------|------|
| | NRZ | RZ | NRZ | RZ |
| $f_{3dB,opt} / R_s$ | 1.2 | 2.35 | 1.15 | 2.7 |
| $f_{3dB,el} / R_s$ | 1.05 | 0.85 | 1.5 | 0.6 |
| R_d [ps/nm] | 855 | 893 | 783 | 1173 |
| τ [ps], $R_d = 0$ ps/nm | 37.5 | 59.5 | 36.6 | 63.4 |
| τ [ps], $R_d = 255$ ps/nm | | 48.7 | | 59.6 |
| τ [ps], $R_d = 510$ ps/nm | | 42.2 | | 53.2 |

Table 4.1 The Optimum optical and electrical filters and the 3-dB tolerances to CD and PMD effects.



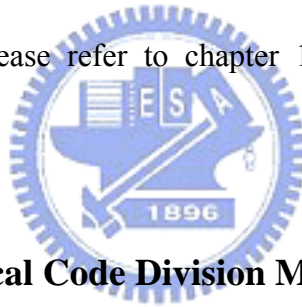
Chapter 5

Optical Code Division Multiplexing

5.1 Introduction

This section describes our proposed OCDMA techniques including 1: the development of a cost-effective optical fast frequency hopping CDMA (OFFH-CDMA) light source using a self-seeded Fabry-Perot laser diode (FP-LD), 2: reduction of the multiple access interference (MAI) for an OFFH-CDMA system by using a frequency interleaved multi-group approach, and 3: the first demonstration of the multi-carrier CDMA (MC-CDMA) for a passive optical network (PON).

For interested readers please refer to chapter 1 and 2 for related backgrounds and overviews.



5.2 Light Source of Optical Code Division Multiple Access (OCDMA)

5.2.1 Introduction

Optical code-division multiple access (OCDMA) has become an attractive technology for local access network (LAN) since it provides a higher bandwidth usage and enhances the transmission security. Due to the power detected nature of the photodiode, the imperfect orthogonality among the developed optical codes would induce a large multiple access interference (MAI) and strongly limits the afforded subscriber number. Thus, to implement a CDMA system in an optical transmission system, the MAI would be an even more serious issue than its counterpart in wireless communication.

An optical fast frequency hopping CDMA (OFFH-CDMA) system by using the fiber Bragg grating array has been proposed for its less MAI [1]. Fiber Bragg grating (FBG) is

cheap, compact, and very simple to tune and thus is a future-proof candidate as an OCDMA en/decoder. Most experimental demonstrations of OCDMA systems use the free running gain-switched FP-LD or super-continuum (SC) light source as a broadband light source for encoding [2-3]. However, the free running gain-switched FP-LD suffers the wavelength-dependent power fluctuations due to the mode competitions in laser cavity and thus is not a good choice for an optical transmission. As for the SC light source, it is really broadband and high speed but the generated output pulses are close to transformed-limited and is not a suitable candidate for incoherent OCDMA.

Recently, a sequentially self-seeded FP-LD combined with the FBGA as an encoded CDMA light source has been proposed without the power fluctuations [4-5]. However, an extra high-cost electric optical modulator (EOM) for gating is required and thus it complicates the whole module.

In this letter, we experimentally demonstrate an OCDMA encoder that uses a FBGA built-in FP-LD based on the configuration of an actively mode-locked fiber laser [6]. The colored optical pulse trains are generated once the self-seeded mechanism has been achieved within the mode-locked laser loop. By inserting the variable fiber delay line (VFDL) in the loop, we can change the transmitting bit rate flexibly without limited by the cavity length. In addition, we save one frequency divider and one extra EOM which are required in the previous method [4-5], thus exhibiting more cost-effective and simple constructed.

5.2.2 Concept

The schematic diagram of the proposed coding scheme is shown in Fig. 5.1. The proposed OCDMA encoding module consists of a RF synthesizer, a FP-LD, a polarization controller (PC), three optical circulators (OC1, OC2, OC3), a fiber Bragg grating array (FBGA), an EDF amplifier, a output coupler, and the variable fiber delay line (VFDL). An external fiber cavity is constructed for providing the feedback optical signal to seeding the FP-LD [5]. The

optical path in the external cavity is FP-LD→PC→OC1 port 3→OC2 port 2→FBGA→ OC 2 port 3→ EDFA→OC 3 port 2→ FBGA→ OC 3 port 3→VFDL→ OC 1 port 2→PC→FP-LD. The PC is used to control the polarization state of the input to the LD for the best seeding efficiency. The embedded FBGA are used to encode the input pulses both temporally and spectrally at the same time, and also used to recombine the encoded chips before being sent into the FP-LD. The cavity length for all optical pulses reflected from the corresponding FBG is the same. The EDFA is used for power compensation in external cavity loop and the VFDL is to control the timing of the feedback pulses.

Figs. 5.2(a)-(c) show the working principle of our proposed scheme. The RF synthesizer drives the FP-LD to emit the free-running pulse trains shown in Fig. 5.2(a). Each pulse is with multiple longitudinal modes $(\lambda_1, \lambda_2, \lambda_3, \lambda_4, \dots, \lambda_M)$ of the FP-LD and the pulse repetition rate is $f = 1/T_{bit}$. After reflected from the FBGA of n FBG sections, the optical pulse train is with the hop pattern of $(\lambda_1, \lambda_2, \lambda_3, \dots, \lambda_n)$, shown in Fig. 5.2(b). The chip duration is equal to the round-trip time between adjacent gratings, $T_{chip} = 2d/v$, where d and v are the grating spacing and optical velocity in fiber, respectively. The encoded pulses will be partially coupled to output for data modulation through a branch of the coupler. Through the other branch of the coupler the encoded pulses will be recombined through the decoding process of the FBGA. Each pulse is with n wavelengths of $(\lambda_1, \lambda_2 \sim, \lambda_n)$ and the pulse duration of T_{bit} . For efficient seeding, the modulation radio frequency should be the harmonics of the fundamental frequency of the external cavity length [5].

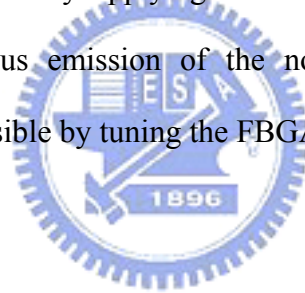
5.2.3 Experimental Results

The optical source is a commercial FP-LD operating at 1555 nm. The mode spacing and the CW lasing threshold are 1.08 nm and 10.1 mA, respectively. The FP-LD is biased at 5.6 mA

and the temperature was set at $23^{\circ}C$. It is gain-switched with a RF signal at $f_{RF} = 475MHz$. The spectrum and the corresponding pulse shape of the FP-LD are shown in Fig. 5.3(a) and (b), respectively. Inset in Fig. 5.3(a) shows the detailed view near the center wavelength. Fig. 5.3(b) shows the width of the output pulse is about 56.4 ps, which is narrow enough for high speed coding. The FBGA we used contains three FBGs for coding. The FBGs are fabricated by masking method and with $d = 5cm$ spacing between gratings for mechanically tuning. Each FBG is with bandwidth of 0.4 nm and reflectivity of over 99%. Fig. 5.4 shows the spectra and the encoded pulse sequence from the coupler (25:75) output after self-seeding. Three FP-LD longitudinal modes at $\lambda_1 = 1548.82nm$, $\lambda_2 = 1549.9nm$, and $\lambda_3 = 1550.98nm$ are coded by the FBGA and the side-mode suppression ratio (SMSR) more than 20 dB is obtained. The observed sequences are with bit duration of about $T_{bit} \approx 2.1ns$ and chip duration of about $T_{chip} \approx 500ps$, which are matched the designed value of radio frequency $f_{RF} = 475MHz$ and the grating spacing $d = 5cm$, respectively. To demonstrate the other possibility of codeword, λ_3 is shifted to $\lambda_4 = 1552.06nm$ by tuning the corresponding grating while the other two modes $\lambda_1 = 1549.9nm$ and $\lambda_2 = 1548.82nm$ are not changed. Their results are shown in Fig. 5.5. The SMSR with more than 20dB is obtained. We continuously monitor the three wavelengths for ten minutes. Power variation of lasing wavelengths is less than 0.4 dB. The power variation increases if the polarization of this system is unstable. According to the self-seeded mechanism [8], only one polarization direction of the feedback light results in the maximum self-seeded efficiency.

The role of EDFA is not only for power compensation for the loss of the fiber cavity loop, but also can be used for power control over network. The signal output power will be controlled by the network manager and it can improve the system performance and efficiency [7]. Since the data bit rate governed by the radio frequency should be harmonics of the

fundamental frequency of the external cavity, it can be any specific value by adjusting the cavity length through the VFDL. The fundamental frequency of system is about 5 MHz, and the cavity length is about 41.38 m. The required cavity length can be flexibly achieved by the VFDL in the system. The only constraint on the RF frequency is to avoid adjacent bit aliasing after encoding, for less MAI in networking [1]. For our case, the RF frequency is upper bounded by $f_{RF} \leq 1/3T_{chip} = 667\text{MHz}$. The usable wavelength number is limited by the FBGA total length. Using the multipassband chirped Moiré grating (CMG) instead, the overall FBGA length can be reduced or more wavelengths can be supported [9]. The tuning range is decided by the FBG tunability and the FP-LD output power. A laser diode with a higher output power over a broad spectral range can enhance the wavelength tuning. The SMSR can be further improved by applying antireflection coating on the diode facet to suppress amplified spontaneous emission of the nonselected cavity mode. In addition, two-dimensional coding is possible by tuning the FBGA properly.



5.2.3 Summary

We propose a novel and simple OFFH-CDMA coding module using self-seeded gain-switched FP-LD combined with the embedded FBGA. We remove the high-cost electro-optic modulator (EOM) required for gating and the complex timing control compared to the previous scheme [4-5]. With the tuneability of each grating in FBGA, we can dynamically change the address code for data destination. We demonstrate the scheme by driving 475 MHz RF frequency to the FP-LD and encoded pulse streams with chip rate of 1.425 GHz. We also demonstrate the possibility of other codeword with different encoded wavelengths. The SMSR of larger than 20 dB is obtained in the two cases and unstable mode competition does not exist. The experimental results show that the demonstrated codeword are with small power variance between chips, which makes the coding module practical. Finally,

the coding module can also be used for two-dimensional OCDMA coding if we insert different optical paths between gratings in FBGA.

5.3 Reduction of the Multiple Access Interference (MAI) in an Optical Fast Frequency Hopping CDMA (OFFH-CDMA) System by Using the Frequency Interleaved Multi-Group Approach

5.3.1 Introduction

Spread spectrum code-division multiple-access (CDMA) has been widely used for wireless communications. Due to its many advantages over traditional multiple access schemes such as TDMA or FDMA, which are scheduled in time or frequency domains, CDMA provides advantages such as larger capacity, asynchronous access, frequency diversity, soft handover, etc. Due to the successful development of wireless CDMA, the use of CDMA in the optical domain has attracted a great deal of research recently. In the late 1970s, the first work on optical CDMA proposed using the fiber delay lines for optical processing which is a scheme of direct-sequence CDMA (DS-CDMA) [10]. Alternative implementations of DS-CDMA are implemented by optical delay lines [11-13], ladder networks [14-15], tunable delay lines [16-18], and recently, superstructure fiber Bragg grating (SSFBG) [19-21]. SSFBG provides not only a low cost en/decoder but also high speed optical processing. Shortcomings of this device is its lower power efficiency since the en/decoding grating must be weakly coupled.

In addition to the DS-CDMA, frequency-encoded CDMA (FE-CDMA) which encodes the signature code on the wavelength domain with coherent or non-coherent method was proposed and analyzed in [22-24]. Since the en/decoding process of these schemes is addressed with a bulk grating, the huge size of the transmitter/receiver is a problem. Although this problem has been resolved using two compact consecutive fiber Bragg gratings (FBGs) [25], the system still requires an ultra-short pulse generator and this will make the system high

price. An alternate scheme sending colored pulses in a predetermined order is the optical fast-frequency hopping CDMA (OFFH-CDMA). The first FFH-CDMA in optical domain is proposed by using an optical frequency synthesizer as the encoder [26-27]. The tunable fiber Bragg grating arrays (FBGA) are used instead of the frequency synthesizer to reduce further the transmitter cost [28-31]. Since the OCDMA is proposed as an access scheme in a local area network (LAN), an OFFH-CDMA system using the FBGA [28] which maintains high performance and potentially low cost is one of the best choices. However, due to the non-fully orthogonality of the optical codes, the maximum capacity is still limited by the multiple access interference (MAI). Therefore, the emerging work for an OFFH-CDMA system is to reduce the MAI and increase the system capacity. Aimed at this, we propose a new scheme which can lessen the multiple-access interference (MAI) of an OFFH-CDMA system.

In this paper, we propose a frequency-overlapping multi-group scheme which reduces the system MAI and enhances the maximum number of the coactive users. This scheme divides the users into different groups, and assigns the users in each group with the frequency slots which are partially overlapping among different groups. Since this assignment makes more efficient use of the optical spectrum than the conventional scheme, in which the frequency gap between any two adjacent Gaussian-shaped frequency slots is wasted, the performance is expected improved.

The rest of this paper is organized as follows. In Section II, we describe the frequency allocation method in a conventional OFFH-CDMA scheme using the FBGA, and then our newly proposed method, which employs a frequency-overlapping multi-group method. In Section III, we analyze the system performance through the development of the codes. We give the constraints required for this new scheme and those codes modified from the previous one-coincidence sequences. The system performance, in terms of the signal to interference ratio (SIR) and the probability of error, are analytically derived with this new codes. In Section IV, we show the numerical results of auto and cross-correlation functions and the

probability of error with different number of groups. It is found that the bit error rate or the maximum number of coactive users will be improved or enhanced by increasing the number of groups. Finally, our conclusions are given in Section V.

5.3.2 Concept

Figure 5.6 shows the architecture of an OFFH-CDMA transmitter and receiver pair. A broadband light source is firstly data modulated using the amplitude shift keying (ASK) format and then encoded by the FBGA, where G_i is the frequency passband of each grating. The matched receiver recovers the transmitted data with a reciprocal FBGA. Optical power received from other transmitters will be randomized and treated as interference. Although there are some other candidates, such as array waveguide gratings (AWGs) or thin-film fillers can employ the OFFH-CDMA system and possibly can apply the scheme we proposed in this paper, it seems that FBGA is the simplest and cost-saving method to modulate or demodulate an OFFH-CDMA signal. Often the multiple access interference is the dominant limiting the number of the coactive user and the performance of a CDMA system, the emerging work for OCDMA is the reduction of the MAI level.

Figure 5.7(a) shows a typical star network of a conventional scheme. All the users are assigned those codes constructed on the discrete non-overlapping frequency slots, i.e.: all the codes used in this network are mapped to the frequency slots shown in Fig. 5.7(b). Each user is assigned a specified hopping sequence $C(l)$ with a code length of N . $C(l)$ is the l -th chip chosen from 0 to $q-1$, where q is the number of available non-overlapping frequency slots. The hopping frequency $f_h(l)$ of the l -th chip can be written as:

$$f_h(l) = f_1 + f_{offset}(l) \quad (5-1)$$

where f_1 is the first frequency slot and the

$$f_{\text{offset}} = C(l) \frac{B}{q} \quad l = 1, \dots, N, \text{ and } 0 \leq C(l) \leq q - 1 \quad (5-2)$$

is the frequency offset around f_1 . B is the total optical bandwidth and B/q is the interval of the frequency slots. This frequency allocation is direct and simple, coming from the ideas of the independent wavelength allocation in a wavelength division multiplexing (WDM) system. However, the spectrum-efficiency is low since no usage is taken around the band-gaps between any two consecutive frequency slots. The band-gaps can be fully used with our multi-group scheme.

In the new scheme, the users are firstly divided into several groups, as shown in Fig. 5.7(c). The first group uses the same frequency allocation as the conventional scheme, in which the frequency slots are discrete and non-overlapping. With a slightly up-shift of the frequency allocation of the first group, we can obtain the allocation of the second group. The allocation of the third group can be obtained further by up-shifting the allocation of the second group, and so on. The frequency allocation is shown in Fig. 5.7(d). The first frequency slots of different groups are assigned as:

$$f_{1,j} = f_1 + j \frac{B}{N_g q} \quad 0 \leq j \leq N_g - 1 \quad (5-3)$$

where $f_{1,j}$ is the first frequency slot of the j -th group, and N_g is the total group number.

The corresponding hopping frequency in the j -th group can be written as:

$$f_{h,j}(l) = f_1 + \frac{B}{q} \left(C_j(l) + \frac{j}{N_g} \right) = f_1 + \frac{B}{N_g q} (N_g C_j(l) + j) \quad (5-4)$$

This formula can be explained as that all users use the same first slot f_1 with the modified code pattern of $N_g C_j(l) + j$ multiplier the slot width $B/(N_g q)$. However, an additional slot with a width of $(B \times j)/(N_g q)$ is required in this new scheme. Since the distribution of the frequency slots is more uniform than the conventional scheme, better spectra-efficiency is

expected. In addition, the reduced overlapping area of the frequency slots between any two different groups implies less correlation, thus lessening the MAI. To promise all the users can communicate with all the other users, each transceiver should equip with a tunable en/decoder.

5.3.3 Code Design and Performance Analysis

A. Hamming Auto- and Cross-Correlation

Multilevel sequences are used to specify which frequency will be used for transmission at any given time. An important requirement in multiple access applications is to keep the mutual interference as small as possible. The interference is generated by the cross-correlation function of the hopping sequences. One of the correlation function measurements is the periodic Hamming cross-correlation function H_{XY} , defined as

$$H_{XY}(\tau) = \sum_{i=0}^{N-1} h(C_X[i], C_Y[i+\tau]_{\text{mod } N}) \quad \text{for } 0 \leq \tau < N \quad (5-5)$$

where

$$(a) \quad h(a, b) = \begin{cases} 0 & \text{if } a \neq b \\ 1 & \text{if } a = b \end{cases}$$

$$(b) \quad C_X = (C_X[0], C_X[1], \dots, C_X[N-1]) \quad \text{and} \quad C_Y = (C_Y[0], C_Y[1], \dots, C_Y[N-1])$$

denote two hopping sequences of length N .

$$(c) \quad C_X \text{ and } C_Y \in \{f_1, f_2, \dots, f_q\}, \text{ where } f_i \text{ is one of the } q \text{ available frequency slots } (q \geq N).$$

The function $H_{XY}(\tau)$ represents the number of the same frequency slots from any two sequences with relative time delay of τ . We will use it to analyze the performance of the developed FFH-codes. If $H_{XY}(\tau) \leq 1$ for any $X \neq Y$, this code set is called as one-coincidence sequence [32] and this gives the smallest interference in an OFFH-CDMA system.

B. Codes for this new scheme

To promise the better performance of this new scheme, in addition to the previous work [33], there are two more constraints should be carefully concerned. The first is that there should not be any two frequency slots of a specific user with a difference smaller than N_g . This allows the gratings in a FBGA independent to each other and hence promises the uniform output chip power after encoded by the FBGA. The second, the new code should still exhibit the so called one-coincidence property. However, since the frequency slots in the new scheme are interleaved with each other, instead of the one-coincidence, the partial-coincidence should be considered. We will define the partial-coincidence later.

For the new scheme, the number of conventional usable discrete frequency slots q is increased to $N_g q$ frequency slots with an interval of $B/(N_g q)$. Since the bandwidth of a grating and their intervals used in the conventional scheme are approximately equal to B/q , the new interval of $B/(N_g q)$ will induce the adjacent N_g frequency slots to overlap. We choose N as the code weight from the available frequency slots q , where $N \leq q$. The code generator can be derived as [33] $C = \{C_0, C_1, \dots, C_{N-1}\}$, where C_i is the element of integers of $d+1, d+2, \dots, q-d-1, d = (q-N-1)/2$ for q odd integers and $d = (q-N-2)/2$ for q even integers. The new codes can be generated as follows.

$$F_{i,j}(k) = G_{i,j}(k) \times N_g + j \quad 0 \leq i \leq M-1, \quad 0 \leq j \leq N_g-1, \quad 0 \leq k \leq N-1 \quad (5-6)$$

where

(a) $F_{i,j}(k)$ is the k -th chip of the i -th user in the j -th group.

(b) $G_{i,j}(k) = [D_0(k) + i + M \times j]_{\text{mod } q}$, and $M = (q-1)/N_g$ is the number of codes

in each group.

$$(c) D_0(k) = [C_0 + C_1 + \dots + C_{k-1}]_{\text{mod } q}.$$

Note that the range of k here is located within $[0, N-1]$ rather than $[1, N]$ defined in [33].

The difference of any two frequency slots of a specific user can be written as:

$$D_{i,j}(k_1, k_2) = |F_{i,j}(k_1) - F_{i,j}(k_2)| = N_g |G_{i,j}(k_1) - G_{i,j}(k_2)| \quad (5-7)$$

It is known that $|G_{i,j}(k_1) - G_{i,j}(k_2)| \geq 1$ for $k_1 \neq k_2$ and hence the difference $D_{i,j}(k_1, k_2)$ should be larger than N_g . Thus, any two slots in a sequence will differ by at least N_g and the uniform output chip power can be promised.

To ensure that the performance of the new scheme outperforms the conventional scheme, the developed codeword should also exhibit the one-coincidence property. Clearly for any two codes from the same group, the one-coincidence nature is still hold. However, if the two codes are from different groups, the partial-coincidence should be considered. We assume that there are two codes from the j -th and the m -th group ($0 \leq j < m < N_g$), respectively. From eq. (5-6), the partial hit occurs only when the difference of two frequency slots is $(m - j)$ or $N_g - (m - j)$. We consider the following two Hamming functions:

$$\begin{aligned} H_1(\tau) &= \sum_{k=0}^{N-1} h(F_{i,j}(k) + (m - j), F_{l,m}(k + \tau)) \\ &= \sum_{k=0}^{N-1} h(G_{i,j}(k), G_{l,m}(k + \tau)) \leq 1 \end{aligned} \quad (5-8)$$


and

$$\begin{aligned} H_2(\tau) &= \sum_{k'=0}^{N-1} h(F_{i,j}(k') - [N_g - (m - j)], F_{l,m}(k' + \tau)) \\ &= \sum_{k'=0}^{N-1} h(G_{i,j}(k'), G_{l+1,m}(k' + \tau)) \leq 1 \end{aligned} \quad (5-9)$$

The corresponding relations and the overlapping areas, which represent the reflective interference power, are shown in Fig. 5.8. The two equations, eq. (5-8) and (5-9), indicate that the normalized maximum interference power of the two sequences is

$H_1(\tau)A_{|m-j|} + H_2(\tau)A_{|N_g-(m-j)|}$, which we defined as the partial coincidence. Note that the shadowing area $A_{|m-j|}$ and $A_{|N_g-(m-j)|}$, as shown in Fig. 5.8, had been normalized to the whole reflective power of a grating, A_0 . Since the sum of $A_{|m-j|}$ and $A_{|N_g-(m-j)|}$ is no greater than one, i.e. $A_{|m-j|} + A_{|N_g-(m-j)|} \leq 1$, the partial coincidence is always no greater than one, i.e. $H_1(\tau)A_{|m-j|} + H_2(\tau)A_{|N_g-(m-j)|} \leq 1$. Since the codes developed above are with this property, the better performance of the new scheme can be promised. The maximum of the partial-coincidence $H_1(\tau)A_{|m-j|} + H_2(\tau)A_{|N_g-(m-j)|} = 1$ holds only when the gratings are with ideal rectangle-shaped spectra.

For example, we construct the 2-group codes with $N = 12$ and $q = 25$. The generator sequence is $C = \{12, 17, 16, 15, 7, 11, 13, 8, 9, 10, 18, 14\}$; the 2-group codes are derived as follows:



| | | | | | | | | | | | | | |
|----------------|---|----|----|----|----|----|----|----|----|----|----|----|----|
| Group 0 | { | 24 | 8 | 40 | 20 | 34 | 6 | 32 | 48 | 16 | 36 | 22 | 0 |
| | | 26 | 10 | 42 | 22 | 36 | 8 | 34 | 0 | 18 | 38 | 24 | 2 |
| | | 28 | 12 | 44 | 24 | 38 | 10 | 36 | 2 | 20 | 40 | 26 | 4 |
| | | 30 | 14 | 46 | 26 | 40 | 12 | 38 | 4 | 22 | 42 | 28 | 6 |
| | | 32 | 16 | 48 | 28 | 42 | 14 | 40 | 6 | 24 | 44 | 30 | 8 |
| | | 34 | 18 | 0 | 30 | 44 | 16 | 42 | 8 | 26 | 46 | 32 | 10 |
| | | 36 | 20 | 2 | 32 | 46 | 18 | 44 | 10 | 28 | 48 | 34 | 12 |
| | | 38 | 22 | 4 | 34 | 48 | 20 | 46 | 12 | 30 | 0 | 36 | 14 |
| | | 40 | 24 | 6 | 36 | 0 | 22 | 48 | 14 | 32 | 2 | 38 | 16 |
| | | 42 | 26 | 8 | 38 | 2 | 24 | 0 | 16 | 34 | 4 | 40 | 18 |
| | | 44 | 28 | 10 | 40 | 4 | 26 | 2 | 18 | 36 | 6 | 42 | 20 |
| | | 46 | 30 | 12 | 42 | 6 | 28 | 4 | 20 | 38 | 8 | 44 | 22 |
| Group 1 | { | 49 | 33 | 15 | 45 | 9 | 31 | 7 | 23 | 41 | 11 | 47 | 25 |
| | | 1 | 35 | 17 | 47 | 11 | 33 | 9 | 25 | 43 | 13 | 49 | 27 |
| | | 3 | 37 | 19 | 49 | 13 | 35 | 11 | 27 | 45 | 15 | 1 | 29 |
| | | 5 | 39 | 21 | 1 | 15 | 37 | 13 | 29 | 47 | 17 | 3 | 31 |
| | | 7 | 41 | 23 | 3 | 17 | 39 | 15 | 31 | 49 | 19 | 5 | 33 |
| | | 9 | 43 | 25 | 5 | 19 | 41 | 17 | 33 | 1 | 21 | 7 | 35 |
| | | 11 | 45 | 27 | 7 | 21 | 43 | 19 | 35 | 3 | 23 | 9 | 37 |
| | | 13 | 47 | 29 | 9 | 23 | 45 | 21 | 37 | 5 | 25 | 11 | 39 |
| | | 15 | 49 | 31 | 11 | 25 | 47 | 23 | 39 | 7 | 27 | 13 | 41 |
| | | 17 | 1 | 33 | 13 | 27 | 49 | 25 | 41 | 9 | 29 | 15 | 43 |
| | | 19 | 3 | 35 | 15 | 29 | 1 | 27 | 43 | 11 | 31 | 17 | 45 |
| | | 21 | 5 | 37 | 17 | 31 | 3 | 29 | 45 | 13 | 33 | 19 | 47 |

From the construction rules we find that codes of the first group are the same as that of previously developed in [33] multiplying the group number by N_g . Fig. 5.9 shows the FBGA

spectra of the first codeword of group 0 and group 1 as solid and dashed lines, respectively. Codewords for other different number of groups can be derived by the same method.

C. Signal to Interference Ratio

Interference will occur when two or more interfered slots and the desired slot with a difference smaller than N_g reach the receiver at the same time. As shown in Fig. 5.8, the interference value of A_i from any two codes will differ depending on the groups where the codes are from. For mathematical convenience, we consider chips to be synchronous but with bit asynchronous interference in SIR and BER approximation. We assume that all users transmit data at an equal rate and with data duration $T_b = NT_c$ in a continuous fashion. Figure 5.10 shows the received signal and the interference in a receiver. The undesired signal from the l -th user from the m -th group with relative chip delay τ_{il} to the i -th user of the j -th group are shown as Fig. 5.10(a) and (b), respectively. Here $b_{l,m,n}$ is the previous or the present data bit of the l -th user from the m -th group for $n = -1$ or 0 , which will be an interference to the desired present data bit of $b_{i,j,0}$. The interference will occur if any two chips of the i -th and j -th users at the same time are with a difference smaller than the group number N_g , i.e.: $|F_{l,m}(t) - F_{i,j}(t)| < N_g$. The interference from the l -th user to the i -th user can be written as:

$$I_{il} = \sum_{d=0}^{\tau_{il}-1} b_{l,m,-1} g(F_{i,j}(d), F_{l,m}(N - \tau_{il} + d)) + \sum_{d=\tau_{il}}^{N-1} b_{l,m,0} g(F_{i,j}(d), F_{l,m}(d - \tau_{il})) \quad (5-10)$$

where

$$g(x, y) = \begin{cases} A_{|x-y|} & \text{for } |x - y| < N_g \\ 0 & \text{for } |x - y| \geq N_g \end{cases} \quad (5-11)$$

where A_i is the normalized interference defined in the previous subsection and its value depends on the grating profile and the frequency interval. The relative delay τ_{il} is assumed uniformly distributed over integers $[0, N-1]$ and the data bits “0” and “1” are transmitted with equiprobability. We assume that there are N_i possible values of interference between any two sequences in the code set, and the probability of each interference can be denoted as $P_n(I_{il} = I_n)$, where n is an integer over $[0, N_i-1]$, and I_n is one of the possible interference values. The average variance of the multi-group codes can be derived as [34]:

$$\sigma^2 = \sum_{m=0}^{N_i-1} \left[I_m - \left(\sum_{n=0}^{N_i-1} I_n \times P_n \right) \right]^2 P_m \quad (5-12)$$

where P_n denotes the average probability of having an cross-correlation value of $I_{il} = I_n$ between any two sequences in the code set. If there are K simultaneous users, the total interference from the other $K-1$ users can be written as

$$I_i = (K-1)\sigma^2 \quad (5-13)$$

So the signal to interference ratio, SIR, can be derived directly as

$$SIR = \frac{N^2}{I_i^2} = \frac{N^2}{(K-1)\sigma^2} \quad (5-14)$$

D. Probability of Error

Here we ignore other noise sources and consider only the MAI, which usually dominates the performance of a CDMA system. Using the Gaussian approximation for multiple access interference and equiprobable data, the bit error rate can be derived as [35]

$$P_e = Q\left(\frac{\sqrt{SIR}}{2}\right) \quad (5-15)$$

where

$$Q = \frac{1}{\sqrt{2\pi}} \int_x^{\infty} e^{-u^2/2} du \quad (5-16)$$

Since we consider only the case of synchronous chips, the error probability will be the upper bound of the exact error probability [28]

$$P_e(\text{exact}) \leq P_e \quad (\text{chip synchronous case}) \quad (5-17)$$

5.3.4 Numerical Results

A. Auto and Cross-Correlation Functions

To estimate the performance of the proposed multi-group scheme, we calculate the auto- and cross-correlation functions for different number of groups. The total optical bandwidth is 7 nm, from 1551.86 to 1558.86 nm, and sliced to 25 non-overlapping frequency slots with a bandwidth of 0.28 nm. Each user is assigned a unique code with length of $N = 12$, and each FBGA consists of 12 gratings corresponding to the code length. To reduce the sidelobes of the grating and increase the slot density, we use the Gaussian apodization for each grating and the gratings are all with a peak coupling coefficient equal to 220 m^{-1} . The length of each grating is 10 mm and the space between adjacent gratings is determined by the required chip rate and the tuneability [28]. Since the sidelobe of each grating is 20 dB lower than the mainlobe, we will ignore its effect and consider the mainlobe only. The interval of the frequency slot Δf is selected allowing the first nulls of successive gratings to overlap for higher slot density, as shown in Fig 5.11.

To evaluate the interference of different group number, one-bit of all the 24 users are synchronously sent to the decoder of the first user, as shown in Fig. 5.12(a). The decoded outputs are shown in Fig. 5.12(b)-(d), where the interference are normalized to the power of the desired signal, which is located at the central peak. The input pulse is Gaussian shaped and has a pulse-width of ~ 0.2 chip duration.

In Fig. 5.12(b), it is found that the cross-correlation is almost as high as the

auto-correlation when all users are active. The system suffers serious interference, which will lose the correct detection window for the receiver and degrade the system performance. Figure 5.12(c) shows the proposed system with the 2-group method. It is found that the cross-correlation function is reduced to only 2/3 of that in the conventional case. The auto-correlation can be easily distinguishable and the performance also improved. Increasing the number of groups, as shown in Fig. 5.12(d) and (e) where $N_g = 6$ and 24, the cross-correlation decreases to a level even lower than half of that in the conventional scheme. There is no apparent difference between the group number of 6 and 24. Since increasing the number of group requires stringent tenability and temperature controllability on the grating, the better group number that tradeoff between signal performance and system complexity might be 6 in this case.



B. Bit Error Rate

The simulation parameters, except that the bit synchronous is changed to the chip synchronous assumption, are the same as the previous section. The average variance and the bit error rates for the proposed multi-group codes are derived from eq. (5-12) and (5-15), respectively. Figure 5.13 gives the probability of error versus the number of asynchronous simultaneous users with two different slot densities. Figure 5.13(a) shows the case with a frequency interval of 0.28 nm, which allows the first nulls of the adjacent gratings to overlap. The performance is increasingly enhanced with the increasing of the group number. The proposed system can support up to 4 extra users for $N_g = 2$ compared to the conventional one at a BER of 10^{-10} and this increase to 8 when the group number N_g exceeds 6. Hence, the system capacity is clearly much improved. However, we found that the enhancement of the BER quickly saturates as the increasing group number. There is only a little improvement from group number of 6 to the group number of 24, but the required tuning and temperature

control for group number of 24 is much stringent since the smallest spacing of two frequency slots is only 0.012 nm and it is expected that slight variation of environmental parameters such as temperature, humidity or stress will degrade the system seriously. It is very costly to maintain the performance of such a system. Thus, a tradeoff between the group number and the system reliability must be made, which will depend on the stability of the FBGA. In this simulation results, it seems that when the group number exceeds 6, the improvement of the BER is not so significant. Therefore, a group number with 6 rather than 24 would be a better choice in this example.

As described in section II, since one additional frequency slot is required in our new scheme, we also simulate the case of the conventional scheme with one more slot in Fig. 5.13(a). However, it is not as that in our multi-group scheme, the improvement is very limited even with the one additional frequency slot.

Figure 5.13(b) is the case with a frequency interval of 0.4 nm. Although the greater spacing of the frequency slots will decrease the slot number over the available bandwidth, the normalized interference, A_i , among different groups becomes smaller. The frequency slots are now reduced to $q = 17$ and the code weight N is left unchanged. The group number of 1, 2, 4, 8, 16 are shown in this figure, which indicates that the performance are getting better with the increasing number of groups. The saturation of the BER improvement is also observed.

Figure 5.14 compares the performance of the two systems with different slot densities. With a smaller group number, the interference mainly results from the users of the same group. This makes the system with lower slot density, $q = 17$, to have higher probability to hit, and exhibits worse performance. When the group number increases, the dominant interference mainly comes from users of different groups. That pushes the system with lower slot density, $q = 17$, to perform better since the smaller overlapping areas between the groups. It can be found that in the case of the maximum number of group, the system with $q = 17$ can support

two more users than that with $q = 25$ at a BER of 10^{-12} . The impairment of a system with lower slot density is that there are fewer codes that can be used and thus limit the maximum available users. In this example, there are 16 usable codes for slot number $q = 17$, while there are 24 usable codes for $q = 25$. However, the lower slot density also means the relaxation to the tuning and temperature controlling requirement, and therefore low cost. Thus, for small size area, the lower slot density is preferred, and for larger area, the higher one could be a better choice. Therefore, the slot density and the group number should be carefully selected depending on the size of the network.

5.3.5 Summary

We propose a novel OFFH-CDMA system using a frequency-overlapping multi-group scheme to make more efficient use of the optical spectrum. Users of different groups are assigned a different frequency allocation which is interleaved with each other. Reduced correlation among codes of different groups and more efficient use of the spectrum enhance the performance of the proposed OFFH-CDMA system. A new code set for this new scheme is developed and analyzed. With two additional constraints of this code set, performance with this code is much improved. The performance of the conventional scheme and the proposed scheme are compared in terms of the correlation function and bit error rate. With a Gaussian profile of each grating, the performance is increasingly enhanced with the increase of the group number. However, it is not a good choice to select the maximum number of group due to the stringent fine tuning and necessary careful temperature control. Trade off must be made between the system performance and the hardware implementation. We also give the performance analysis with different frequency slot density. The system with lower slot density will outperform that with higher slot density, in a larger group number, and lessens the requirement for tuning accuracy and temperature control. The corresponding shortcoming is the fewer usable codes in the system. Which one is better depends on the size and cost of the

network.

Another important issue is that in our simulation, the used profile of a grating is approximately Gaussian. If a flat-top profile grating has been used in our proposed scheme for better power efficiency, the interference is the same as the conventional scheme and no gain will obtain with this scheme. However, with a Gaussian or other non-flat-top grating, the interference can be largely reduced at a price of lower power efficiency. Hence, an appropriate profile should be selected under the considerations of both the power efficiency and the multi access interference.

5.4 Multi-Carrier CDMA (MC-CDMA)

5.4.1 Introduction

Orthogonal frequency division multiplexing (OFDM) alleviates the need for in-line compensation in optical links since the channel's bandwidth is divided into several narrower sub-channels and high speed signals are transmitted over multiple lower rate subcarriers, enabling a very simple equalization in electrical domain [36, 37]. Dividing the spectrum into several narrow sub-channels is based on fast Fourier transform (FFT) algorithms which can be simply implemented by commercially available FFT chips. Despite OFDM is new in optical communications, results show that it can be a promising transmission technique [37].

In [38], orthogonal frequency multiple access (OFDMA) was introduced as a technique for sharing the channel in passive optical networks (PONs) that has the advantages of OFDM. This scheme is a subcarrier multiplexing (SCM) technique in which depending on the required bandwidth of an optical network unit (ONU), a number of subcarriers is assigned to that ONU. The disadvantage of this method is that the bandwidth of the channel is not effectively consumed when some ONUs are not operating in the network because each ONU has a predetermined frequency range that other ONUs are unable to use.

In code division multiple access (CDMA) networks, multiple users transmit data at the same time and over the same spectrum in a shared medium. This feature allows users to efficiently utilize the available bandwidth since unlike TDMA or WDM, a time slot or a frequency range is not allocated to a certain user that can potentially be inactive from time to time. Moreover, flexibility, increased security, and plug-and-play functionality have made CDMA a promising candidate for PONs [39].

Multicarrier-CDMA (MC-CDMA) is the combination of CDMA and OFDM, thus taking the advantages of both techniques [40]. This multiple access method has been studied and demonstrated in wireline and wireless radio communications and in this paper for the first time we demonstrate MC-CDMA in optical fibres.

5.4.2 Concept

The general concept of MC-CDMA for one user is presented in Fig. 5.15. At the transmitter, data of user i , d_i , is mapped to QAM symbols, s_i . Then the user's unique signature code, c_i , encodes the symbols into chip sequences. The serial to parallel converter receives a chip sequence of length N and copies them to its output and then the Inverse FFT (IFFT) block performs inverse Fourier transform, generating N equally spaced subcarriers at its output. Finally, the parallel to serial converter places the subcarriers side by side in time domain.

At the receiver, the reverse processes plus equalization are performed on the signal. The equalizer is a memoryless block that multiplies each input (subcarrier) by a complex number. This number is the inverse of the channel response at the subcarrier frequency and it can be obtained using a preamble sequence and channel estimation. This simple equalization is inherent of OFDM and it is based on the fact that subcarriers bandwidth is very narrow [36]. Finally, each user correlates the output of the equalizer with its own signature code, and since each pair of codes has a low cross-correlation, any user is able to recover its symbols from other users. In this paper we have used Walsh-Hadamard (WH) codes that are completely

orthogonal to each other in synchronous systems; therefore, this demonstration is suitable for downlink since the central network unit is capable of synchronously transmitting data to the users in the network. However, using other codes such as m-sequence enables implementation of MC-CDMA for downlink, uplink, and peer to peer communication.

5.4.3 Experimental Setup and Results

The experimental setup is shown in Fig. 5.16. The input data for all the users is a random sequence of ones and zeros generated in computer. Then QAM mapping, CDMA encoding, IFFT, and adding the cyclic prefix are all done in MATLAB and the output of all these processes is loaded to an arbitrary waveform generator (AWG). The cyclic prefix is necessary for synchronization of the receiver. The waveform generator modulates a CW laser through a single arm Mach-zehnder modulator (MZM) which is biased at the quadrature point. Then the directly modulated signal is amplified by an Erbium doped fiber amplifier (EDFA) and sent through a 70 km of single mode fiber (SMF). The transmission length ensures the maximum coverage in a PON. At the receiver, a photo-detector converts the optical signal to the electrical signal which is sampled by a real-time oscilloscope. The output of the scope is connected to a computer and FFT, cyclic prefix removing, equalization, CDMA decoding, QAM demapping, and bit error rate (BER) measurements are all implemented in MATLAB.

The signal bandwidth is fixed at ~ 2.5 GHz. This relaxes the bandwidth requirement for the laser and receiver in a PON [41]. Therefore, the frequency spacing of subcarriers is equal to $2.5/N$ (GHz) and thus the symbol time $T_s = N/2.5$ (nSec), where N is the number of subcarriers. The bit rate per user depends on the constellation size of the QAM symbols. If QAM size is M , the bit rate will be equal to $R_b = (\text{Log}_2 M)/T_s = (2.5 \text{Log}_2 M)/N$ (Gbits/sec). For the QAM mapping we have used Gray coding to minimize the BER. The maximum number of users (the number of code words) that a WH set can support is equal to the code length, L ,

so the global bit rate of the whole network is equal to $R = LR_b = (2.5L/N)\text{Log}_2M$ (Gbits/sec).

The BER curves are obtained by averaging over the BER of all active users. Figure 5.17 shows the BER of three different numbers of active users while $N = L = 64$ and the symbols are 16 QAM. It can be seen there is almost no penalty after 70-Km SMF compared to the back to back case. As the number of users is increased from 4 to 64, less than a 2 dB penalty is observed.

In Fig. 5.18, BER curves for different constellation sizes are presented while the number of subcarriers is $N = 256$ and the code length is $L = 256$. As the constellation size is increased, due to a higher spectral efficiency, the bit rate is also increased, but on the other hand the performance is more degraded. Choosing appropriate values for M , L , and N enables accomplishing the required specifications of different users in the network. For example, based on different required bit rates, different users of the network can employ different QAM mapping. This flexibility is another advantage of MC-CDMA.

5.4.4 Summary

Optical multicarrier-CDMA is experimentally demonstrated for the first time. The system supports up to 256 users at a total bit rate of 15 Gb/s with almost no penalty after 70-km transmission.

Reference

- [1] H. Fathallah, L. Rusch and S. Larochelle, "Passive optical fast frequency-hop CDMA communications system," *IEEE J. Lightwave Technol.*, vol. 12, pp. 397-405, 1999.
- [2] X. Wang, K. T. Chan, Y. Liu, L. Zhang, and I. Bennion, "Novel temporal/spectral coding technique based on fiber Bragg gratings for fiber optic CDMA application," in *Dig. OFC/IOOC'99*, 1999, paper WM50, pp.341-343.
- [3] N. Wada, H. Sotobayashi, and K. Kitayama, "2.5Gbit/s time-spread/wavelength-hop optical code division multiplexing using fiber Bragg grating with super-continuum light source," *Electron. Lett.*, vol. 36, pp. 815-817, 2000.
- [4] X. Wang, K. L. Lee, C. Shu, and K.T. Chan, "Multiwavelength self-seeded Fabry-Perot laser with subharmonic pulse-gating for two-dimensional fiber-optic CDMA," *IEEE Photon. Technol. Lett.*, vol. 13, pp. 1361-1363, 2001.
- [5] X. Wang, and K. T. Chan, "A sequentially self-seeding Fabry-Perot laser for two-dimensional encoding/decoding optical pulse," *IEEE J. Quantum Electron.*, vol. 39, pp. 83-90, 2003.
- [6] S. Li, and K. T. Chan, "A novel configuration for multiwavelength actively mode-locked fiber lasers using cascaded fiber Bragg gratings," *IEEE Photon. Technol. Lett.*, vol. 11, pp. 179-181, 1999.
- [7] E. Inaty, H.M.H. Shalaby, P. Fortier, and L. A. Rusch, "Multirate optical fast frequency hopping CDMA system using power control," *IEEE J. Lightwave Technol.*, vol. 20, pp. 166-177, 2002.
- [8] M. Schell, D. Huhse, W. Utz, J. Kaessner, D. Bimberg, and I. S. Taraov, "Jitter and dynamics of self-seeded Fabry-Perot laser diodes," *IEEE Journal of Selected Topics in Quantum Electronics*, vol. 1, pp. 528-534, 1995.
- [9] L. R. Chen, and P. W. E. Smith, "Demonstration of incoherent wavelength-encoding/time-spreading optical CDMA using chirped Moire Gratings," *IEEE*

Photon. Technol. Lett., vol. 12, pp. 1281-1283, 2000.

[10] E. Marom and O. G. Ramer, "Encoding –decoding optical fiber network," Electronic lett., vol. 14, no. 3, pp. 48-49, 1978.

[11] P. Prucnal, M. Santoto, and T. Fan, "Spread spectrum fiber optic local area network using optical processing," J. Lightwave Technol., vol. 4, no. 5, pp. 307-405, 1986

[12] W. Kwong, and P. Prucnal, "Synchronous CDMA demonstration for fiber optic networks with optical processing," Electronic lett., vol. 26, no. 24, pp. 2219-2220, 1990.

[13] W. C. Kwong, P. Perrier, and P. R. Prucnal, " Performance comparisons of asynchronous and synchronous code-division multiple-access techniques for fiber-optic local area networks," IEEE Trans. Commun., vol. 39, no. 11, pp. 1625-16, 1991.

[14] A.S. Holmes, and R. Syms, "Switchable all-optical encoding and decoding using optical fiber lattices," Optical Comm., vol. 86, no. 1, pp. 25-, 1991.

[15] A.S. Holmes, and R. Syms, "All optical CDMA using 'quasi-prime' codes," J. Lightwave Technol., vol. 10, no. 2, pp. 279-, 1991.

[16] J. G. Zhang, and G. Picchi, "Tunable prime-code encoder/decoder for all optical CDMA applications," Electronic lett., vol. 29, no. 13, pp. 1211-1212, 1993.

[17] J. G. Zhang, and W. C. Kwong, "Novel designs of programmable all-optical synchronous code-division multiple-access encoders and decoders," vol. 34, no. 7, pp. 2109-, 1995.

[18] L. Tancevski, and I. Andonovic, "Block multiplexing codes for incoherent optical ladder network correlators," IEEE Photon. Technol. Lett., vol. 6, no. 2, pp. 309-311, 1994

[19] P. C. Teh, P. Petropoulos, M. Ibsen, and D. J. Richardson, "A comparative study of the performance of seven- and 63-chip optical code-division multiple-access encoders and decoders based on superstructured fiber Bragg gratings," J. Lightwave Technol., vol. 19, no. 9, pp. 1352-1365, 2001.

[20] P. C. Teh., M. Ibsen, J. H. Lee, P. Petropoulos and D. J. Richardson, "Demonstration of a four channel WDM/OCDMA system using 255-chip 320-Gchip/s quaternary phase coding

gratings,” IEEE Photon. Technol. Lett., vol. 14, pp. 227-229, Feb., 2002.

[21] J. H. Lee, P. C. Teh, P. Petropoulos, M. Ibsen, and D. J. Richardson, “A grating-based OCDMA coding-decoding system incorporating a nonlinear optical loop mirror for improved code recognition and noise reduction,” J. Lightwave Technol., vol. 20, no. 1, pp. 36-46, 2002.

[22] J. A. Salehi, A. M. Weiner, and J. P. Heritage, “Coherent ultrashort light pulse code-division multiple access communication,” J. Lightwave Technol., vol. 8, pp. 478-, 1990.

[23] D. J. Hajela, and J. A. Salehi, “Limits to the encoding and bounds on the performance of coherent ultrashort light pulse code-division multiple access,” IEEE Trans. Commun., vol. 40, no. 2, pp. 325, 1992.

[24] D. Zaccarin, and M. Kavehrad, “An optical CDMA system based on spectral encoding of LED,” IEEE Photon. Technol. Lett., vol. 4, no. 4, pp. 479-482, 1993.

[25] A. G. Jepsen, A. E. Johnson, E. S. Maniloff, T. W. Mossberg, M. J. Munroe, and J. N. Sweetser, “Fibre Bragg grating based spectral encoder/decoder for lightwave CDMA,” Electronic Lett., vol. 35, no. 13, pp. 1096-1097, 1999.

[26] K. Kiasaleh, “Fiber optic frequency hopping multiple access communication system,” IEEE Photon. Technol. Lett., vol. 3, no. 2, pp. 173-175, 1991.

[27] K. Kiasaleh, “Performance of packet-switched fiber-optic frequency-hopping multiple-access networks,” IEEE Trans. Commun., vol. 43, no. 7, pp. 2241-2253, 1995.

[28] H. Fathallah, L. Rusch and S. Larochelle, “Passive optical fast frequency-hop CDMA communications system,” J. Lightwave Technol., vol. 12, pp. 397-405, 1999.

[29] H. Fathallah, and L. Rusch, “Robust optical FFH-CDMA communications: coding in place of frequency and temperature control,” J. Lightwave Technol., vol. 17, no. 8, pp. 1284-1293, 1999.

[30] E. Inaty, H. M. H. Shalaby, and P. Fortier, “A new transmitter-receiver architecture for noncoherent multirate OFFH-CDMA system with fixed optimal detection threshold,” J. Lightwave Technol., vol. 20, no. 11, pp. 1885-1894, 2002.

- [31] E. Inaty, H. M. H. Shalaby, P. Fortier, L. Rusch, "Multirate optical fast frequency hopping CDMA system using power control," *IEEE J. Lightwave Technol.*, vol. 20, no. 2, pp. 166-177, 2002.
- [32] A. A. Shaar, and P. A. Davies, "A survey of one-coincidence sequences for frequency hopped spread spectrum systems," *Proc. Inst. Elec. Eng. Pt. F, Commun., Radar Signal Processing*, pp. 719-724, 1984.
- [33] L. Bin, "One coincidence sequences with specified distance between adjacent symbols of frequency-hopping multiple-access," *IEEE Trans. Commun.*, vol. 45, no. X, pp. 408-410, 1997.
- [34] G. C. Yang, and W. C. Kwong, "Performance analysis of optical CDMA with Prime codes," *IEE Electronic Lett.*, vol. 31, no. 7, pp. 569-570, 1995.
- [35] J. Salehi, "Code division multiple-access techniques in optical fiber networks—Part 2: Systems performance analysis," *IEEE Trans. Commun.*, vol. 37, pp. 834-842, 1989.
- [36] A. J. Lowery et al., "Performance of Optical OFDM in Ultralong-Haul WDM Lightwave Systems," *IEEE J. Lightwave Technol.*, vol. 25, pp. 131-138, 2007.
- [37] S. L. Jansen et al., "Coherent Optical 25.8-Gb/s OFDM Transmission Over 4160-km SSMF," *J. Lightwave Technol.*, vol. 26, pp. 6-15, 2008.
- [38] D. Qian et al, ECOC'07, paper 5.4.1
- [39] A. E. Willner et al, "Advanced Techniques to Increase the Number of Users and Bit Rate in OCDMA Networks," *IEEE J. Selected Topic Quantum Electron.*, vol. 13, pp. 1403-1414, 2007.
- [40] S. Hara et al, "Overview of Multi-carrier CDMA," *IEEE Comm Mag.*, vol. 35, pp. 126-133, 1997.
- [41] Y. M. Lin et al, "Demonstration and Design of High Spectral Efficiency 4Gb/s OFDM System in Passive Optical Networks," OFC'07, paper OThD7.

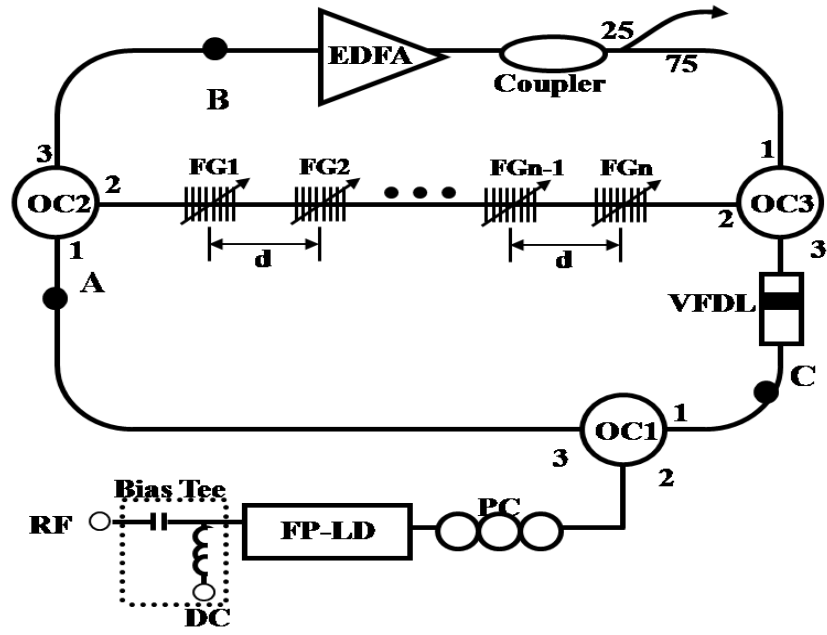


Fig. 5.1 Experimental setup of the proposed OFFH-CDMA light source module.

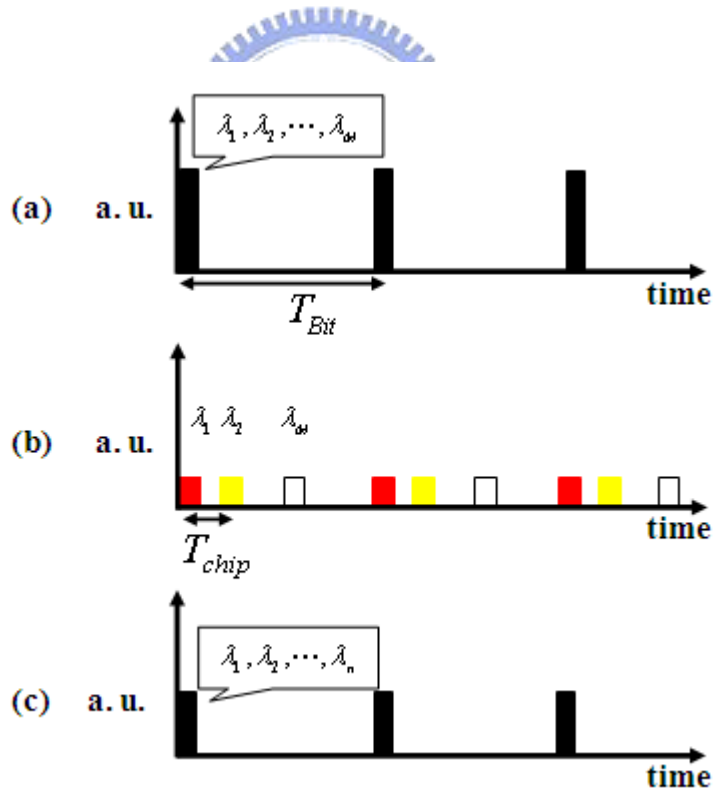


Fig. 5.2 Time domain waveforms at positions of A, B, and C, respectively.

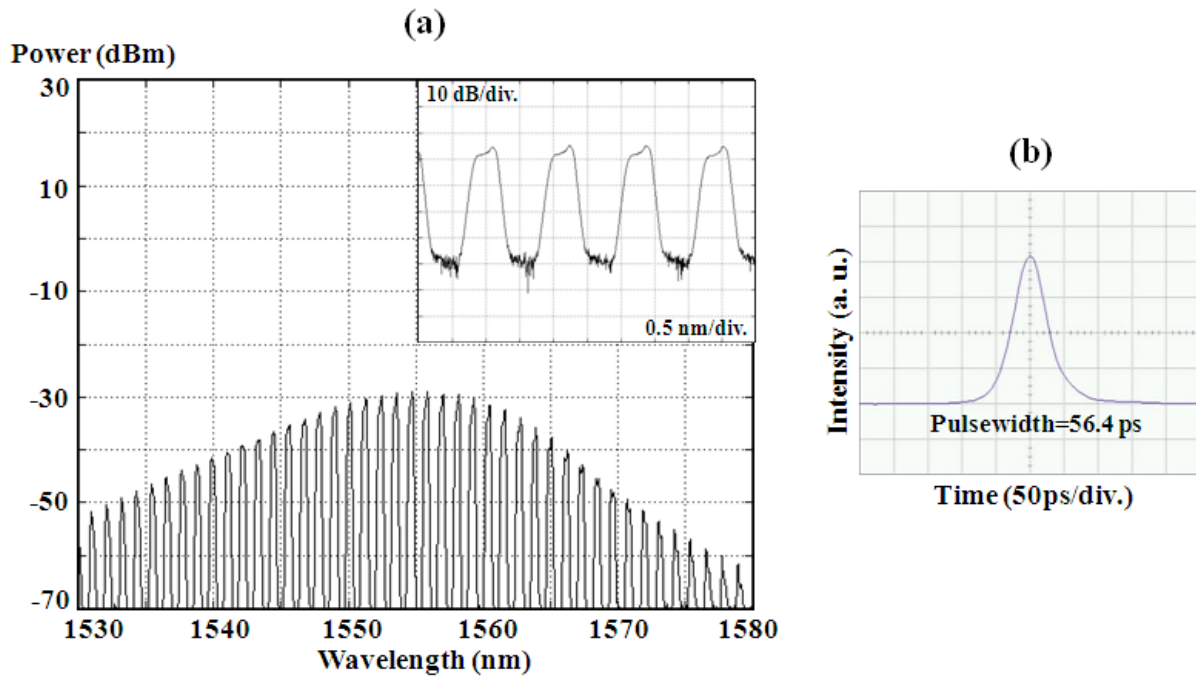
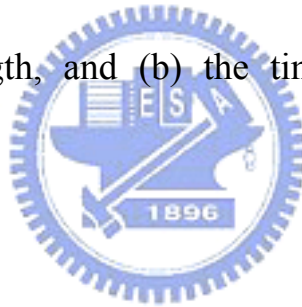


Fig. 5.3 (a) Optical spectrum of the FP-LD output. The inset shows the detail near the center wavelength, and (b) the time domain single pulse with a pulse-width of ~ 56.4 ps.



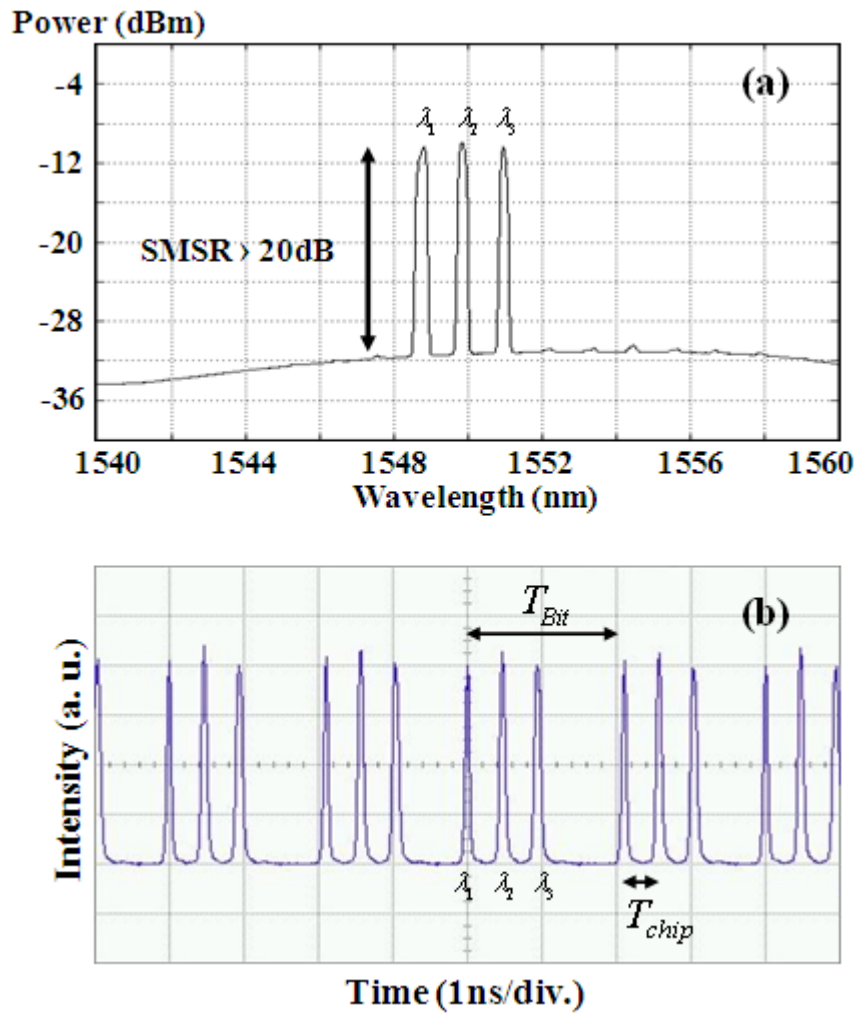


Fig. 5.4 (a) The output spectrum after encoding, where, $\lambda_1=1548.82$ nm, $\lambda_2=1549.9$ nm, and $\lambda_3=1550.98$ nm. (b) Encoded waveform with a bit and chip durations of 2.1 ns and 500 ps, respectively. The sequence order in time domain is $\lambda_1 \rightarrow \lambda_2 \rightarrow \lambda_3$.

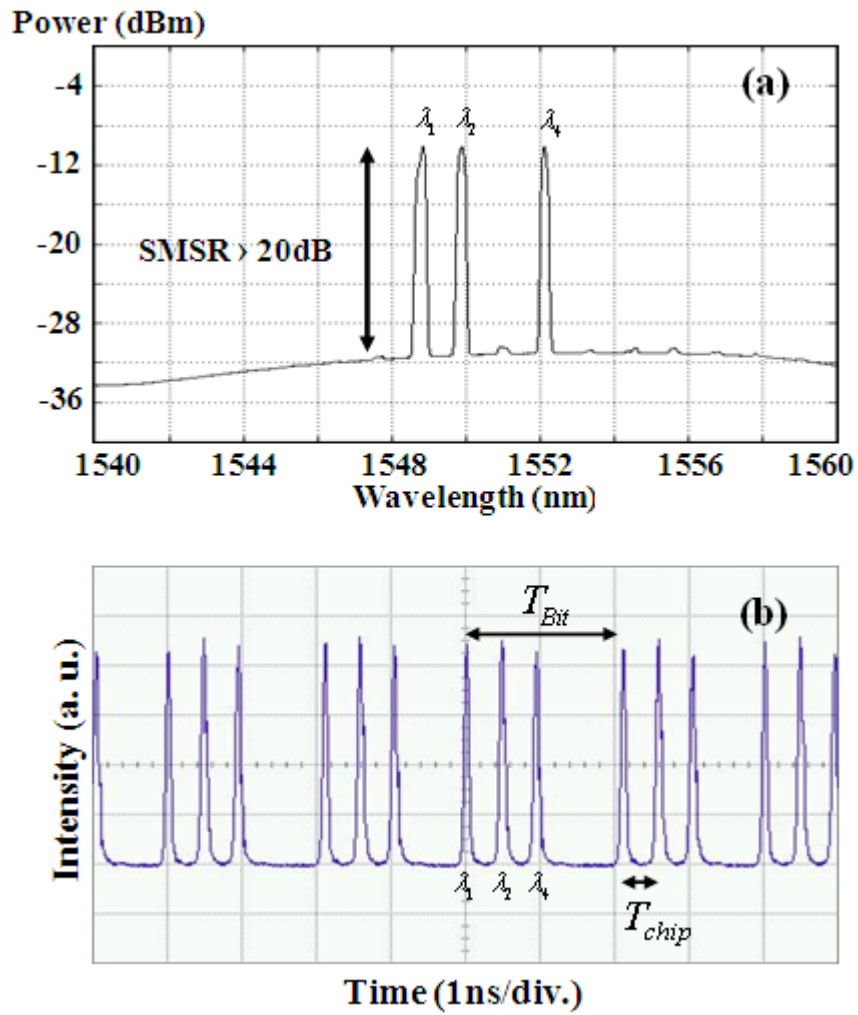


Fig. 5.5 (a) The output spectrum after encoding, where $\lambda_1=1548.82$ nm, $\lambda_2=1549.9$ nm, and $\lambda_4=1552.06$ nm. (b) Encoded signal with bit and chip durations of 2.1ns and 500ps, respectively. The sequence order in time domain is $\lambda_1 \rightarrow \lambda_2 \rightarrow \lambda_4$.

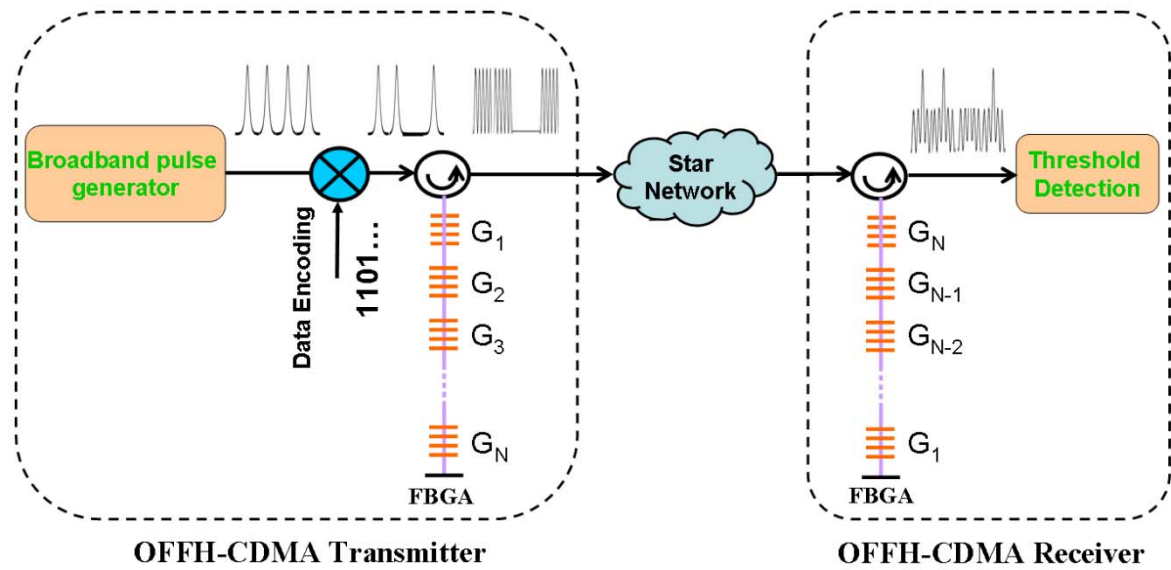


Fig. 5.6 The transmitter and receiver for an OFFH-CDMA system with the fiber Bragg grating (FBGA) as the encoder and decoder.

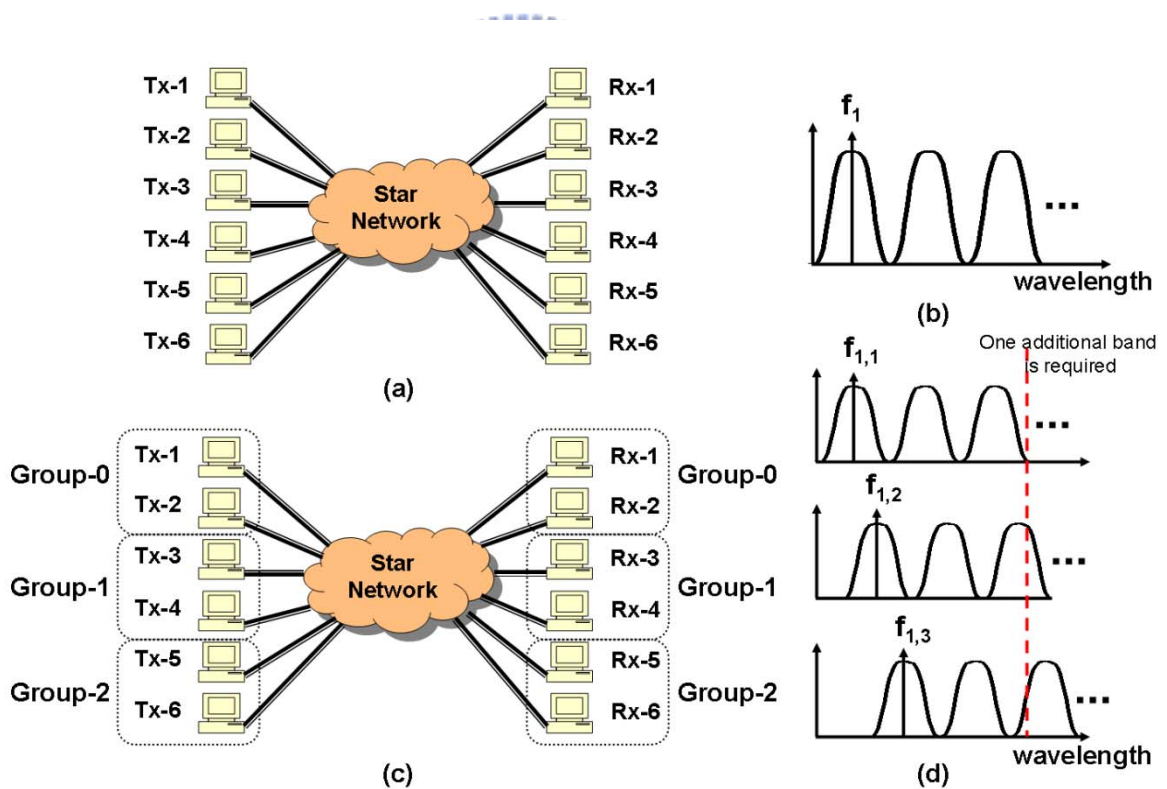


Fig. 5.7 (a) and (b), a star network and the frequency allocation approach for conventional scheme. (c) and (d), a star network and the frequency allocation approach with our proposed multi-group scheme.

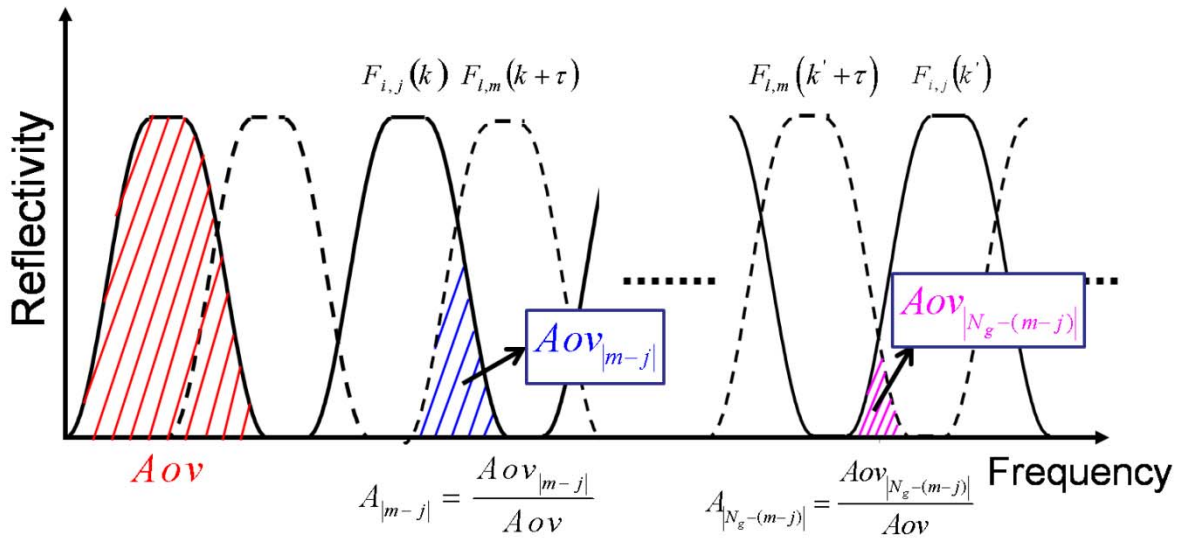


Fig. 5.8 The frequency slots assigned to the i -th and the j -th group. The reflected optical power by a grating is denoted as Aov and the two possible partial reflected power shown in figure are denoted as $A_{|m-j|}$ and $A_{|N_g-(m-j)|}$.

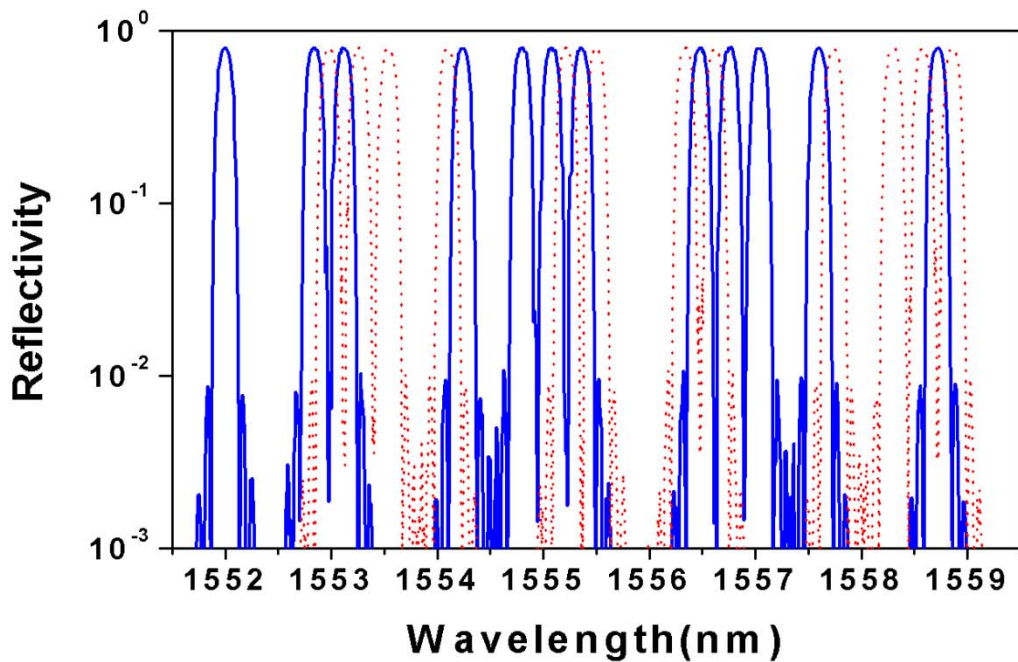


Fig. 5.9 The FBGA spectra of the 2-group codes. Note the frequency slots of different groups are overlapping.

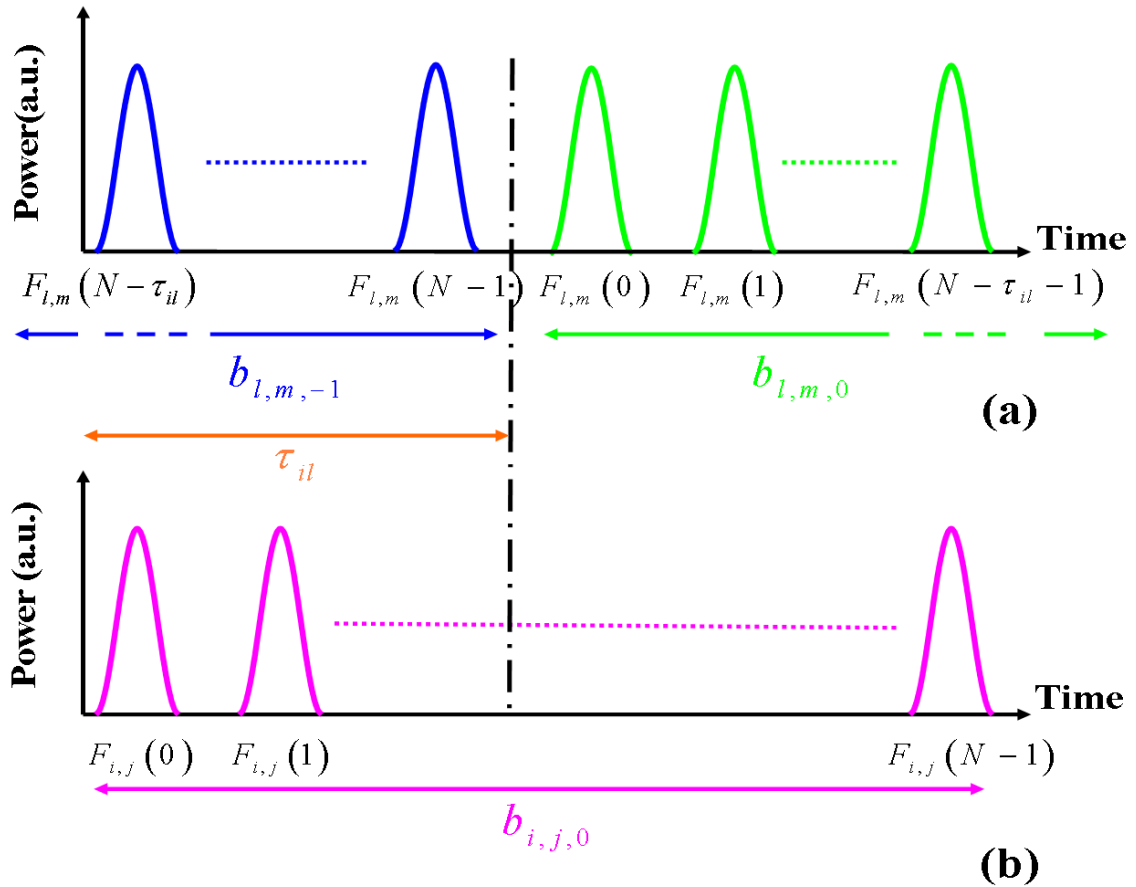


Fig. 5.10 Received signals at the i -th receiver from j -th group. (a) Interference in the l -th transmitter from the m -th group. The used code is denoted as $F_{l,m}$. (b) Received signal of the desired transmitter, the i -th transmitter from j -th group. The used code is denoted as $F_{i,j}$. “ $b_{l,m,n}$ ” is the earlier or the present bit of the l -th transmitter from the m -th group when $n = -1$ or $n = 0$. τ_{il} represents the relative delay chips between the two inputs.

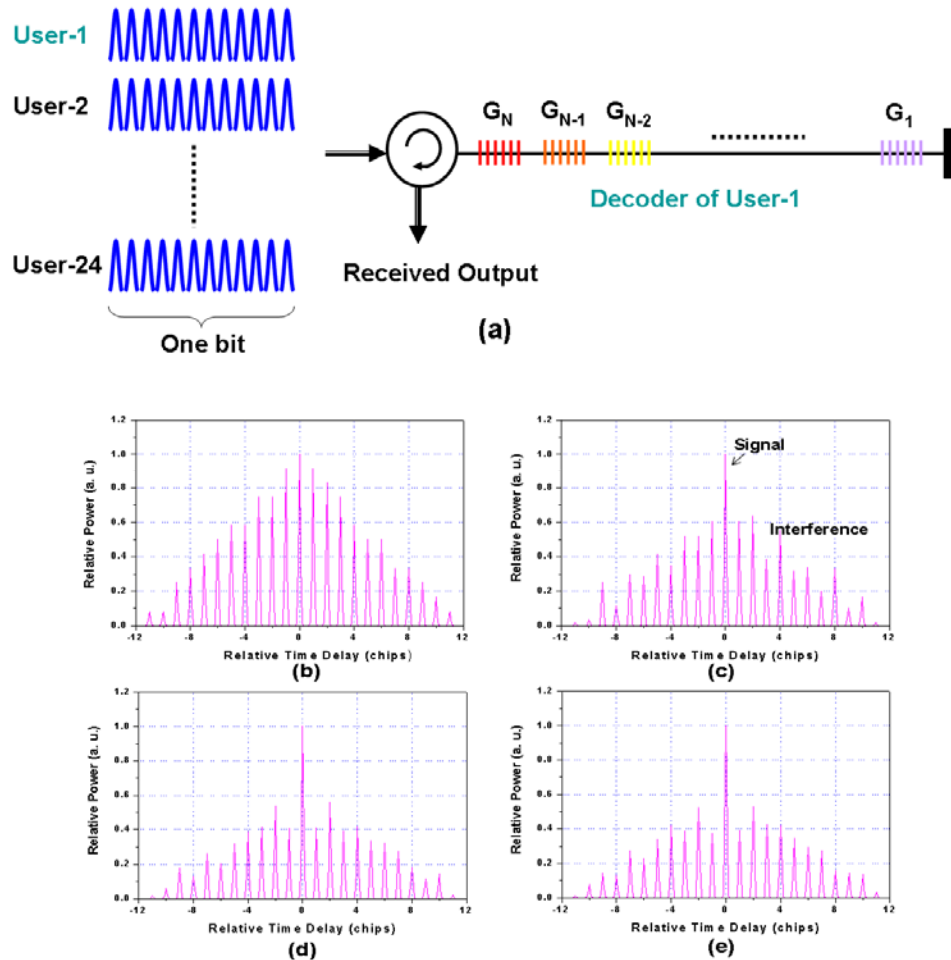


Fig. 5.11 (a) One-bit of all the 24 users are synchronously sent to the decoder of the first user to evaluate the interference, (b) to (e) correspond to group number of 1, 2, 6, 24 for code lengths of 12, from 25 available un-overlapping frequency slots and 24 simultaneous users. The center shows the auto-correlation peaks and the side lobes are the cross-correlation interference.

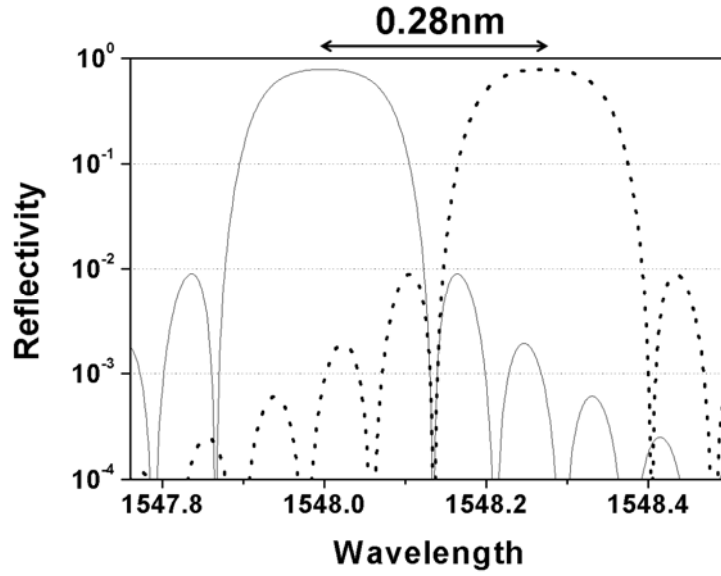


Fig. 5.12 The adjacent non-overlapping Gaussian apodization grating spectra. The spacing is determined that the first nulls are coincided to increase the spectra efficiency.

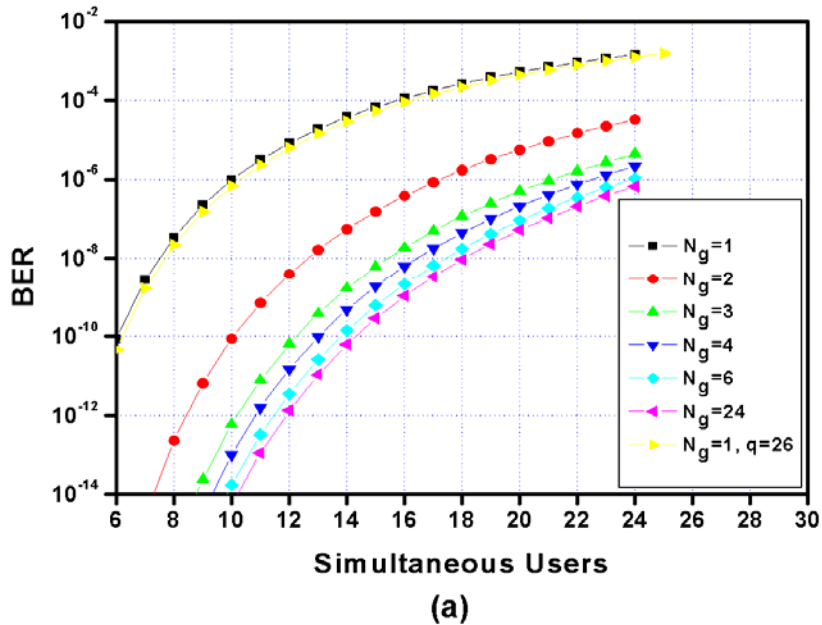


Fig. 5.13(a) BER versus simultaneous users with different group numbers. The number of frequency slots q and the code weight N are equal to 25 and 12, respectively.

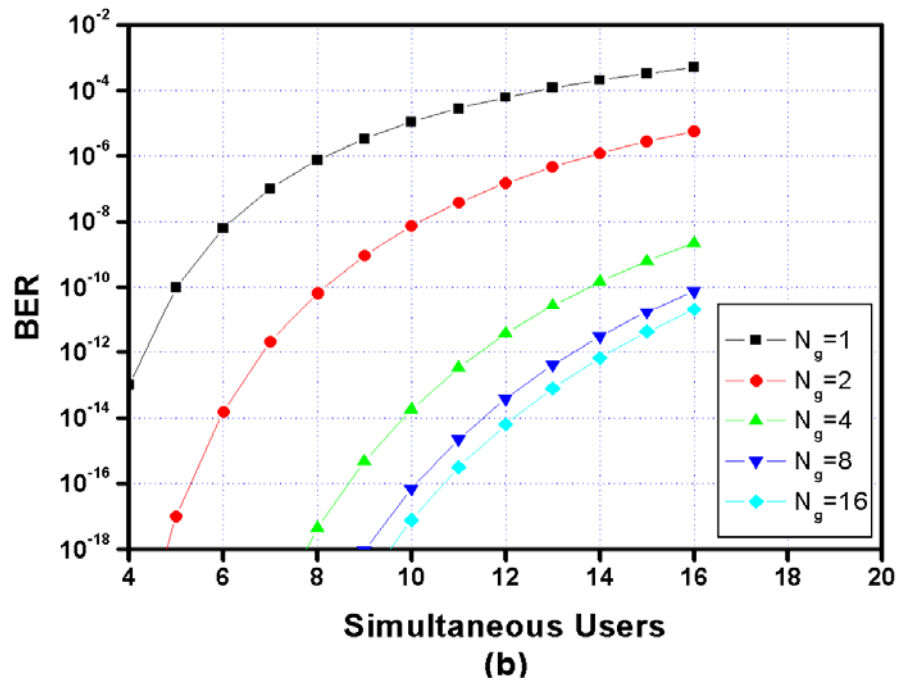


Fig. 5.13(b) The number of frequency slots q and the code weight N are equal to 17 and 12, respectively.

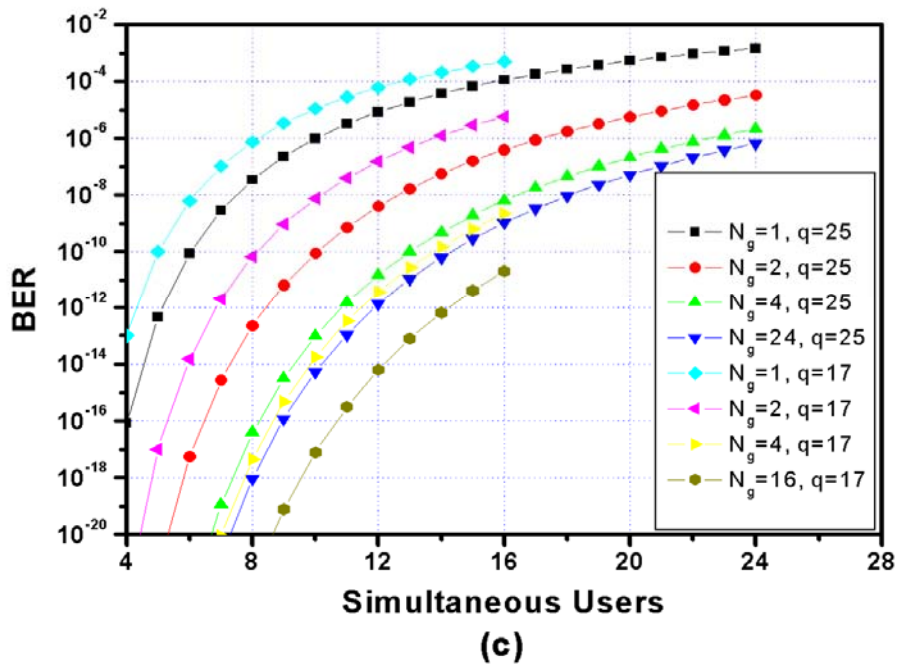


Fig. 5.14 BER of systems with parameters $(q, N) = (17, 12)$ and $(q, N) = (25, 12)$.

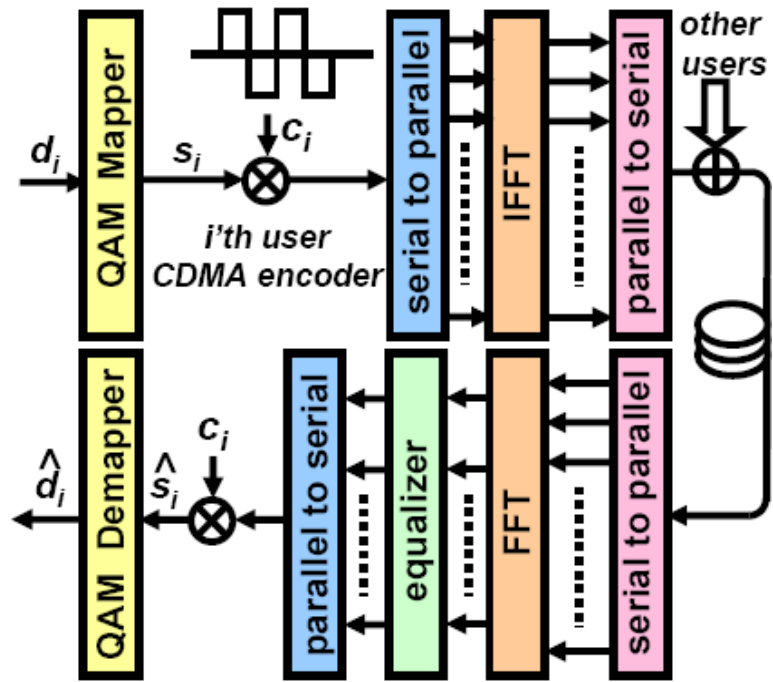


Fig. 5.15 Block diagram of MC-CDMA, upper part is the transmitter and lower part is the receiver.

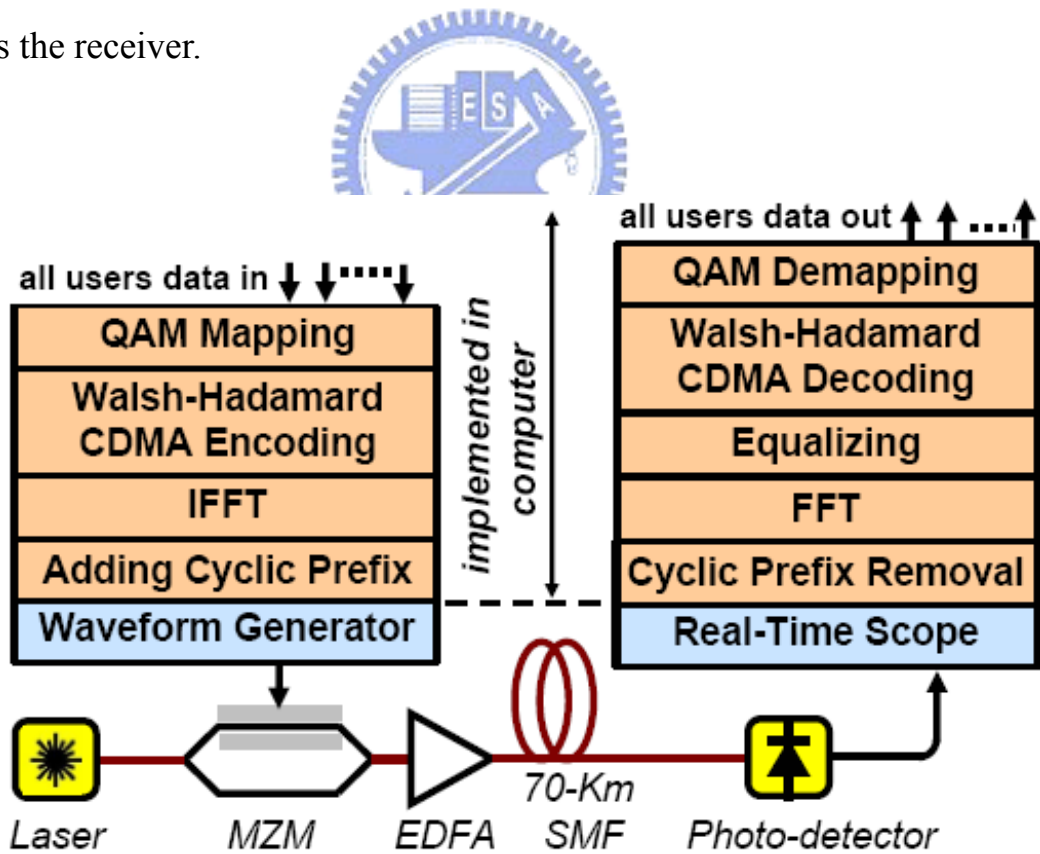


Fig. 5.16 Experimental setup of MC-CDMA

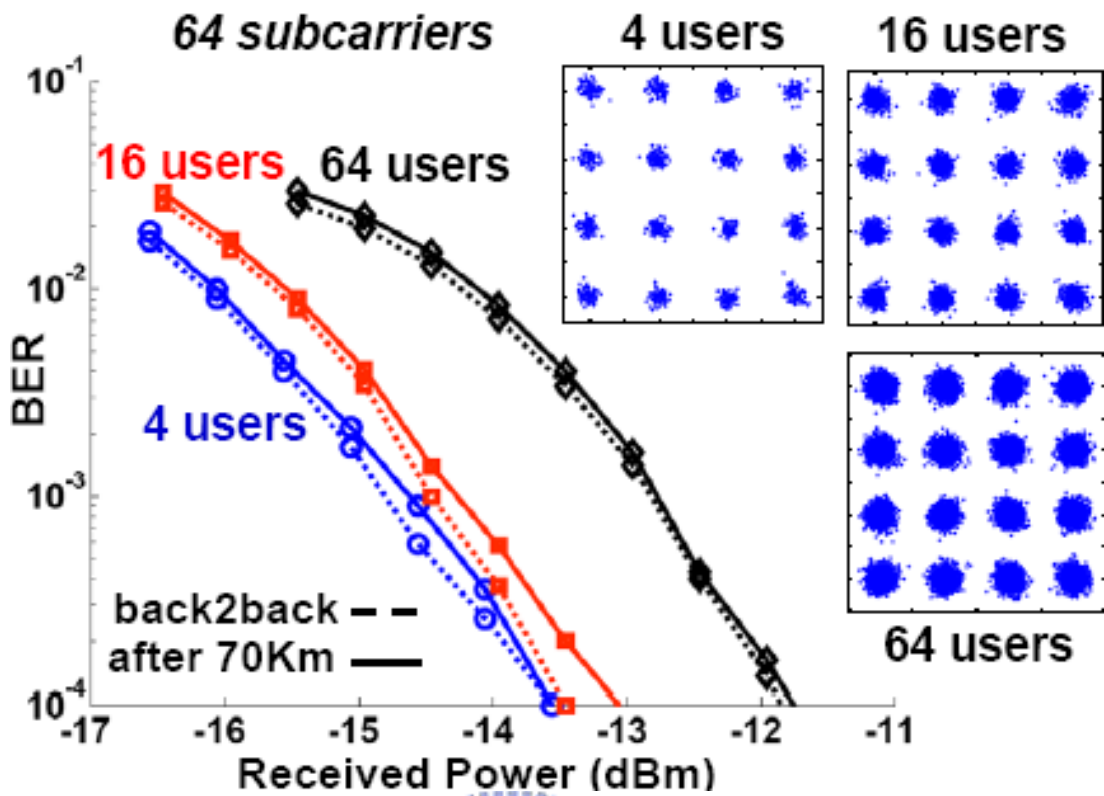


Fig. 5.17 BER curves of different number of active users and corresponding equalized constellations.

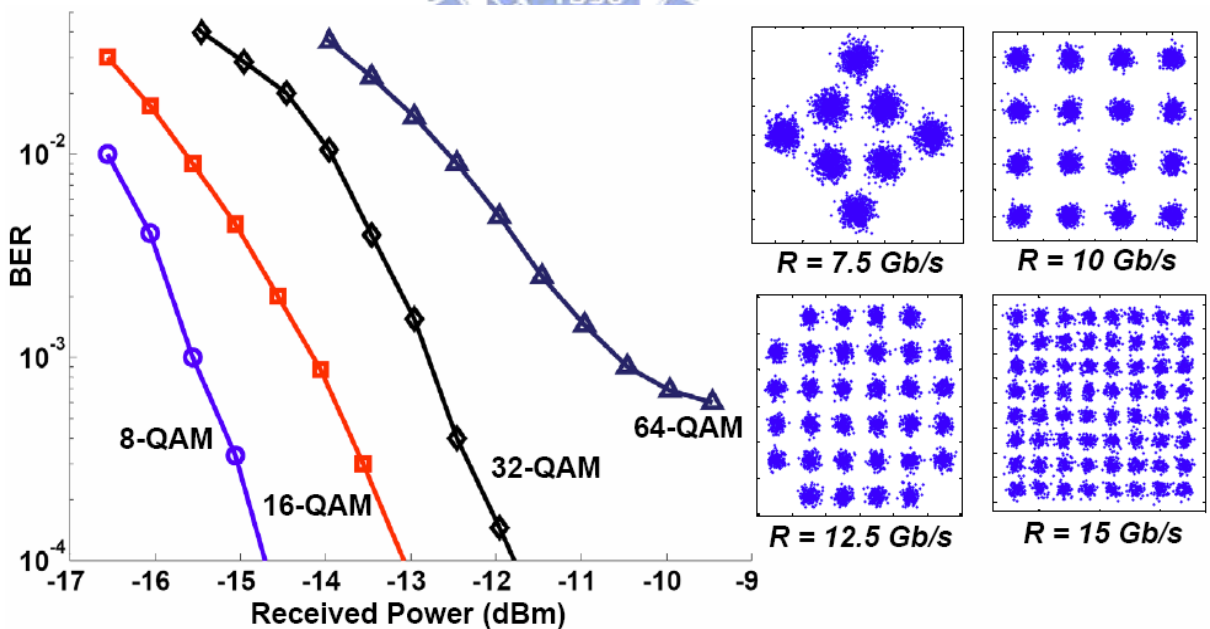


Fig. 5.18 BER curves and equalized constellations for different QAM mappings.

Chapter 6

Conclusions

6.1 Conclusions

Aimed to solve some of the issues described in chapter 2, we list as follows the main contributions of this dissertation.

(i) OFDM

1. *RF-tone assisted OFDM*

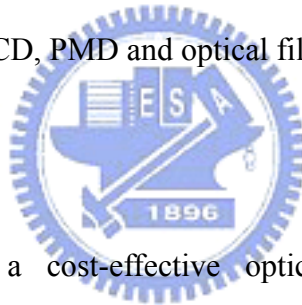
- a) We propose the RF-tone assisted OFDM system with a 5 dB better sensitivity and a more robust CD tolerance (almost immune to CD).
- b) We firstly propose the 2×2 matrix equalizer which jointly compensates the impairments resulted from both the MZM imbalances and the fiber CD.
- c) The first demonstration of wavelength conversion for OFDM signal. This proves the possibility for OFDM to be employed in an all-optical wavelength routing network.
- d) We provide a semi-analytical approach to accurately evaluate the BER for OFDM systems. This would help people design and optimize the OFDM systems.

2. *Virtual Single Sideband OFDM*

- a) We propose the VSSB-OFDM which has an ~ 2 dB gain and saves half of DAC's bandwidth compared to the previous direct detected OFDM system. In addition, there is almost no penalty observed after 340 km SSMF transmission.
- b) We further propose the GVSSB-OFDM which inserts an optimized frequency gap between the RF tone and the signal. The new system has only 3 dB transmission penalty after 1600 km uncompensated SSMF transmission.

(ii) Advanced Modulation Formats

- a) Experimental demonstrations of the DQPSK signal generation using a dual-drive Mach-Zehnder modulator (DD-MZM). We show that using RZ impulse shaping can exceed more than 5 dB gain over NRZ with this generation scheme. The theoretical investigations of optical spectrum and bit error rate are also given.
- b) Encoding the ASK labeled RZ-DPSK signal by using one DD-MZM. Compared to the previous approach this cost-effective scheme has a 2 dB gain for the label and a comparable performance for the payload after 120 km fiber transmission.
- c) We also evaluate the quantum limit for 4ASK with optimum level spacing. Compared to OOK format, there is around 5 dB penalty due to multi-level detection.
- d) A phase modulated 4ASK (PM-4ASK) format is proposed with the advantages of better tolerances to the CD, PMD and optical filtering effects.



(iii) OCDMA

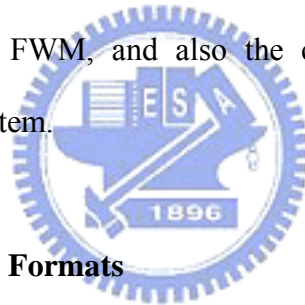
- a) The development of a cost-effective optical fast frequency hopping CDMA (OFFH-CDMA) light source using a self-seeded Fabry-Perot laser diode (FP-LD).
- b) Reduction of the multiple access interference (MAI) for an OFFH-CDMA system by using a frequency interleaved multi-group approach.
- c) The first demonstration of the multi-carrier CDMA (MC-CDMA) for a passive optical network (PON).

6.2 Future Work

(i) OFDM

One of the big issues for OFDM would be its vulnerability to nonlinearity. There are various nonlinear sources throughout the link including the electrical drivers, MZM, fiber nonlinearities, optical amplifiers, photodiodes, and post-electrical amplifiers. The

nonlinearities in the transmitter and the receiver can be easily evaluated and compensated for in advanced, while the fiber nonlinearities is a different story since it strongly depends on various operation parameters like the input power per span, signal bandwidth, subcarrier spacing, the number and polarizations of WDM channels, transmission distance and the type of the transmitted fiber. Thus, a dynamic nonlinear equalizer would be imperatively required. So far there are couples of nonlinear compensation techniques proposed for single channel transmission [1-2]. Unfortunately, all of these proposals only mitigate the effects of self-phase modulation (SPM). However, both the four wave mixing (FWM) and the residual SPM effects would still seriously degrade the transmission performance. Thus, a laudable goal would be to provide a nonlinear equalizer which could dynamically compensate the SPM, FWM, and also the cross-phase modulation (XPM) when operated in a WDM system.



(ii) Advanced Modulation Formats

During the years around 2001~2005, there are various different modulation formats such as DPSK, DQPSK, ADPSK, 4ASK and duo-binary (DB) are proposed at that time. In 2005 the DPSK and DQPSK won out and became the next generation formats. At the same time (2005), the DSP-assisted long-haul transmission using pre-equalizer had been proposed by a company, Nortel. To date, the most promising technique for next generation communication would be the coherent PDM-QPSK, which can carry 40 Gbps data rate with only 10 GHz bandwidth. The PDM-QPSK is virtually immune to all linear impairments like the CD, PMD, and optical filtering effects [3-4]. In the near future when the demand for a higher bandwidth keeps increasing, we can expect that the coherent PDM-MPSK with a higher spectral-efficiency would be the next interesting topic for “optical people” [5].

(iii) **OCDMA**

One of the important issues in all-optical CDMA systems would be the choice of the optical en/decoding modules. The most general devices performing the en/decoding would be the fiber Bragg gratings because of the tuneabilities of their center wavelength and the compatibilities to the single mode fiber. Despite of these advantages, their bulky size and the slow tuning speed are still the issues existed in OCDMA systems. Recently, people consider replacing the FBGs by the smaller-sized microring devices [6]. The microring device is a nano-structured optical filter of which the center wavelength could be controlled via the input voltage employed on it. The smaller size could allow the transceiver has a longer code-length and thus increase the system capacity in a LAN; while the voltage-controlled tuneability would increase the tuning speed and thus could reduce the transient time preparing the next destination code.

On the other hand, the poor tolerance to the CD resulted from the typically used broadband light source is another detrimental issue for an OCDMA system. One of the possible solutions would be to employ the post-signal processing after transmission. With the explosive studies and investigations of DSP these years, the OCDMA combined with the DSP could further extend its maximum reach and in the future become the standard transmission system for next generation passive optical network.

References

- [1] J. Lowery, "Fiber Nonlinearity Mitigation in Optical Links That Use OFDM for Dispersion Compensation," *IEEE Photon. Technol. Lett.*, vol. 19, pp.1556-1558, 2007.
- [2] W. Shieh, H. Bao, and Y. Tang, "Coherent optical OFDM: theory and design," *Optics Express*, vol. 16, pp. 841-859, 2008.
- [3] S. J. Savory et al., "Electronic compensation of chromatic dispersion using a digital coherent receiver," *Opt. Express*, vol. 15, pp. 2120-2126, 2007.
- [4] C. Laperle et al., "Wavelength Division Multiplexing (WDM) and Polarization Mode Dispersion (PMD) Performance of a Coherent 40Gbit/s Dual-Polarization Quadrature Phase Shift Keying (DP-QPSK) Transceiver", OFC 2007, Paper PDP16.
- [5] X. Zhou et al., "8x114 Gb/s, 25-GHz-spaced, PolMux-RZ-8PSK transmission over 640 km of SSMF employing digital coherent detection and EDFA-only amplification," OFC2008, Paper PDP01.
- [6] K. Takiguchi, "Integrated photonic devices for OCDMA using silica planar lightwave circuit technology," OFC2008, Paper OThE3.

Publication

International Journals:

1. **Wei-Ren Peng**, Bo Zhang, Xiaoxia Wu, Kai-Ming Feng, Alan E Willner, and Sien Chi, “Experimental Demonstration of 1600 km SSMF Transmission of a Generalized Direct Detection Optical Virtual SSB-OFDM System,” to be *submitted to IEEE Photon. Technol. Lett.*
2. **Wei-Ren Peng**, Bo Zhang, Xiaoxia Wu, Kai-Ming Feng, Alan E Willner, and Sien Chi, “Experimental Demonstration of Compensating the I/Q Imbalance and Bias Deviation of the Mach-Zehnder Modulator for an RF-Tone Assisted Optical OFDM System,” *to be submitted to IEEE Photon. Technol. Lett.*
3. **Wei-Ren Peng**, Kai-Ming Feng, Sien Chi, and Alan E. Willner, “Bit Error Rate Calculation for a Single Sideband OFDM Signal with Direct Detection Optically Pre-Amplified Receivers,” *submitted to Optics Express*.
4. **Wei-Ren Peng**, Xiaoxia Wu, Vahid R. Arbab, Bishara Shamee, Jeng-Yuan Yang, Louis C. Christen, Kai-Ming Feng, Alan E. Willner, and Sien Chi, “Experimental Demonstration of 340 km SSMF Transmission Using a Virtual Single Sideband OFDM Signal that Employs Carrier Suppressed and Iterative Detection Techniques,” *submitted to IEEE Photon. Technol. Lett.*
5. **Wei-Ren Peng**, Xiaoxia Wu, Vahid R. Arbab, Bishara Shamee, Louis C. Christen, Jeng-Yuan Yang, Kai-Ming Feng, Alan E. Willner and Sien Chi, “Experimental Demonstration of a Coherently Modulated and Directly Detected Optical OFDM System Using an RF-Tone Insertion,” to be *submitted to IEEE Photon. Technol. Lett.*
6. **Wei-Ren Peng** and Sien Chi, “Quantum limit of optimum four-level ASK signals with direct detection optically preamplified receivers,” *Optics Express*, vol 15, pp. 6790-6797, 2007.

7. **Wei-Ren Peng**, Wen-Piao Lin, and Sien Chi, "Improved FBGA OFFH-CDMA System Using a Novel Frequency-Overlapping Multigroup Method," *IEEE/OSA Journal of Lightwave Technol.*, vol. 24, pp. 1072-1081, Mar. 2006.
8. **Wei-Ren Peng**, Peng-Chun Peng, Yu-Ting Hsueh, Sien Chi "Performance Comparisons of External Modulated Hybrid Analog/Digital Signals in Electrical and Optical Domains," *IEEE Photonics Technology Letters*, vol. 17, no. 11, pp. 2496-2498, Nov. 2005.
9. **Wei-Ren Peng**, Yu-Chang Lu, Jason (Jyehong) Chen, and Sien Chi "Encoding ASK Labeled CSRZ-DPSK Payload by Using Only One Dual-Drive Mach-Zehnder Modulator with Enhanced Label Performance," *IEEE Photonics Technology Letters*, vol. 17, pp. 2227-2229, Oct. 2005.
10. **Wei-Ren Peng**, Peng-Chun Peng, Wen-Piao Lin, Kuei-Chu Hsu, Yin-Chieh Lai, and Sien Chi "A Cost-Effective Fast Frequency-Hopped Code-Division Multiple Access Light Source Using Self-Seeded Fabry-Perot Laser with Fiber Bragg Grating Array," *IEEE Photonics Technology Letters*, vol. 16, no. 11, pp. 2550-2552, November 2004.
11. Chun-Ting Lin, **Wei-Ren Peng**, Peng-Chun Peng, Jason (Jyehong) Chen, Cheng-Feng Peng, Bi-Shiou Chiou, and Sien Chi, "Simultaneous Generation of Baseband and Radio Signals Using Only One Single-Electrode Mach-Zehnder Modulator With Enhanced Linearity," *IEEE Photonics Technology Letters*, vol. 18, pp. 2481-2483, Dec. 2006.
12. Peng-Chun Peng, **Wei-Ren Peng**; Kai-Ming Feng, Hung-Yu Chiou, Chen, J., Hao-Chung Kuo, Shing-Chung Wang; Chi, S., "OCDMA light source using directly modulated Fabry-Perot laser diode in an external injection scheme," *IEEE Photonics Technology Letters*, vol. 18, pp. 1103-1105, May 2006.
13. Peng-Chun Peng, **Wei-Ren Peng**, Jia-He Lin, Wen-Piao Lin, and Sien Chi, "Generation of wavelength-tunable optical pulses using EDFA as external-injection light source and amplifier for Fabry-Perot laser diode," *IEEE Photonics Technology Letters*, vol. 16, no. 11, pp. 2553-2555, November 2004.

14. Wen-Piao Lin, **Wei-Ren Peng**, Sien Chi, “Dynamic wavelength allocation in WDM radio-over-fiber access network,” *Japanese Journal of Applied Physics*, 44 (3): 1282-1286 MAR 2005.
15. Peng-Chun Peng, **Wei-Ren Peng**, Wen-Piao Lin, and Sien Chi, “Dynamic Encoder and Decoder Based on Fiber Bragg Gratings for Optical Security System,” *Japanese Journal of Applied Physic*, 43 (12): 8101-8102 DEC 2004.
16. Peng-Chun Peng, Kai-Ming Feng, **Wei-Ren Peng**, Hung-Yu Chiou, Ching-Cheng Chang, and Sien Chi “Long-Distance Fiber Grating Sensor System using Fiber Ring Laser with EDWA and SOA,” *Optics Communications*, vol. 1, no. 1, pp. 127-131, Aug. 2005.
17. Peng-Chun Peng, Kai-Ming Feng, Hung-Yu Chiou, **Wei-Ren Peng**, Jason (Jyehong) Chen, Hao-Chung Kuo, Shing-Chung Wang, and Sien Chi "Reliable Architecture for High-Capacity Fiber-Radio Systems," *Optical Fiber Technology*, vol. 13, pp. 236-239, 2007.
18. Chun-Ting Lin, Jason (Jyehong) Chen, Peng-Chun Peng, Cheng-Feng Peng, **Wei-Ren Peng**, Bi-Shiou Chiou, and Sien Chi, “Hybrid optical access network integrating fiber-to-the-home and radio-over-fiber systems,” *IEEE Photonics Technology Letters*, vol. 19, pp. 610-612, Apr. 2007.
19. Yu-Chang Lu, Jason (Jyehong) Chen, Kai-Ming Feng, Pao-Chi Yeh, Tzu-Yen Huang, **Wei-Ren Peng**, Ming-Fang Huang, and Chia-Chien Wei, “Improved SPM Tolerance and Cost-Effective Phase-Modulation Duobinary Transmission over 230 km Standard Single-Mode Fiber Using A Single Mach-Zehnder Modulator,” *IEEE Photonics Technology Letters*, vol. 17, pp. 2754-2756, Dec. 2005.

International/Domestic Conferences:

1. **Wei-Ren Peng**, Bo Zhang, Xiaoxia Wu, Kai-Ming Feng, Alan E Willner, and Sien Chi, “Experimental Demonstration of 1600 km SSMF Transmission of a Generalized Direct

Detection Optical Virtual SSB-OFDM System,” *ECOC2008*, Paper Mo.3.E.6.

2. **Wei-Ren Peng**, Bo Zhang, Xiaoxia Wu, Kai-Ming Feng, Alan E Willner, and Sien Chi, “Experimental Demonstration of Compensating the I/Q Imbalance and Bias Deviation of the Mach-Zehnder Modulator for an RF-Tone Assisted Optical OFDM System,” *ECOC2008*, Paper Mo.4.D.3.
3. Xiaoxia Wu, **Wei-Ren Peng**, Vahid R. Arbab, and Alan E. Willner, “Tunable Optical Wavelength Conversion of a 10 Gb/s OFDM Data Signal using a Periodically-Poled Lithium Niobate Waveguide,” *ECOC2008*, Paper P.3.1.
4. Vahid R. Arbab, **Wei-Ren Peng**, Xiaoxia Wu, and Alan E. Willner, “Experimental Demonstration of Multicarrier-CDMA for Passive Optical Networks,” *ECOC2008*, Paper We.1.F.1.
5. **Wei-Ren Peng**, Kai-Ming Feng, Sien Chi, and Alan E. Willner, “Bit Error Rate Calculation for a Single Sideband OFDM Signal with Direct Detection Optically Pre-Amplified Receivers,” *CLEO2008*, Paper CWN3.
6. **Wei-Ren Peng**, Xiaoxia Wu, Vahid R. Arbab, Bishara Shamee, Jeng-Yuan Yang, Louis C. Christen, Kai-Ming Feng, Alan E. Willner, and Sien Chi, “Experimental Demonstration of 340 km SSMF Transmission Using a Virtual Single Sideband OFDM Signal that Employs Carrier Suppressed and Iterative Detection Techniques,” *OFC2008*, Paper OMU1.
7. **Wei-Ren Peng**, Xiaoxia Wu, Vahid R. Arbab, Bishara Shamee, Louis C. Christen, Jeng-Yuan Yang, Kai-Ming Feng, Alan E. Willner and Sien Chi, “Experimental Demonstration of a Coherently Modulated and Directly Detected Optical OFDM System Using an RF-Tone Insertion,” *OFC2008*, Paper OMU2.
8. Jeng-Yuan Yang, Lin Zhang, Teng Wu, Xiaoxia Wu, Louis C. Christen, Scott Nuccio, Omer F. Yilmaz, **Wei-Ren Peng**, and A. E. Willner, “Chromatic Dispersion Monitoring of 40-Gb/s RZ-DPSK and 80-Gb/s RZ-DQPSK Data Using Cross-Phase Modulation in

Highly-Nonlinear Fiber and a Simple Power Monitor,” *OFC2008* Paper OTuG5.

9. **Wei-Ren Peng** and Sien Chi, “Improving the Transmission Performance for an Externally Modulated Baseband Single Sideband OFDM Signal Using Nonlinear Post-compensation and Differential Encoding Schemes,” *ECOC 2007*, Paper P078.
10. Chun-Ting Lin, Peng-Chun Peng, Chen, J., Cheng-Feng Peng, **Wei-Ren Peng**, Bi-Shiou Chiou, Chi, S, “Hybrid Optical Access Network Integrating Baseband and Radio Signals Transmitted on a Single Wavelength,” *CLEO 2007*, Paper CFP4.
11. Chun-Ting Lin, Cheng-Feng Peng, Peng-Chun Peng, Jyehong Chen, **Wei-Ren Peng**, Bi-Shiou Chiou, Sien Chi, ”Simultaneous Modulation and Transmission of FTTH Baseband and Radio Signals on a Single Wavelength,” *OFC2007*, Paper OThM7.
12. **Wei-Ren Peng**, Jason (Jyehong) Chen, Shen-You Tsai, Cheng Tsao, and Sien Chi, “Evaluation of the Inherent Ripple Effects on the Performance of an Optical DQPSK Signal Generated by Using Only One MZM,” *Photonics in Switching (PS2006)*, Paper P08.
13. **Wei-Ren Peng**, Jason (Jyehong) Chen, Shen-You Tsai, Cheng Tsao, and Sien Chi, “The Impact of Inherent Ripples on the Performance of an Optical DQPSK Signal Generated by Single One DD-MZM,” *2006 International Topical Meeting on Microwave Photonics (MWP'2006)*, Paper P50.
14. **Wei-Ren Peng**, Shen-You Tsai, Jason (Jyehong) Chen, and Sien Chi, “Comparing the performances of optical DQPSK signal generated by single modulator with and without pulse carver,” *Coherent Optical Technologies and Applications (COTA 2006)*, Paper JWB25.
15. Hung-Yu Chiou; Peng-Chun Peng; Kai-Ming Feng; **Wei-Ren Peng**; JyeHong Chen; Hao-Chung Kuo; Shing-Chung Wang; Sien Chi, “ A star-ring bus architecture for WDM fiber-wireless system,” *Optical Fiber Communication Conference 2006 (OFC 2006)*, Paper OFM5.

16. **Wei-Ren Peng**, Yu-Chang Lu , Jye-Hong Chen, Sien Chi, “ASK/RZ-DPSK Labelled Signal Generation Using Only One Mach-Zehnder Modulator,” *ECOC2005*, Paper Mo4.4.6.
17. Yu-Chang Lu, Jason (Jyehong) Chen, Kai-Ming Feng, Pao-Chi Yeh, Tzu-Yen Huang, **Wei-Ren Peng**, Ming-Fang Huang, Chia-Chien Wei, and Sien Chi, “A Cost-Effective Phase-Modulation-Enhanced Duobinary Modulation to Improve SPM Tolerance Using Only One Mach-Zehnder Modulator,” *ECOC2005*, Paper Th1.2.4.
18. **Wei-Ren Peng**, Wen-Piao Lin, Hung-Chang Chien, Sien Chi, “A novel scheme for better performance in optical code-division multiple access,” *IQEC and CLEO-PR 2005*, Paper CThC3-P30, Tokyo, Japan.
19. **Wei-Ren Peng**, Peng-Chun Peng, JyeHong Chen , Shen-You Tsai , Sien Chi, “Performance comparisons between direct NRZ and gain-switched RZ modulation on Fabry-Perot lasers,” *IQEC and CLEO-PR 2005*, Paper CWAB3-P75, Tokyo, Japan.
20. **Wei-Ren Peng**, Peng-Chun Peng, Yu-Ting Hsueh, and Sien Chi, “Performance study of multiple radio channels in a hybrid analog radio and digital baseband fiber link with external modulation,” *the Tenth Optoelectronics and Communications Conference/Third International Conference on Optical Internet (OECC/COIN2004)*, pp. 560-561, Korea, July 4-8, 2005.
21. Peng-Chun Peng, Kai-Ming Feng, **Wei-Ren Peng**, Hung-Yu Chiou, Ching-Cheng Chang, and Sien Chi, “Long-Distance FBG Sensor System using Fiber Ring Laser with Hybrid Amplifier,” *Optical Fiber Sensors Conference (OFS-17)*, Paper P2-67, Bruges, Belgium, May 2005, SPIE.
22. Wen-Piao Lin, **Wei-Ren Peng** and Sien Chi, “A novel bidirectional wavelength add-drop multiplexer in the WDM radio-over-fiber ring network,” *Proceeding of IEEE Conference on OECC/COIN’04*, Pacifico Yokohama, Yokohama, Japan, pp. 378-379, July 2004.
23. Peng-Chun Peng, **Wei-Ren Peng**, Wen-Piao Lin, and Sien Chi, “A Novel Dynamic

Encoder and Decoder using Fiber Bragg Gratings and Optical Switches for Optical Security System,” *the Ninth Optoelectronics and Communications Conference/Third International Conference on Optical Internet (OECC/COIN2004)*, pp. 234-235, Japan, July 12-16, 2004.

24. Wen-Piao Lin, **Wei-Ren Peng**, and Sien Chi, “A robust architecture for WDM radio-over-fiber access networks,” *Optics Fiber Communication Conference’04 (OFC2004)*, FG-3, pp. 49 - 51, 2004.
25. **Wei-Ren Peng**, Yu-Ting Hsueh, Peng-Chun Peng, Wen-Piao Lin, and Sien Chi, “Simultaneous Transmission of Baseband and Microwave Signals using a Novel Radio over Optical FSK scheme,” *Proceeding of Optics and photonics Taiwan’04*, PB-SU1-67, (OPT 2004).
26. **Wei-Ren Peng**, Peng-Chun Peng, Wen-Piao Lin, and Sien Chi, “Reconfigurable Coding Module for Optical CDMA Using the Fiber Ring Laser with Embedded Fiber Bragg Gratings,” *Proceeding of Optics and photonics Taiwan’04*, B-SU-VII5-4, (OPT 2004).
27. Peng-Chun Peng, **Wei-Ren Peng**, Wen-Piao Lin, and Sien Chi, “Wavelength-Tunable Pulse Generation using Fiber Amplifier as External-Injection Light Source and Amplifier for Fabry-Perot Laser,” *Proceeding of Optics and photonics Taiwan’04* _B-SA-VII1-1, (OPT 2004).
28. Shu-Ling Li, **Wei-Ren Peng**, Wen-Piao Lin, and Sien Chi, “WDM Fiber-Radio Network Based on A Dynamic Wavelength Allocation Structure,” *Proceeding of Optics and photonics Taiwan’03* (OPT 2003), PC2-1, pp.232-234, 2003.

博士候選人資料

姓名：彭煒仁

性別：男

出生年月日：1978年10月8日

學歷：

| 學校 / 科系 | 學位 | 起訖年月 |
|---------|----|-------------|
| 交大光電所 | 博士 | 92年9月~97年6月 |
| 交大光電所 | 碩士 | 90年9月~92年6月 |
| 台大電機系 | 學士 | 86年9月~90年6月 |

經歷：

| 服務單位 | 職位 | 起訖年月 |
|-------------------|-----|--------------|
| 美國南加州大學 電機工程學系 | 研究員 | 96年5月~97年5月 |
| 台灣工研院 機械所 | 研究員 | 90年1月~90年12月 |